Spring 1-1-2021

Dispersion, Self-assembly, And Rheological Characterization of Dna-complexed Boron Nitride Nanosystems

Venkateswara Rao Kode
Cleveland State University

DISPERSION, SELF-ASSEMBLY, AND RHEOLOGICAL CHARACTERIZATION OF DNA-COMPLEXED BORON NITRIDE NANOSYSTEMS

VENKATESWARA RAO KODE

Bachelor of Technology in Chemical Engineering

Jawaharlal Nehru Technological University

May 2015

Master of Science in Chemical Engineering

Cleveland State University

May 2017

Submitted in partial fulfillment of requirements for the degree

DOCTOR OF PHILOSOPHY IN CHEMICAL ENGINEERING

at the

CLEVELAND STATE UNIVERSITY

MAY 2021

We hereby approve this dissertation for

VENKATESWARA RAO KODE

Candidate for the Doctor of Philosophy in Chemical Engineering degree for the

Department of Chemical and Biomedical Engineering

and the CLEVELAND STATE UNIVERSITY'S

College of Graduate Studies by

Dissertation Committee Chairperson, Geyou Ao, Ph.D.

Chemical and Biomedical Engineering, 05/08/2021

Dissertation Committee Member, Christopher L. Wirth, Ph.D.

Chemical and Biomedical Engineering, 05/08/2021

Dissertation Committee Member, Orhan Talu, Ph.D.

Chemical and Biomedical Engineering, 05/08/2021

Dissertation Committee Member, Chandra Kothapalli, Ph.D.

Chemical and Biomedical Engineering, 05/08/2021

Dissertation Committee Member, Petru S. Fodor, Ph.D.

Department of Physics, 05/08/2021

Date of Defense: April 21, 2021

ACKNOWLEDGEMENT

I take this opportunity to express my deepest and sincere indebtedness to my advisor Dr. Geyou Ao, a source of constant motivation, for her mentorship and support throughout these years. Once again, thank you very much Dr. Ao, for believing in me and giving the opportunity to work in the lab, which has been the most rewarding and unforgettable journey in my life. I would like to thank the committee members: Dr. Christopher Wirth, Dr. Orhan Talu, Dr. Chandra Kothapalli, Dr. Petru Fodor for their collaborations, valuable suggestions, and feedback.

I would like to thank Rebecca Laird, Darlene Montgomery, Miroslav Bogdanovski, Dave Epperly and Karen Jackson for their assistance along the way.

My special thanks to my parents and family members for their love, sacrifices, and tremendous encouragement in advancing my education. I wanted to sincerely thank my elder brothers Narendra Kode and Sreekanth Tummala for their unconditional support.

To my best friends and colleagues, specifically, Dr. Aidin Rashidi, Dr. Gautam Mahajan, Harsha Nuthalapati, Selwin Varghese, Fjorela, Jiarui Yan, Michael Cantwell, Jacob Vitale, Michael Thompson, Jamil Jamal, Ana Dilillo, Rushik Bandodkar, Bindu Gandra, Anjana, Chennupati Vamsi, Ram Sekhar, Dr. Gude, Phanita Mannava, Aneesha Avasthi, Anand Tummala, Aravind Kommineni, Sai Mamillapalli, Naveen Morampudi, Satwic Mudigulam, a big thank you guys for making this journey a great learning yet so much enjoyable at Cleveland State and being with me in my life.

This work would not have been possible without the generous financial support from Cleveland State University Faculty Research and Development Award, TeCK fund, and Graduate Student Research Award. I wanted to acknowledge the Office of Research,

College of Graduate Studies and Robert W. Lyczkowski for recognizing my research efforts at CSU.

DISPERSION, SELF-ASSEMBLY, AND RHEOLOGICAL CHARACTERIZATION OF DNA-COMPLEXED BORON NITRIDE NANOSYSTEMS

VENKATESWARA RAO KODE

ABSTRACT

Stable liquid dispersions and the subsequent self-assembly of boron nitride (BN) nanostructures are a vital precursor for translating their exceptional electrical, mechanical, thermal, and optical properties into large-area assemblies with controlled properties. However, achieving individually dispersed BN nanomaterials including BN nanotubes (BNNTs) and hexagonal BN nanosheets (hBN) in almost any solvent has been hindered by strong van der Waals interactions among nanomaterials.

In this dissertation work, we reported a comprehensive study on developing an efficient dispersion, self-assembly, and rheological characterization of BN nanomaterials. Particularly, we reported a highly efficient dispersions of BNNTs through noncovalent complexation while exploiting the solvent-nanotube-dispersant interactions using biopolymer DNA and various solvents including water and alcohol. The subsequent purification by membrane filtration revealed that the raw BNNT material constitutes ≈ 45.2 mass % of non-nanotube impurities. Of the alcohols tested, isopropyl alcohol (IPA) was found to be an efficient solvent, resulting in a dispersion yield of as high as ≈ 48 % nanotubes in an IPA/water mixture with 60 vol % IPA by mild bath sonication. Molecular dynamics simulations further revealed that IPA played a pseudosurfactant role in solvating BNNTs by replacing water molecules in the solvation layer while IPA is added. The dispersion techniques developed for BNNTs has been extended for aqueous dispersions of

hBN as well. Additionally, we demonstrated the formation of solid BNNT films comprised of spontaneously aligned nanotubes through drop drying of DNA-wrapped BNNTs.

The overall properties of solid BNNT assemblies are directly influenced by the physical properties of nanotubes, including the tube lengths. Conventional surface deposition method by imaging dried samples on a substrate revealed inconsistencies in the average lengths of the parent BNNTs coated by DNA and SDC, due to the differential binding of DNA-BNNTs to a substrate. Therefore, we determined the nanotube lengths using an alternative method - rheological characterization - by measuring the viscosity of dilute dispersions of DNA-BNNTs, highlighting the Brownian rigid rod behavior of BNNTs. Combined, our study on the dispersion, self-assembly and rheology of BN nanomaterials paved a way for producing BN assemblies with controlled properties while offering green chemistry and multifunctionality.

TABLE OF CONTENTS

Page

LIST OF TABLES

LIST OF FIGURES

CHAPTER I

INTRODUCTION

The multi-dimensional boron nitride (BN) polymorphs, including fullerenes, nanotubes and nanosheets, have spurred a special attention in a wide range of applications due to their unique structural, mechanical, electrical, optical, and thermal properties. These are classified as inorganic or non-carbon nanomaterials, which are primarily produced synthetically and more recently, discovered in nature.[1] BN nanomaterials are structural analogs to carbon but substituted with equal number of covalently bonded boron (B) and nitrogen (N) atoms on a hexagonal carbon lattice. Like graphitic nanomaterials including graphene and carbon nanotubes (CNTs), studies on synthesis of various forms of BN nanostructures including boron nitride nanotubes (BNNTs), BN nanowires, hexagonal-boron nitride (hBN) nanosheets, nanofibers and BN nanocages have been reported.[2]–[6] These BN classified materials have been of great research interest as they possess unique features that are unavailable in many existing nanomaterials. Some of the excellent characteristics offered by BN nanostructures, including, but are not limited to, high thermal stability, superior mechanical strength, chemical inertness, and excellent ultraviolet protection and thermal stability. More importantly, they offer unique combination of

properties of electrically insulating and thermally conductive properties, unlike carbon nanomaterials. These advantages make BN nanomaterials a promising material for potential application developments in various fields including thermal interface materials,[7],[8] waste-water treatment,[9]–[11] energy harvesting,[12],[13] cosmetics,[14],[15] electrocatalysts[16] and advanced polymer composites.[17], [18] In addition, due to their imaging contrast and strong neutron capture abilities, and enhanced biocompatibility, they have been taken advantage in biomedical applications, biosensing[19] and drug and gene delivery.[20], [21]

Undoubtedly, compared to the carbon nanomaterials, the BN nanomaterials have remained much less explored. However, such a shortage of research work does not necessarily reflect the fact that BN systems have been downplayed relative to carbon nanomaterials. This is due to the lack of well-controlled conditions and techniques for synthesis of BN-based nanostructures, which have been different from already well-established routes of carbon nanomaterial synthesis. As a result, the final properties of the macroscopic artifacts fabricated by BN nanomaterials could possibly be inhibited by the low quality as-synthesized BN material, which is used as a precursor for liquid phase processing and subsequent application developments. More importantly, achieving individually dispersed nanomaterials in almost any solvent has been hindered by strong van der Waals interactions among nanomaterials. One of the most promising routes to accomplish stable dispersions of BN nanomaterials is via noncovalent complexation using dispersant molecules in a solvent media using sonication, enabling minimal damage to BN lattice structure and reduced energetic cost.

One of the primary goals of our research group is to develop BN nanomaterial dispersion methodology and effective characterization, which is the fundamental criteria for developing and achieving the final product with desired optimum properties. My role, as detailed in this thesis, was to develop highly efficient dispersions of BN nanostructures, specifically, BNNTs and hBN nanosheets, aided by biomolecules such as DNA using non-covalent complexation in solvent media. This effort utilized the various characterization techniques including UV-vis spectrophotometer, thermogravimetric analysis, optical microscopy, scanning electron microscopy, and rheology to characterize and optimize the dispersion quality and yield.

This thesis is formatted mainly into two sections: the first section, which is the major portion of this dissertation work, includes the solvent/cosolvent assisted dispersions, purification, rheological characterization, self-assembly of BNNTs by DNA. The second section includes the noncovalent complexation of hBN sheets using DNA in phosphate buffered saline solution. Specifically, chapter II includes a broader background knowledge about BNNTs and hBN nanosheets and various approaches that are previously employed for surface modification, exfoliation, rheology of dilute dispersions, bottom-up assembly and other relevant information.

Chapter III is the published paper on purification and assembly of DNA-stabilized BNNTs into aligned films. We report a dispersion methodology of BNNTs in an aqueous environment using DNA and produced assembled solid films with improved nanotube alignment and purity. We chose to initially work with $(GT)_{20}$ single-stranded DNA, which has emerged as a sequence controlled biopolymer of choice to effectively sort chirality-defined SWCNTs[22] and enable controlled assembly and technological applications of

SWCNTs with enhanced biocompatibility.[23], [24] ***The main intellectual contribution from this effort was the formation of films comprising aligned DNA/BNNT bundles that has not been previously achieved.***

Chapter IV is our second manuscript submitted on a high throughput dispersion of BNNTs by DNA in various cosolvents. We used a natural and cost-effective DNA source in this study. Our results showed that the bath sonication not only unleashes the production of long pristine BNNTs surface coated by DNA, but also produces highly stable dispersions with improved nanotubes yield, dependent on the alcohol/water mixture composition. Molecular dynamic simulations were used to examine the solvation behavior of BNNTs in IPA/water mixtures, revealing the pseudosurfactant role of IPA in dispersing BNNTs. The similarities and differences in estimated average BNNT lengths are addressed using SEM and rheology. In addition, we showed that BNNT dispersions exhibit the rheological behavior of dilute Brownian rigid rods, which is a vital prerequisite for subsequent liquid crystalline phase behavior study of BNNTs in future work. ***The main intellectual contribution from this effort was the production of highly efficient and stable dispersions of DNA-BNNTs in IPA/water and their subsequent length characterization by rheological measurements of dilute dispersions, demonstrating the Brownian rigid rod behavior of BNNTs.***

Chapter V presents the preliminary work on the liquid dispersions of hBN nanosheets through a non-covalent complexation using DNA in phosphate buffered saline solution. We applied our prior knowledge from BNNT work to produce hBN dispersions assisted by DNA in Dulbecco's Modified Eagle Medium for cytotoxicity studies. To start with, we used UV-vis spectrophotometer and SEM to characterize and determine the

dispersion yield of hBN samples. Successful completion of work will lead to the development of potential hBN cosmetic and sunscreen applications with enhanced biocompatibility. ***The main intellectual contribution from this effort was the production of highly concentrated yet stable dispersions of hBN by DNA in phosphate buffered saline solution.***

Chapter VI states conclusions and the recommendations for future work. Briefly, a systematic approach of processing BNNTs including dispersion, purification, and assembly into solid aligned films was achieved using short ssDNA as a highly efficient dispersant for stabilizing BNNTs in water. In addition, a quick and efficient way of cosolvent assisted dispersions of BNNTs using natural DNA and their length characterization techniques by SEM and rheology is reported. Molecular dynamic simulations were utilized to understand the solvation energies and dynamics of BNNT dispersions in IPA as a cosolvent. Our preliminary findings on liquid dispersions of hBN nanosheets by DNA in PBS are also reported. The thesis is concluded with a discussion of the future direction for the work.

CHAPTER II

BACKGROUND

Boron nitride nanosystems including BNNTs and hBN possess the exceptional optical, mechanical, chemical, and thermal properties for various scientific and industrial applications. The synthesis techniques and fundamental studies of BN nanomaterials continued to gain attention due to their unique properties that are not available in many existing nanomaterials. Particularly, recent advances in the large-scale synthesis techniques of BNNTs have led to growing interests in liquid phase processing and their macroscopic assemblies including films and fibers with improved properties. The effective translation of unique properties of individual nanomaterials into macroscopic assemblies requires a starting material with well-defined properties. In order to accomplish this, a prerequisite is to obtain nanotubes in an individually dispersed state in a liquid medium, which will allow developing films and fibers. However, obtaining BNNT dispersions has been hindered by multiple challenges, including strong van der Waals interactions between nanotubes, "lip-lip" interactions, polydispersity, and impure BN raw material. Our goal is to bridge the gap between ill-defined as-synthesized BN materials available in the market and potential applications development with enhanced properties of a final product through

liquid phase processing with minimal energetic cost and enhanced biocompatibility and green chemistry.

This chapter provides general background information relevant to this dissertation including boron nitride nanotubes, boron nitride nanosheets and their surface modification techniques in solvent media. In addition, this section includes the theoretical and experimental knowledge on understanding the rheological behavior of Brownian rigid rod systems in dilute region. Furthermore, this section covers briefly about different thin film fabrication techniques that are previously employed in the literature, as well as in this work for macroscopic assembly of nanomaterials into aligned films.

2.1. Boron Nitride Nanotubes

BNNTs are one-dimensional (1D) tubular nanostructures consisting of hexagonal-boron and nitrogen bonding patterns.[2], [25] Structurally, BNNTs are close analogues to CNTs, which can be classified as single-wall boron nitride nanotubes (SWBNNTs) and multi-wall boron nitride nanotubes (MWBNNTs).[26], [27] SWBNNTs in general, imagined as a rolled up single-layered hexagonal BN nanosheet (Figure 2.1A). Similar to the atomic structure of CNT, there are several classification of BNNT chirality depending on the chiral index (*n, m*) as shown in Figure 2.1B.[28] For instance, a tube is said to be "zig-zag", if the direction of sheet is parallelly oriented to the tube axis, i.e., m = 0. On the other hand, it is called "arm-chair", if the orientation of sheet is along with the tube axis, i.e., m = n. All other (*n, m*) species corresponds to "chiral" BNNTs. The majority of the BNNTs investigated previously depicted "zig-zag" model systems, although "arm-chair" and "chiral" nanotubes are also observed to a certain extent, unlike CNTs, which are typically found in equal proportions statistically.

On the other hand, MWBNNTs are nested arrangement of SWBNNTs in two or up to maximum 8 coaxial cylinders with typical diameters between 2 to 8 nm and length ranging up to a 200 μm.[26] The BNNTs with number of walls that are most commonly found are 2 to 5 as shown by a representative transmission electron microscope (TEM) image in Figure 2.1C. BNNTs exhibits a partial ionic nature due to their electronegativity difference between B and N bonding. As a result, unlike CNTs,[27] BNNTs are electrically insulating with a wide band gap of ≈ 5-6 eV, which is independent of tube wall number and chirality.[25], [29] In fact, several studies were reported by several research groups on modifying the electronic structure of BNNTs, by electric field,[30] doping,[31] introducing defects[32] and engineering the tube surface to fit them in a broader applications.[33] In addition, BNNTs are stable under air oxidation up to 1000 °C which is almost two times greater than the thermal stability of CNTs and have optical absorbance, fluorescence features in the ultraviolet range and transparent in visible, unlike CNTs.[34], [35] Furthermore, BNNTs are inherently noncytotoxic and exhibit excellent hydrophobicity.[36]

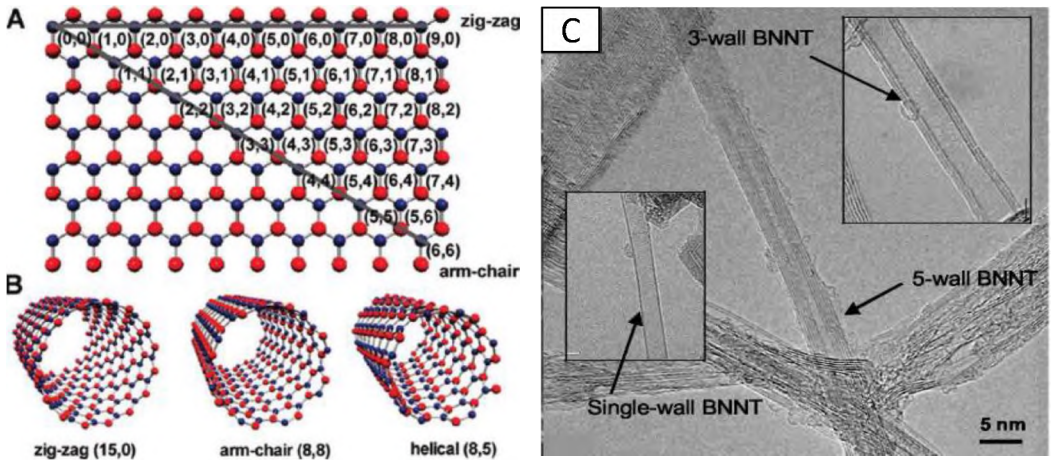

Figure 2.1. (A) The structural model of multiple single-layered BNNTs indicating "zig-zag" (15,0), "arm-chair" (8,8), and a "chiral" (8,5) models by wrapping the planar monoatomic hexagonal BN nanosheet. Boron and nitrogen are colored in blue and red, respectively. [reproduced from ref. [28]] (B) A TEM image of typical one-, three- and five-wall BNNTs, produced by PVC/HTP method. [reproduced from ref. [26]]

In 1994, Rubio et al. reported the first theoretical prediction of perfect tubular model of boron nitride structure.[37] Subsequently, the first experimental synthesis was reported in 1995 using the arc-discharge method.[2] Later, various synthesis techniques of BNNT raw material have been published based on primarily, the type of material produced and temperature conditions, in fact, a few of them are adapted from the well-known techniques of CNTs production. The techniques that are classified in a low temperature category are ball-milling,[38] substitution reaction method,[39] and catalysts based chemical vapor deposition (CVD).[40] The temperature employed in the processing chamber is way below the vaporization temperature of pure boron (4000 ˚C). The arc-discharge method[41] was reported in a high temperature synthesis category of BNNTs, where the energy generated by the high intensity laser/arc discharge is targeted into an elemental B source until it gets vaporized in a production chamber. The vaporized elemental B reacts with the nitrogen source in the ambient temperature conditions and condense into the solid state to form BNNTs. However, the arc discharge method make use

of catalysts and produces low length-to-diameter ratio BNNTs.[42] Although small quantities (i.e. milligrams of the BNNTs) can be formed using the HTP method, the tubes are of high quality and crystalline, few-wall nanotubes, high aspect ratio BNNTs and with a minimal side-wall defects.[26]

More importantly, the raw BNNT material used in this work was synthesized from pressurized vapor/condenser method (PVC)/high-temperature-pressure method (HTP), reported by a group at NASA.[26] This technique produced highly crystalline, very long and small-diameter BNNTs in the absence of any catalysts. It involves the force condensation of an ascending plume of pure boron vapor, which was produced by a targeted heating using a laser. These boron vapors at an elevated ambient pressure, typically 20 times higher than atmospheric pressure, was allowed to react with the surrounding high-pressure nitrogen gas in the chamber. As a result, the strong buoyancy force was generated due to the density difference between boron vapors (over 4000˚C) and nitrogen gas maintained at room temperature. The boron droplets from a cooled metallic wire which acts as a condenser in a chamber, will eventually be collided with the supplied nitrogen gas molecules to help grew BNNTs in a form of cotton like shaped raw material. This raw BNNT material (Figure 2.2) is stabilized into a puffball shaped with a bundled, and interlocked network of nanotubes along with the presence of unwanted non-nanotubes impurities.[43], [44] Some of the impurities include elemental boron, oxides of boron, boron nitride cages and hBN nanostructures. In fact, the gray color of the raw material was due to the presence of boron impurities.[44], [45] Subsequently, several refinements have been carried out on BNNTs by both commercial companies and research groups to obtain the raw material with improved purity. While techniques to purify elemental boron from

the as-synthesized material were known, but the selective removal of hBN from BNNTs is challenging due to their chemical similarities.[45], [46] More recently, Marincel et al. reported the wet-thermal etching technique, which utilizes the presence of defect sites on the surface of hBN nanosheets to selectively purify from BNNTs at a low temperature of 715 ˚C, despite their chemical similarities.[43] A maximum yield of 10 wt. % of pure BNNTs was reported while showing that BNNT defect sites can withstand to damage during purification.[43] Nevertheless, the production of pristine BNNTs especially in large quantities with high purity and small diameters during the synthesis still remains challenging and negatively impacts the potential technological developments and applications.[42],[43] Therefore, the process optimization coupled with the controlled arrangement of boron and nitrogen sources in the reaction chamber could potentially improve the BNNT quality in the as-synthesized raw BNNT material.

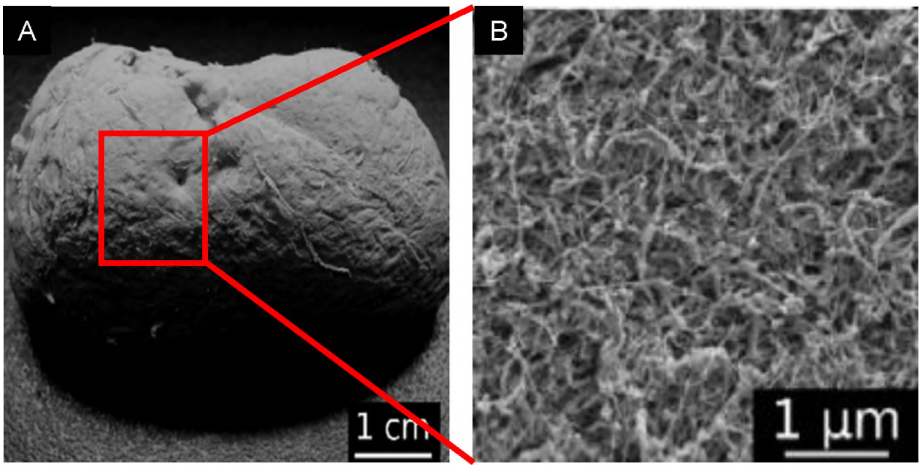

Figure 2.2. SEM of as-synthesized raw BNNT material. [reproduced from ref.[43]]

2.2. Hexagonal Boron Nitride Nanosheets

Two-dimensional hexagonal boron nitride nanosheets (hBN), also often referred as 'white graphene' powder or "non-carbon graphene" because of its white color. These sheets can be mono- to several layers thick with an alternating B and N atoms in a

honeycomb BN lattice structure (Figure 2.3A).[48] However, it has been challenging practically to produce single-layered planar monoatomic hBN nanosheets, unlike graphene, as the interaction caused by van der Waals forces among BN layers are much stronger. As a result, studies involving monoatomic BN graphene-like layers have been limited.[49]–[51] Figure 2.3B shows the representative TEM image of hBN displaying several nanosheets with a heavily stacked structure in different orientations.[52] These hBN nanosheets possess a high Young's modulus (865 GPa),[53] that is four times higher than that of steel by itself and a measured thermal conductivity of 600 W m^{-1} K^{-1} for a single-layer hBN nanosheet, which decreases as the count of hBN layers increases.[54] They have a wide energy band gap of 5.9 eV, very high chemical, mechanical, and thermal stabilities.[51],[52] These advantages make BN a promising material for application developments in various fields including next generation polymer matrix composites,[57] hydrogen storage,[58] field emitters,[59] neutron capture,[60] electrocatalysts,[61] sorbents,[62] and cosmetic sunscreens.[63], [64]

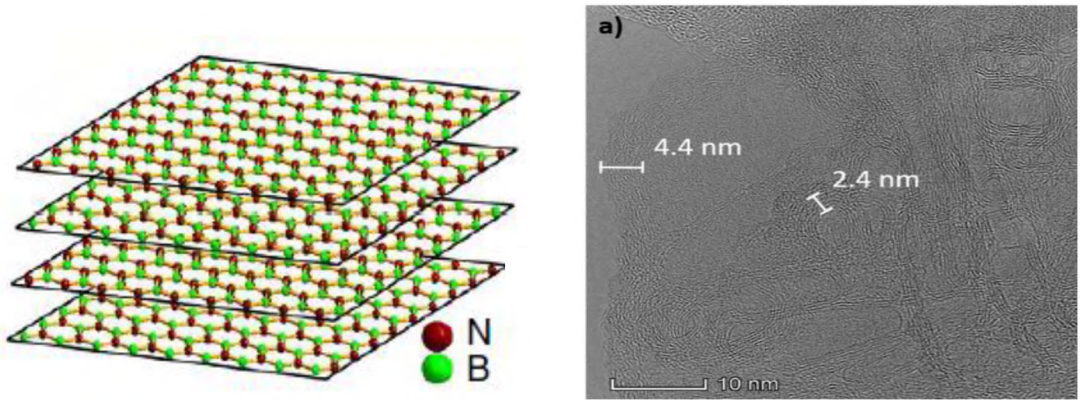

Figure 2.3. (A) The structural model of a multi-layered hexagonal boron nitride nanosheets representing the alternating boron and nitrogen in green and red, respectively. [reproduced from ref. [48]] (B) TEM image of several-layered hBN representing multiple randomly oriented stacked sheets. [reproduced from ref. [52]]

Several synthesis techniques have been reported previously to produce high-quality hBN nanosheets. Some of the techniques include chemical vapor deposition,[65] plasma arc method,[66] laser ablation,[67], [68] and plasma-enhanced pulsed laser deposition.[69] For instance, in a CVD technique, which was previously employed to grow BNNTs, a volatile precursor such as borazine ($B_3H_6N_3$), are typically subjected to interact on the surface of a substrate in the presence of catalysts such as Ni_2B particles that are maintained at temperatures of 1100 °C to condense the desired hBN as-synthesized material.[65] On the other hand, researchers have utilized a combination of multiple precursors including BF_3-NH_3, BCl_3-NH_3, and B_2H_6-NH_3 to grow hBN thin films on a metallic substrates like Ni (111) for deposition of hBN nanomaterials.[70] Some of the advantages this technique generally offers are minimal energetic cost, greater purity, and scalability. Whereas the latter synthesis techniques usually utilize high energy input of up to 2000 °C and these are not studied as extensively as the techniques discussed before.

2.3. Dispersions of Boron Nitride Nanomaterials

In spite of these amazing properties and possible applications, the real applications of BN nanomaterials are greatly hindered by a lack of high-quality dispersions. Also, the structural factors including purity, diameter, defects that are directly associated with the synthesis process is problematic, which would negatively impact the final properties, functionalities of large area assemblies and interfacial quality of polymer composites. Liquid phase processing of BN nanomaterials including 1D BNNTs and 2D hBN nanosheets that are used in this work, is a promising approach to effectively translate fascinating properties of individual BN nanomaterials into macroscopic assembled materials for application developments. However, liquid phase processing is limited by

poor dispersibility of nanomaterials in almost any solvent medium due to the strong van der Waals interactions and high surface energy of BN nanomaterials. In fact, BN nanomaterials have significantly higher chemical inertness compared to well-known graphitic materials, as the peculiar stacking sequence of monoatomic layers of BN nanomaterials lead to the "lip-lip" interactions among the BN layers.[71], [72] More importantly, due to the difference in electronegativity between B and N, the covalent BN bonds are partially ionic, unlike carbon-carbon bonding in graphene polymorphs, which makes them tougher to chemically modify.[73] In the literature, there have been several successful studies that are reported on surface functionalization and exfoliation of BN nanomaterials. Some of the approaches include covalent functionalization, non-covalent complexation and solid-state surface functionalization including ball milling, plasma-assisted and thermal treatment methods, which will be discussed further in detailed in the following sections.

2.3.1. *Solid-state surface functionalization*

First, via thermal treatment,[68],[69] BN nanomaterials are subjected to elevated temperatures up to 1000 °C in the presence of air in a furnace to introduce hydroxyl (-OH) groups by generating defect sites on edges or surface of nanomaterials. The resulting hydroxylated BN nanomaterials are dispersed in a desired solvent to produce stable dispersions of nanomaterials. However, this technique typically produces byproducts in the form of oxides of boron such as B_2O_3 post heat-treatment, resulting in inhibiting the dispersion yield of hydroxylated BN nanomaterials. In addition, although the thermal treatment minimizes the usage of solvents that are often toxic and corrosive, the limitations

are nevertheless be considered, as they utilize high-energetic cost, and it is solely capable of oxidizing nanomaterials.

Secondly, high-energy radiation including plasma, X-ray, and electron beam, have been often conducted by altering both chemical and physical structures of nanomaterials. This technique was previously used by researchers for a precise targeted surface functionalization of hBN nanomaterials. This induce covalent bonds at the active sites or the attack of reactive species via Lewis acid-base interactions on B and N atoms with a tunable parameters.[76]–[78] It offers several advantages including a significantly lower reaction time, utilization of diversified functional groups, nondestructive surface morphology.

Third, ball-milling treatment, which was predominantly used for exfoliation of hBN nanosheets relative to BNNTs, involves the mechanical force to break down highly crystalline hBN nanosheets while generating disorders or defect sites on the surface of BN. Here, the treatment time with ball milling was reported to be directly proportional to the extent of chemical reactivity of hBN nanosheets.[79] In order to fabricate applications, an additional step of further modification of treated hBN powders is typically required. For example, Lei et al. reported a urea-assisted exfoliation of water-soluble hBN nanosheets through a solid-state ball milling technique, resulting in a stable hBN dispersions of concentrations as high as 30 mg/mL (Figure 2.4).[48] These dispersions with few-layer hBN nanosheets were later used to fabricate the low density aerogels and freestanding thin-film membranes through a cryo-drying and filtration techniques, respectively.[48]

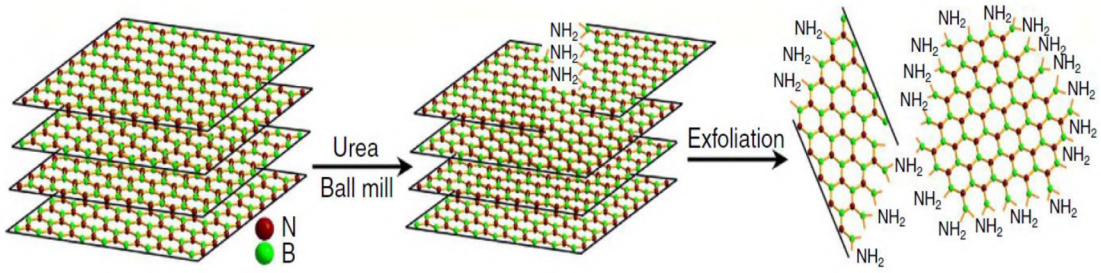

Figure 2.4. The schematic showing the production of few-layer hBN based on urea-assisted solid-state surface functionalization. [reproduced from ref.[48]]

2.3.2. *Covalent functionalization*

Covalent functionalization, one of the most widely studied chemical modification technique to help disperse both graphitic and BN nanomaterials. This utilizes functional groups that can create new bonds on the surface of nanomaterials. Here, the BN structure is generally functionalized covalently by adding two similar or different groups to a neighboring B-N bonds on the basal plane sites. The generated novel bonds are always expected to be at an even number to satisfy the overall charge when functional groups form bonds as the BN conjugated π bonds are opened.[80], [81]

Due to intrinsic partial ionic nature of a B-N bond, B and N atoms are partially positive and negative charged, respectively. This enables BN materials to be interactive with both nucleophilic and electrophilic groups. Most covalent modification procedures consist of two steps. Firstly, hBN are modified to introduce a variety of chemical groups including hydroxyl,[76], [82]–[84] amino,[85], [86] amine,[87], [88] alkyl,[89], [90] acyl,[91] halogen groups[92] on BN surfaces. Secondly, these one-step functionalized BNs can be directly utilized in many applications, at the same time, can be further modified to decorate more functional groups to engineer into desired properties. Researchers reported a multi-step reaction by utilizing a oxosilane to interact with the hydroxylated BNNTs

followed by a grafting of polyhedral oligosilsesquioxane structures.[93] In addition, researchers reported hydroxylated BNNTs and hBN nanosheets that are being used as precursors for further alteration by perfluorobutyric acid ($CF_3CF_2CF_2COOH$) or thioglycolic acid ($HSCH_2COOH$).[82],[84] However, this often required highly corrosive oxidants such as concentrated acids. While the high temperature and pressure conditions utilized in these techniques to chemically modify BN surfaces would negatively impact the intrinsic properties of nanomaterials.

Studies over the past few decades showed that a facile and effective covalent functionalization can be accomplished via the direct surface modification on BN network by chemical reduction. The covalent alkylation of reduced BNNTs was reported using 1-bromohexane (Figure 2.5).[90] BNNTs were in this case mixed in sodium napthalide/tetrahydrofuran solution in the presence of argon gas to enable chemical reduction.[90] Then, 1-bromohexane was added to the reduced BNNTs as a precursor and mixed for 48 hours for alkylation. More recently, Marti et al. reported BNNTs that are covalently functionalized by dodecyl chains via Billups-Birch reaction utilizing reagents of lithium and 1-bromododecane.[94] This study revealed the existence of alkyl chains on the surface of BNNTs. As a result, this led to increased efficiency of dispersions in different solvents.[94] A similar strategy was also reported for dispersing hBN nanosheets, where the highest chemical modification was achieved at a 1:20 BN/Lithium as demonstrated by thermogravimetric analysis and spectroscopic measurements.[52] However, these covalent modification techniques involve the usage of strong reducing and oxidation conditions, which will hinder the novel physiochemical functions and achieving nondestructive pristine physical structure, as this enables the major alteration of its properties.

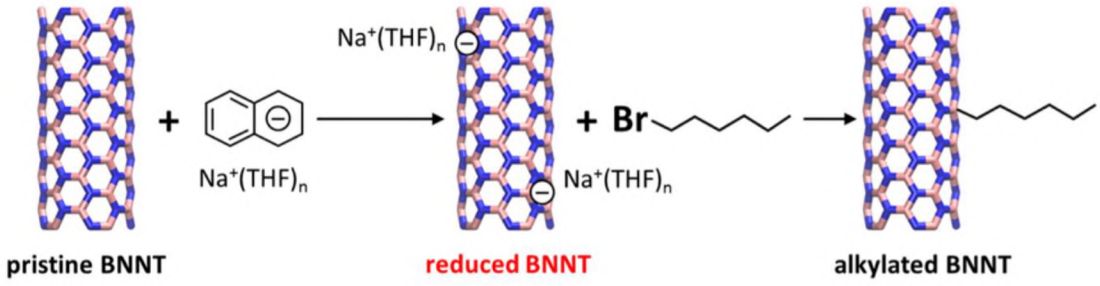

Figure 2.5. The schematic illustration of 1-bromohexane assisted-covalent alkylation of BNNTs through chemical reduction. [reproduced from ref.[90]]

2.3.3. *Noncovalent complexation*

In contrast, non-covalent modification technique does not substantially alter the properties of the nanomaterials structure. This technique has been explored by many researchers as this can widen up dispersing a broader range of nanomaterials including graphene structures, BNNTs and hBN nanosheets, using several dispersant molecules in both volatile and nonvolatile solvents.[84], [95], [96] This technique not only induces diversity in usage of dispersant molecules via attaching different alien molecules to the sidewall of nanotubes, but also preserves the intrinsic properties of nanomaterials. In general, these dispersant molecules would wrap around or interact with the sidewall of BN nanomaterials based on weak inter-molecular interactions including $\pi - \pi$ stacking,[97] cation- π interactions[98] and hydrogen bonds.[99] In most cases, these processes are regarded to be reversible as the bonding between dispersant molecules and hBN nanomaterials is usually is much weaker as that in covalent functionalization, retrieving pristine nanotube surface.

Over a decade, various surfactants,[100]–[102] aromatic molecules,[103] polymers[104]–[106] and biomolecules such as DNA,[35], [107] peptides,[108] and polysaccharides[109] have been utilized to disperse BN nanomaterials through

noncovalent complexation in common aqueous and cosolvents. The noncovalent functionalization of BNNTs with π -conjugated polymer of poly [*m*-phenylenevinylene-co-(2, 5-dioctoxy-*p*-phenylenevinylene)] (PmPV) was first confirmed by Zhi et al.[110] Thereafter, several synthetic and water soluble polymers such as poly(xylydiene tetrahydrothiophene), poly(sodium styrene sulfonate), poly(sodium vinyl sulfonate), and poly(sodium acrylate), were used for dispersing BNNTs through strong $\pi - \pi$ interactions in aqueous medium using a simple sonication technique.[111] However, these synthetic polymers are expensive and required precise synthesis techniques. Moreover, the dispersions in water as a solvent is preferred in many biological applications, but only a few studies have been reported to dispersing BNNTs in aqueous phase. More recently, Marti et al. reported the dispersions of BNNTs in aqueous solutions of both nonionic and ionic surfactants.[112] Although all surfactants produce individualized BNNTs, they reported that high molecular weight nonionic surfactants resulted in the higher dispersion yield of BNNTs, while ionic surfactants assisted in eliminating the majority of hBN impurities. Even more recently, a similar dispersion strategy was used by the same research group to disperse hBN nanosheets by both nonionic and ionic surfactants in aqueous solution.[113] It was reported that large-molecular weight nonionic surfactants tend to disperse hBN at high concentrations with the assistance of low centrifugal force. In contrast, ionic surfactants tend to produce high dispersion yield samples of hBN aided by high centrifugal force while maintaining high dispersion stability.

On the other hand, researchers also explored alternative approaches to noncovalently functionalize surfaces of BN nanomaterials solely based on the interactions of strong physical adsorption of acid molecules via $\pi - \pi$ stacking. For instance, Okamoto

et al. reported noncovalently functionalized hBN nanosheets with a maximum dispersion yield of ~25% in strong acids such as chlorosulfonic acid (CSA) using sonication.[114] They observed a significant increase in in- and through-plane thermal conductivities of noncovalently functionalized hBN nanosheets as high as 10 W m^{-1} K^{-1} in thermoplastic polymer composite films that are fabricated via a simple wet-process. More recently, Zhao et al. reported an ultrahigh in-plane thermal conductivity of 70.3 W m^{-1} K^{-1} for free-standing composite PVA films of tannic acid-functionalized hBN nanosheets that are exfoliated using sonication, resulted in the dispersion yield of ≈ 42 % (Figure 2.6).[115] Similarly, CSA has been used by Talmon et al. and Pasquali et al. for a spontaneous dissolution of BNNTs into disentangled individually dispersed nanotubes without sonication or use of dispersant agents.[116], [117] Later, these extracted BNNTs were processed into macroscopic assemblies including thin films, gels and aerogels.

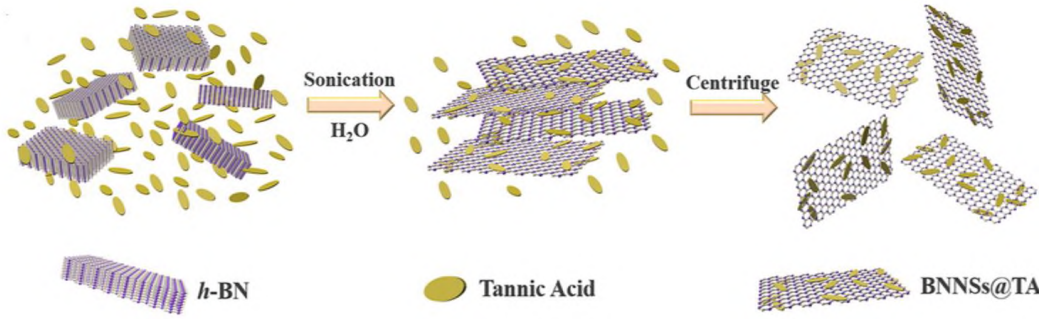

Figure 2.6. The schematic representation of noncovalent complexation of hBN nanosheets by tannic acid in water. [reproduced from ref.[115]

Over the years, many biomolecules have been used as dispersing agents for noncovalent complexation of CNTs. Some of them are peptides, proteins, DNAs, saccharides, and lipids. Serizawa et al. reported the flavin mononucleotide, which is a phosphorylated derivative of vitamin B2, functionalized BNNTs exfoliated under a mild sonication for 3 hours at 20 °C in water (Figure 2.7).[118] Studies revealed the presence of

strong $\pi - \pi$ interactions between dispersant molecules and BNNTs hybrids, which were reported to be highly fluorescent and can be potentially used for visible-light emitters applications.[118] Lee et al. reported the lipids assisted functionalization of BNNTs in water, which can be stable up to 3 months.[119] Despite the chemical similarities of BN nanomaterials, many biomolecules are expected to be similarly efficient for dispersing and functionalizing of both BNNTs and hBN nanosheets. However, the interactions between these biomolecules and BN materials are very complicated and yet to be fully understood. Several molecular dynamic simulation studies have been reported to understand the structural dynamics, solvation and interaction phenomena of DNA biomolecules on the sidewall of BNNTs and hBN nanosheets.[107], [120]

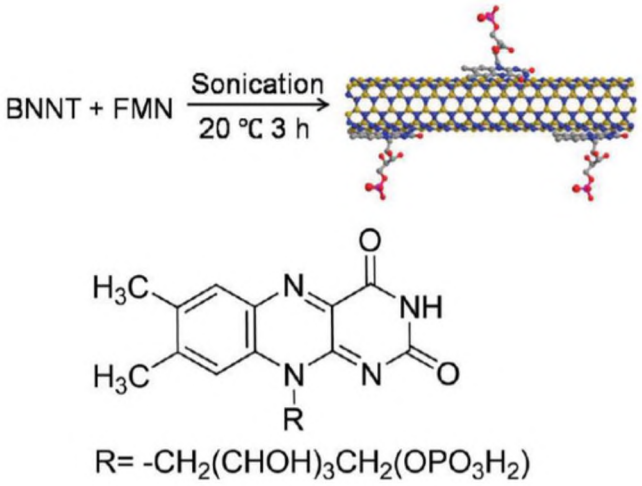

Figure 2.7. The formation process of BNNTs wrapped by flavin mononucleotide. [reproduced from ref.[118]]

2.4. Noncovalent Complexation of Boron Nitride Nanotubes by DNA

Among all, the biomolecule DNA, nature's most important building block has been widely studied for the application developments of nanomaterials like CNTs due to its advantageous properties including potential enhanced biocompatibility, green chemistry and multifunctionality.[23], [24], [121] In addition, understanding the interactions of

BNNTs and biopolymer DNA is essential to explore other biomolecules and polymers to better manipulate BNNTs in future work. For instance, single-stranded DNA (ssDNA) has emerged as a sequence controlled biopolymer of choice to effectively sort chirality-defined SWCNTs.[22], [122] DNA is composed of repeating units of nucleotides (A,T,G,C) with nitrogen containing aromatic bases, a negatively charged phosphate-sugar DNA backbone. Theoretically, the dispersion mechanism of BNNTs interacting with short single nucleotide repeats revealed the formation of DNA wrapping structure on BNNTs *via* $\pi - \pi$ stacking of hydrophobic DNA nucleotide bases and the hydrophobic surface of an aromatic BNNT as shown in Figure 2.7.[120] Furthermore, DNA-BNNT hybrids are stabilized by electrostatic interactions due to the charge-carrying phosphate-sugar DNA backbone that is exposed in the aqueous environment. This allows BNNTs to remain individually dispersed in aqueous environments.

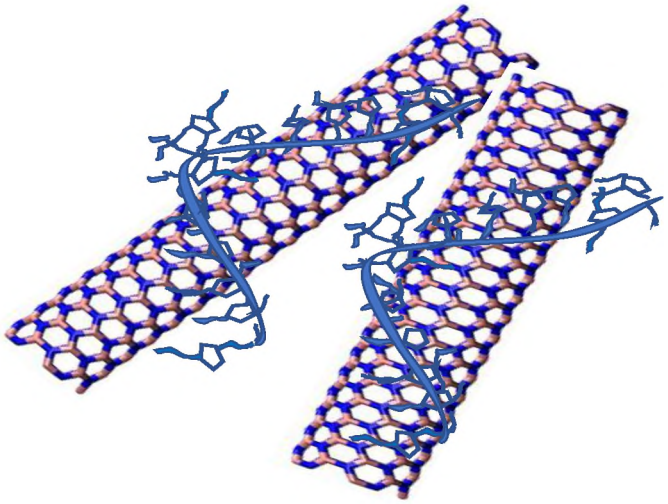

Figure 2.8. The schematic representation showing the noncovalent complexation of single-stranded DNA sequence on the surface of BNNT. [reproduced from ref.[120]]

Zhi et al. reported denatured salmon DNA and thiol-modified short single-stranded DNA of 27-mer to disperse multi-wall boron nitride nanotubes with an average diameter

of ≈ 50 nm in water.[35] A thermogravimetric analysis suggested that 20 wt% DNA were wrapped around the surface of BNNTs, yielding 0.2 wt% BNNTs using a single-stranded DNA at optimized experimental conditions. A clear shift was identified in spectroscopic measurements of BNNTs and DNA, indicating the presence of strong π-π stacking interactions of BNNT and DNA. They attempted to assemble them *via* filtering DNA-BNNT dispersions through a filter sheet and the resulting DNA-BNNT mat was dried for characterization. However, there were still several unsolved problems and drawbacks in that work. The DNA-BNNT hybrid started to aggregate as the concentration increased. The purification of DNA-BNNT dispersions was not reported. The dried mat of DNA-BNNTs showed a locally orientated but globally isotropic morphology of BNNTs with impurities on a smaller length scale of $< 3\ \mu m$. The orientated morphology only consisted of a few DNA-BNNT bundles. In addition, the authors suggested that a nematic ordering of BNNT ensembles observed for the dried mat could correlate to the formation of a nematic liquid crystal phase during filtration. The orientated morphology only consisted of a few DNA-BNNT bundles. In addition, the authors suggested that a nematic ordering of BNNT ensembles observed for the dried mat could correlate to the formation of a nematic liquid crystal phase during filtration. This is problematic as the DNA-BNNT hybrids were not stable in water at higher than 0.2 wt% BNNTs, which is more than an order of magnitude lower than the critical concentration for forming a liquid crystalline phase from rodlike BNNTs with the given aspect ratio of ≈ 20-60. Moreover, it was not clear whether the BNNT assembly was mediated by DNA or was simply due to the aggregation of BNNTs.

2.5. Rheology of Fluid Dispersed Brownian Rods in Dilute Regime

Rheometer is a powerful tool that can study the deformation and flow behavior of all kinds of materials as a function of rate or frequency of deformation. It translates the rheometer parameters into the material parameters by considering the predefined sample shape or flow field. For liquids, it imposes a shearing flow in a liquid and measures the resulting stresses acting on a surface per unit area, parallel to the direction of fluid flow, or alternatively, impose the shear stress and measure the resulting shear rate. This phenomenon can be illustrated by considering a simple Sliding-Plate-Model or Parallel-Plate-Model as shown in the Figure 2.8. The shear stress (τ) is defined as the force (F) acting on the upper plate over a shear area A, resulting in a deflection of *s*. Shear rate ($\dot{\gamma}$) is defined the velocity (v) of moving plate due to applied force F, divided by the gap (h) between two plates. Here, the lower plate is held stationary ($v = 0$). Therefore, $\dot{\gamma} = v/h$. The shear viscosity η, is then defined as $\tau/\dot{\gamma}$. After a steady shearing flow has been imposed on a liquid for a certain period, along the coordinate direction (x_1), the shear stress often attains a steady state $\tau(\dot{\gamma})$ while the velocity varying perpendicular in a direction of coordinate (x_2). Then the steady-state shear viscosity $\eta(\dot{\gamma})$ is defined as $\tau(\dot{\gamma})/\dot{\gamma}$

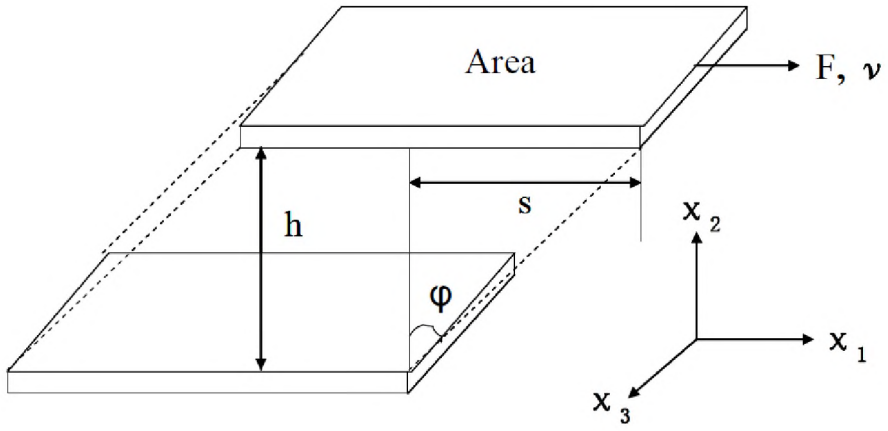

Figure 2.9. The Sliding-Plate-Model illustrating a simple shear test with relative coordinate system.

A reliable characterization of aspect ratio (length-to-diameter) of rodlike molecules dispersed in fluids is important for a precise quantification of final mechanical, thermal, electrical properties of BNNT macroscopic assemblies and nanocomposites. This can be accomplished using a method based on measuring the viscosity of a macroscopic sample of dilute suspended rods, which was previously reported to determine the apparent lengths of nanorods.[123], [124] However, applicability of this rheological method to new systems such as BNNTs requires Brownian rigid rod behavior or the collapse of viscosity versus shear rate curves from samples of different concentrations onto a single master curve (Figure 2.9).[123] BNNTs being a rodlike 1-D tubular nanostructures with a high length-to diameter ratio (L/D), they have a greater tendency to behave as Brownian rigid rods in dilute region. A more recent study on real-time visualization and dynamics of BNNTs undergoing Brownian motion showed that 3.6 μm long BNNTs behaved as ideal rigid rods, yielding a persistence length of ≈ 7 mm that is 100-fold higher than the SWCNT.[125] Previously, dilute dispersions of SWCNTs in superacid of an average aspect ratio ≈ 500

exhibited a Brownian behavior.[126] However, the Brownian behavior of SWCNTs dispersed in dsDNA solution was not observed.[127] This could be attributed due to the presence of excess amounts of semiflexible dsDNA in the dispersions as well as the limitations of rheological measurements in the lower shear rate region. For instance, Wierenga et al. characterized the aspect ratio of CNTs using a similar viscosity method.[128] In addition, Boluk et al. determined the aspect ratio of cellulose nanocrystals, as this was a reliable and simple method to estimate the aspect ratios of cellulose nanocrystals.[129] However, applicability of this rheological method to new systems such as BNNTs requires Brownian rigid rod behavior in dilute regime. In general, the Brownian motion of rods is induced by the random fluctuation of the solvent molecules. In the dilute region, rods should be able to rotate or translate freely and without being influenced by the neighboring rods. In addition, Doi-Edwards's theory (1986) stated that the volume, a single long rod can sweep out by rotation about its center of mass must be large (around L^3). For instance, in the dilute region, the concentration range of dsDNA-stabilized SWCNTs of an average aspect ratio 600 in supernatant dispersions was reported as $\leq$ 912 ppm.[127] However, it was much higher than the concentration range of SWCNTs in superacid which was $\leq$ 94 ppm.[126]

If the Brownian forces dominate, the relative amount of time the rods take to orient themselves parallelly with the direction of flow field at a given shear rate is significantly higher. This results in the least influence on viscosity of a fluid in dilute regime.[130] At high enough shear, the viscosity of rods decreases with shear rate as the rods orient and therefore results in a shear thinning behavior.

The rate at which a rod reorients by Brownian motion in dilute solution can be calculated using the rotary diffusivity of the particle D_{ro}. The rotary diffusivity of a rod is given as

$$D_{ro} = \frac{3\kappa_B T(\ln\left(\frac{L}{D}\right)-0.8)}{\pi\eta_s L^3} \quad (1)$$

Where η_s is solvent viscosity, κ_B is Boltzmann's constant, L is length, D is diameter, and T is temperature.

The zero-shear viscosity, η_O, as given in equation 2, of Brownian rigid rods in a dilute dispersion can be expressed as sum of solvent viscosity and viscosity contribution from the suspended rods.

$$\eta_O \equiv \lim_{\dot{\gamma}\to 0}\eta\left(\dot{\gamma}\right) = \eta_s\left(1+\frac{4}{5}\kappa_B T\tau_{rot}\nu\right) \quad (2)$$

Where, $\tau_{rot} \equiv \xi L^3/(72\kappa_B T)$ is the rod rotational relaxation time, and ξ is the perpendicular drag coefficient. The number concentration of rods is given in terms of the volume fraction ϕ as $\nu \equiv \phi/(\pi R^2 L)$.

The perpendicular drag coefficient ξ on a slender cylinder is $\xi = 4\eta_s\varepsilon f(\varepsilon)$. Where, $\varepsilon = \frac{1}{ln(L/R)}$ and $f(\varepsilon) = \frac{1+0.64\varepsilon}{1-1.5\varepsilon} + 1.659\varepsilon^2$

By substituting the above expressions, yields the Kirkwood-Auer-Batchelor (KAB) relationship:

$$[\eta] \equiv \lim_{\phi\to 0}\frac{\eta_0-\eta_s}{\eta_s\phi} = \frac{2\ (L/R)^2}{45\ [ln\ (L/R)]}\left[\left(\frac{1+\frac{0.64}{ln\ (L/R)}}{1-\frac{1.5}{ln\ (L/R)}}\right)+\frac{1.659}{(ln\ (L/R))^2}\right] \quad (3)$$

Kirkwood and Plock estimated the viscosity of a dilute sample of monodisperse rods in terms of Weissenberg number ($\tau_{rot}\dot{\gamma}$), which is a product of shear rate and rotational relaxation time, and the viscosity over viscosity at vanishingly low shear rates,

i.e., (η/η_0). It is noted that the rods contribution to the viscosity falls within the power law coefficient with a terminal slope of -0.5. For monodisperse dilute rods, the shear thinning region is expected to start at $\tau_{rot}\dot{\gamma} \approx 0.2$ and that they reach the terminal region at $\tau_{rot}\dot{\gamma} \geq 1$. These results can be represented using the Carreau-Yasuda equation as follows.

$$\eta(\dot{\gamma}) = \eta_s + (\eta_o - \eta_s)[1 + (\lambda\dot{\gamma})^a]^{\frac{n-1}{a}} \quad (4)$$

Where η_s is the solvent viscosity, and η_0 is the zero-shear viscosity of the rods; λ, a, n are fitting parameters: n controls the slope of the viscosity curve at high shear rates, a controls the breadth of the transition from Newtonian behavior to terminal region, and λ controls the onset of shear thinning region.

Here, the intrinsic viscosity as shown in equation 3 is independent of the concentration of nanotubes and dispersants used to prepare dilute dispersions. For example, Parra-Vasquez et al. showed that the SWCNTs from the same batch of synthetic material were dispersed using two different surfactants resulted in the same average aspect ratio of nanotubes in the dilute region.[123] Wu et al. found out that the intrinsic viscosity of cellulose nanocrystals is dependent on surface charge density due to the electric double layers, indicating NaCl concentrations should be optimized to determine the precise length-to-diameter ratio of cellulose nanocrystals.[131] The average aspect ratio can be obtained from the low shear rate plateau of a master curve generated from dilute dispersions of rods at different concentrations. The experimental data of average reduced viscosities $\eta_{red} \equiv \frac{\eta - \eta_s}{\eta_s \phi}$ of rigid Brownian rods are fit to the Carreau-Yasuda model[132] to extract the intrinsic viscosity from low shear rate plateau. With the intrinsic viscosity in hand, the KAB for monodisperse Brownian rods in dilute regime,[123], [133], [134] can be solved for <L/D> to determine the lengths of rods.

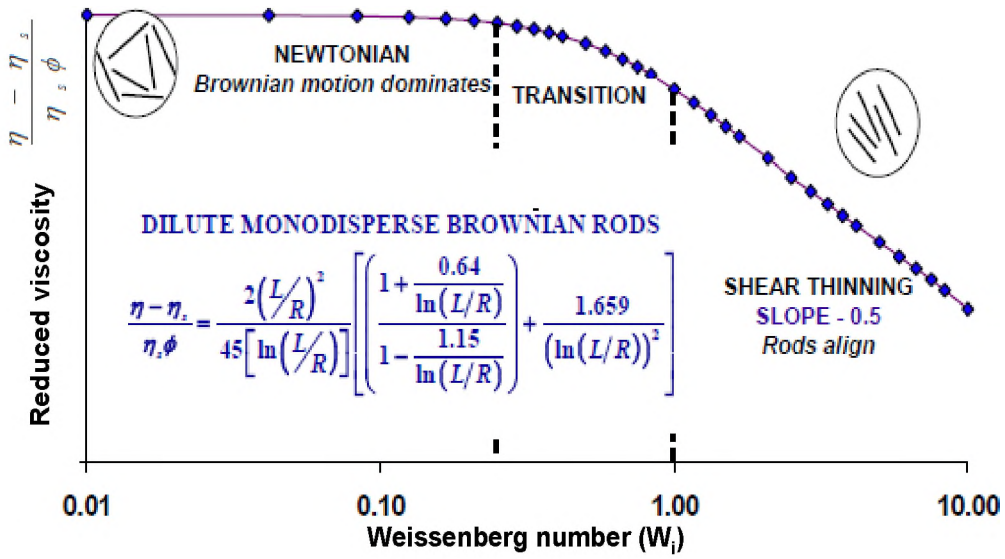

Figure 2.10. The universal shear thinning curve of monodisperse Brownian rigid rods. [reproduced from ref.[123]]

2.6. Bottom-Up Assembly of Boron Nitride Nanotubes

The ability to produce starting dispersion material system with well-defined properties has spurred research interest in the fundamental potential bottom-up assembly for application developments. In this section, the various fabrication techniques that are previously employed for fabricating thin films of nanorods are described. Some of the techniques include spray-coating,[135], [136] dip-coating,[137] spin-coating,[138] and vacuum filtration.[139] Briefly, in a spray-coating method, nanotube dispersions are sprayed onto a heated substrate, allowing the uniformly coated droplet to undergo pyrolytic decomposition on the surface of substrate. Substrates including glass, quartz or silicon wafer are typically being used in this method. In fact, it was reported that substrates could be pre-treated to improve the film properties including conductivity by tuning the adhesion properties of a substrate.[135] This spray-coating technique can produce large area and thick films.

In the dip-coating technique (Figure 2.10a), the substrate is dipped into a dispersion at constant rate and pulled off after a certain amount of time. Here, the thin layer of dispersion will be formed along the surface of substrate after the drying process. The thickness of the film is controlled by many constraints including dispersion viscosity, dipping time, pull-up rate and the interaction between the dispersion and substrate. The dip-coating technique is known for its scalability, minimal need of sophisticated apparatus. For instance, SWCNTs/polyvinyl butyral composite films were fabricated using this simple dip-coating method, where the thickness of the composite films was controlled by optimizing the concentration of precursor dispersions.[137] On the other hand, spin-coating (Figure 2.10b) utilizes the centrifugal force to produce a thin film by spinning the substrate at a certain speed, allowing dispersion to uniformly spread over the substrate to form a thin film. However, quite a few drawbacks exit for this technique that limits the large-scale coating and lacks material efficiency.

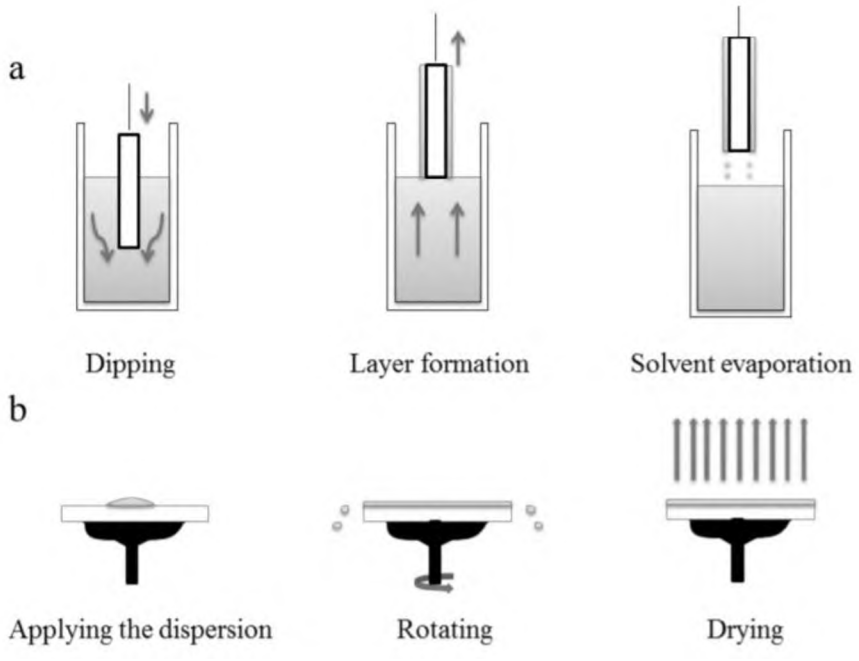

Figure 2.11. Schematic representation of thin film fabrication using (a) dip-coating (b) spin-coating. [reproduced from ref.[140]]

Vacuum filtration utilizes the pressure gradient between Buchner funnel, where the dispersions can pass through the filter to separate retentate and permeate. Later, the thin film formed is then peeled off from the filter paper after the drying process. This technique was previously used to fabricate the BNNT buckypapers from purified dispersions of BNNTs in methanol via vacuum filtration through a polycarbonate membrane of 20 μm pore size.[141] The resulting films were peeled off from membrane filtration and further dried at elevated temperatures. However, this technique produces relatively thick films, thus may not be preferred for certain applications. Especially, the alignment of nanorods in films is considered to be an important factor to obtain large area assemblies with improved properties, which has been demonstrated extensively for aligned films and fibers produced from lyotropic LCs of carbon nanotubes,[142]–[144] CdSe nanorods,[145] silver nanorods.[146] For instance, macroscopic films were obtained by spreading cholesteric double-stranded DNA/SWCNT dispersions of concentration 2 vol.% onto copper tape by roller coating.[144] This resulted in 20 μm translucent thick films post drying exhibiting typical birefringence that are unique to lyotropic liquid crystals when rotated at different angles under cross polarizers. Interestingly smooth surface morphology of SWCNTs films was observed, which could be due to the uniform coatings of DNA. More recently, the assembly of BNNTs into macroscale articles via solution processing with chlorosulfonic acid was reported (Figure 2.11).[116] Later, these stable nanotubes were fabricated into BNNT films and mats of thickness 1-1.5 μm by filtering the high concentrated supernatant of BNNTs and transferred to perfluoro alkoxy substrates which were peeled off with tweezers to test under SEM.[116] In addition, BNNTs with a mass concentration of 2000 ppm were fabricated into 1 cm^3 steel mesh cages to produce 1 cm x 1 cm x 1 cm aerogels

by coagulating in cold ether. However, the individually dispersed BNNTs were not aligned in a self-standing film which limit the benefits of incorporating the inherent properties of nanotubes in the final product.

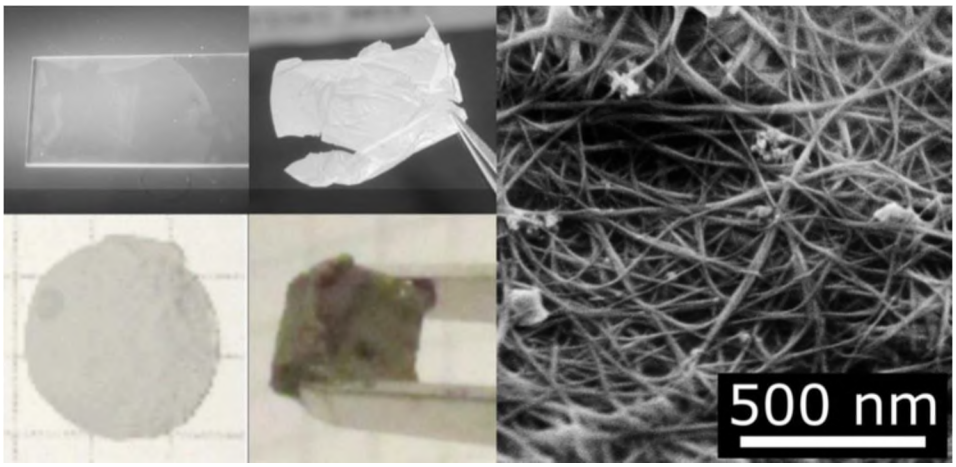

Figure 2.12. Macroscopic assemblies of BNNTs in chlorosulfonic acid including thin film, freestanding 1-1.5 μm film, 2.5 cm diameter mat, 1 cm x 1 cm x 1 cm aerogel. [reproduced from ref.[116]]

In this study, we used a simple drop casting technique as shown in Figure 2.12, to produce aligned films of BNNTs stabilized by DNA. 2 μL of highly concentrated purified BNNT dispersion is deposited on to a substrate such as silicon wafer, allowing it to dry and scribed to see the alignment of nanotubes underside the film. This offers advantages including a minimal utilization of sophisticated apparatus and lower volume of samples.

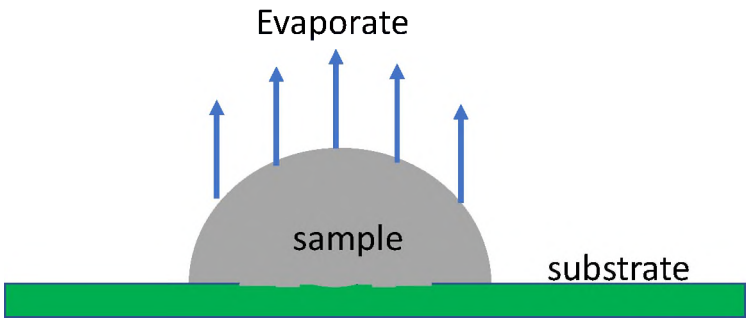

Figure 2.13. Schematic representation of a drop casting method on the substrate.

CHAPTER III

PURIFICATION AND ASSEMBLY OF DNA-STABILIZED BORON NITRIDE NANOTUBES INTO ALIGNED FILMS

This chapter is a reprint of the paper, "Purification and Assembly of DNA-Stabilized Boron Nitride Nanotubes into Aligned Films", published in *ACS Applied Nano Materials* **2019**, 2(4), 2099-2105

3.1. Introduction

Boron nitride nanotubes (BNNTs) have promising optical,[147] mechanical,[148] and thermal properties[34] for developing thermal interface material and electronic and optoelectronic applications.[149]–[151] Recent advances in high-throughput synthesis of BNNTs have led to growing effort in scalable processing solution for making macroscopic assemblies of BNNTs.[26], [141],[142] The one-dimensionality and symmetry restrictions in high-aspect-ratio BNNTs, resembling that of carbon nanotubes, render new structural characteristics and unique properties that are not available in many existing nanomaterials.[25] Compared to electronic structures of single-wall carbon nanotubes (SWCNTs), which can be metals, quasi-metals, or semiconductors,[27] BNNTs with diameters larger than 1.2 nm behave as wide bandgap semiconductors independent of wall number and chirality.[37] In addition, BNNTs are stable under air oxidation up to 900 °C[34] and have optical absorbance and fluorescence features in the ultraviolet range.[35]

These distinct properties make BNNTs one of the most promising material candidate for producing multifunctional, protective films with remarkable thermal and chemical stabilities and ultraviolet radiation shielding.[25]

The effective translation of unique properties of individual BNNTs into macroscopic assemblies requires a starting material with well-defined properties. Current scalable synthesis of BNNTs *via* a high-temperature-pressure (HTP) process[6,][153] typically produces a mixture of few-wall BNNTs and large percentages of non-nanotube impurities, such as elemental boron, boron oxide (B_2O_3), and hexagonal boron nitride (*h*-BN) structures such as nanosheets and nanoshells.[47] The post synthesis purification of BNNTs has been previously performed using acid and heat treatments, however, those techniques are mainly focused on the selective removal of elemental boron.[153] The alignment of nanotubes is also considered as an important factor to obtain assembled solid materials with improved properties, which has been demonstrated extensively for aligned films and fibers produced from carbon nanotubes.[142] In order to purify and align BNNTs through liquid phase processing as demonstrated in this work, a prerequisite is to obtain nanotubes in an individually dispersed state in a liquid medium.

To date, various surfactants,[100], [112] aromatic molecules,[103] biomolecules,[154] including DNA,[35] and other polymers[104] have been utilized to disperse BNNTs through noncovalent complexation in an aqueous environment. BNNTs that are noncovalently complexed with single-stranded DNA (DNA-BNNTs) are of particular interest. Single-stranded DNA (ssDNA) has emerged as a sequence controlled biopolymer of choice to effectively sort chirality-defined SWCNTs[22] and enable controlled assembly and technological applications of SWCNTs with enhanced

biocompatibility.[23], [24] The interactions of single-wall BNNTs and short ssDNA revealed theoretically the wrapping conformation of DNA on the BNNT, resembling that of a DNA-SWCNT hybrid, *via* $\pi - \pi$ stacking of hydrophobic DNA nucleotide bases and the hydrophobic surface of an aromatic BNNT.[120] Furthermore, DNA-BNNT hybrids are stabilized by electrostatic interactions due to the charge-carrying phosphate-sugar DNA backbone that is exposed in the aqueous environment. The adsorption of DNA on BNNTs is dominated by the van der Waals interaction with a minor contribution from the electrostatic interaction as determined by the molecular dynamics simulation.[120] Notably, the ionic nature of the BN bond[25], [37] and few-wall BNNTs[26] used in this study could lead to a drastically different DNA conformation on the surface of BNNTs. In addition, DNA-mediated assembly of a BNNT mat by membrane filtration was reported for multi-wall BNNTs of an average diameter of ≈ 50 nm, however, a uniform dispersion at higher than ≈ 0.2 mass % BNNTs was not obtained due to nanotube aggregations.[35] Understanding the interactions of BNNTs and biopolymer DNA is essential to explore other biomolecules and polymers to better manipulate BNNTs in future work.

Here, we report a systematic study of aqueous dispersion, purification, and self-assembly of BNNTs using DNA. We demonstrated a highly efficient, aqueous dispersion of BNNTs using $(GT)_{20}$ ssDNA and the subsequent removal of non-nanotube impurities from aqueous dispersions of as-synthesized material by a membrane filtration approach. Furthermore, aqueous dispersions of purified DNA-BNNTs remained uniform at a nanotube concentration of as high as ≈ 11.5 mass %, which resulted in aligned BNNT films after solvent evaporation.

3.2. Experimental Section

3.2.1. *Materials*

Boron nitride nanotubes (BNNTs, Puff Ball, lot no: 44171) synthesized by the high-temperature-pressure (HTP) method[153] were purchased from BNNT, LLC. Custom-made DNA was purchased from Integrated DNA Technologies. Sodium chloride (NaCl, Sigma-Aldrich), sodium thiocyanate (NaSCN, Sigma-Aldrich), and polyethylene glycol (PEG, MW 6kDa, Alfa Aesar) were used as received.

3.2.2. *BNNT dispersion and purification by membrane filtration*

For dispersion of BNNTs with a given DNA sequence, a total volume of 1 mL of the DNA and as-synthesized BNNT mixture material in deionized (DI) water with 0.1 M NaCl was bath sonicated at room temperature for 1 h followed by a probe tip ultrasonication with a 2 mm diameter probe in an ice bath for 1 h at a power level of 8 W (model VCX 130, Sonics and Materials, Inc.). The BNNTs/DNA mass ratio was varied from BNNTs:DNA = 1:0 up to 1:6 while keeping the BNNT mixture concentration constant at 1 mg/mL. Bath sonication was used to loosen the BNNT puff balls, while the majority of BNNT materials remained undispersed. After tip sonication, brown colored dispersions were obtained, which are composed of individually dispersed DNA-BNNT hybrids as well as small and large bundles of nanotubes and impurities. However, nanotubes did not disperse in the absence of DNA after tip sonication. To remove large BNNT bundles and undispersed impurities, sonicated samples were centrifuged at 19 °C and 17,000 g in 100 μL aliquots for 90 min. The supernatant was collected and used as a stock DNA-BNNT dispersion. The purification of BNNTs from non-nanotube structures remaining in the supernatant was performed using a membrane filtration method.

Specifically, the stock DNA-BNNT supernatant was purified using a Microcon® centrifugal filter with a molecular weight cutoff (MWCO) of 30 kDa by centrifugation at 19 °C and 17,000 g for 15 min. The leftover sample in the filter was washed with DI water 3 times before re-dispersing in water by vortex mixing. The purification yield of DNA-BNNT hybrids is ≈ 19.6 %. The estimation of the % yield of purified DNA-BNNT hybrids is calculated over the total mass of a synthetic BNNT mixture in the starting material. For improved stability of purified DNA-BNNT dispersion for long-term storage or concentrating to obtain macroscopic films, an additional amount of DNA was added to a final concentration of ≈ 100 μg/mL and bath sonicated at room temperature for 30 min. All BNNTs/DNA ratios of various nanotube dispersions are reported in mass ratios.

3.2.3. *UV-vis absorbance measurements*

The UV-vis absorbance measurements were performed on a Shimadzu UV-2600/Jasco V-760 spectrophotometer over the wavelength range of 185-800 nm using a 10 mm path length quartz cuvette. Absorbance spectra were plotted up to ≈ 400 nm due to the fact that absorption peaks of aqueous dispersion of BNNT synthetic materials were observed in the UV region. Excess DNA not bound to BNNTs was removed from the sample by a precipitation method[155] previously reported for carbon nanotubes to allow for resolution of BNNT absorption features in the UV region. Specifically, final concentrations of 1 M NaSCN and 6 mass % PEG were added to the sample, and the mixture was incubated overnight at 4 °C and then centrifuged at 17000 g for 30 min. After centrifugation, the supernatant was removed, and the pellet was re-dispersed in water by bath sonication for 30 min.

3.2.4. *Thermogravimetric analysis*

The percentage of impurities and thermal stability of a synthetic BNNT material was tested by the thermal gravimetric analyzer (TA instruments Q50 series) by heating a BNNT puff ball up to 1000 °C under dry air at 20 °C/min ramp. The system was equilibrated to reduce the momentum created by the ramping temperature to the successive isothermal step. Isothermal temperatures were maintained at 120 °C and 240 °C for 15 min and at 425 °C for 25 min in order to ensure the maximum removal or oxidation of various components of the synthetic BNNT material, such as a moisture content, elemental boron, and boron oxide (B_2O_3) at critical temperatures.

3.2.5. *Scanning electron microscopy*

High-resolution field emission scanning electron microscope Inspect F50 by FEI, equipped with an Everhart-Thornley detector with variable grid bias was used to characterize dispersed DNA-BNNT hybrids as well as aligned DNA-BNNT films. The gold sputtered silicon wafer substrate was used to image dilute dispersions of DNA-BNNTs. For the densely packed DNA-BNNT films a bare silicon substrate was used instead, which was plasma treated to promote uniform transfer of the films to the substrate. The sample was scribed to reveal the underside of the film. SEM imaging was performed at 5 kV.

3.2.6. *Optical microscopy*

Optical microscopy was performed on an Olympus BX51W1 optical microscope with a Hamamatsu ORCA-R2 digital deep-cooled CCD camera (C10600) using precleaned glass slides and coverslips. Images of dilute and concentrated dispersions of DNA-BNNTs

were taken in transmission with and without cross-polarized light using 20x and 40x objectives.

3.2.7. *Formation of DNA-BNNT films by evaporation*

A total of 20 mL stock DNA-BNNT dispersion was purified by membrane filtration and was concentrated 10 times to obtain a total volume of 2 mL concentrated dispersion. An additional amount of corresponding $(GT)_{20}$ DNA was added to a final concentration of 0.1 mg/mL to maintain the dispersion stability of DNA-BNNTs at higher concentrations of nanotubes. This yields a mass ratio of free DNA:DNA-BNNT hybrids ≈ 1.1:1 in the dispersion. The 2 mL sample vial was placed on a stir table with a rotational speed between 100-150 rpm at room temperature. In addition, the mass of solvent evaporated was tracked to calculate the concentration of DNA-BNNT hybrids. The dried BNNT film was obtained by evaporation of ≈ 11.5 mass % DNA-BNNT dispersion on a plasma treated silicon substrate which was later tested under SEM.

3.3. Results and Discussion

The liquid phase processing including dispersion, purification, and macroscopic assembly of boron nitride nanotubes (BNNTs) is both scientifically interesting and technologically important. Short single-stranded DNA (ssDNA) has been the biopolymer of choice to achieve efficient surface functionalization and assembly of carbon nanotubes, which are structural analogs to BNNTs. Here, we report a systematic study of the aqueous dispersion of DNA-stabilized BNNTs *via* a noncovalent functionalization approach and a first example of self-assembly of individually dispersed BNNTs into aligned films. Using $(GT)_{20}$ ssDNA, we show that the dispersion efficiency of BNNTs in an aqueous environment is dependent on the BNNTs/DNA mass ratio. The surface coating of BNNTs

by DNA creates uniform dispersions at a nanotube concentration of as high as ≈ 11.5 % by mass leading to the formation of aligned BNNT films after solvent evaporation. Our work demonstrates the highly efficient dispersion of BNNTs using DNA, providing a general methodology that may be used to guide the processing of BNNTs using any dispersants for nanotubes, such as surfactants and polymers. In addition, it provides important insights to better understand the interactions between nanotubes and biomolecules and opens new routes for producing BNNT films with potential enhanced biocompatibility as well as controlled morphology and properties.

A systematic approach of processing BNNTs including dispersion, purification, and assembly into solid aligned films was achieved using short ssDNA as a highly efficient dispersant for stabilizing BNNTs in water (Scheme 1).

Scheme 1. Purification and Assembly Processes of DNA-BNNT Hybrids

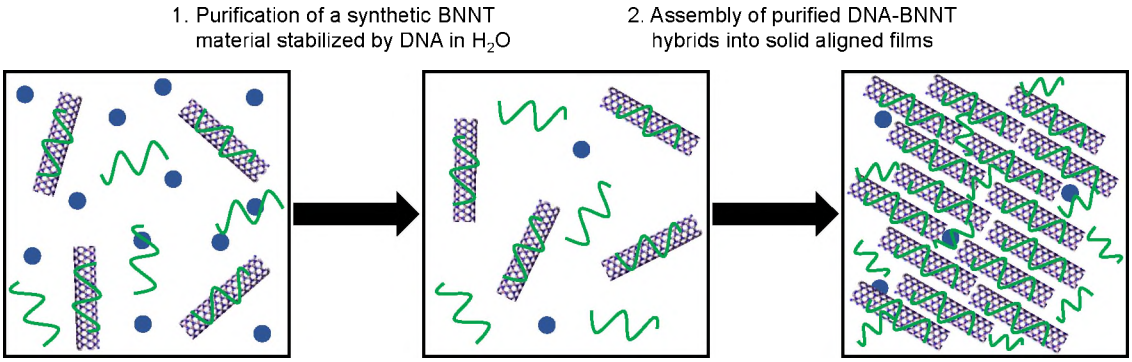

DNA confers a number of advantages including the potential to stabilize nanotubes through $\pi - \pi$ interactions in various solvents such as water and alcohols,[156] assist large area assemblies of nanotubes,[144], [157] and offer green chemistry and multifunctionality. We first examined the capability of DNA to disperse BNNTs individually in an aqueous environment based on its potential for $\pi - \pi$ interactions.[120] In general, under the dispersion condition of BNNTs:DNA = 1:1 by mass, all short DNA

sequences we tested yielded good BNNT dispersions. We compared the dispersion yield of BNNTs by 8-mer single-nucleotide repeats of A_8, C_8, G_8, and T_8, as shown in Figure 3.1A. The BNNT dispersion yield follows the order of $G_8 > C_8 > T_8 > A_8$ based on absorbance values of DNA-BNNT hybrids at 205 nm. The difference in absorbance spectra of G_8-BNNT dispersion between 235 nm and 285 nm compared to that of other DNA-BNNT dispersions could be caused by the formation of G-quadruplexes for G_8 sequence[158] exhibiting different interaction behavior with nanotubes. It may also be possible that G-quadruplexes remain in a dispersion after a precipitation and re-dispersion process. In Figure 3.2B, the effect of DNA lengths on the dispersion yield of nanotubes was tested using $(GT)_n$ sequences where n= 3, 5, 10, 15, 20. We found that sequences composed of G/T nucleotides led to effective dispersions of BNNTs regardless of the length of $(GT)_n$ sequences used, indicating that the DNA length is not a determining factor for forming a stable DNA-BNNT hybrid within the range of DNA length tested. In fact, it has been previously proposed for a $(GT)_n$-SWCNT system that the binding strength of specific DNA sequences towards nanotubes is the primarily determinant of the hybrid stability rather than the DNA length used and the DNA surface coverage created on nanotubes.[121] Consequently, we selected $(GT)_{20}$ ssDNA, which is one of the best known recognition sequences to effectively disperse and purify SWCNTs due to its ability to fold onto a nanotube to form a stable DNA-wrapped SWCNT hybrid.[22] The folding conformation of $(GT)_{20}$ on BNNTs in this work could be different from that of DNA-SWCNTs due to the ionic BN bonding and few-wall structures of BNNTs. Nonetheless, stock dispersions of DNA-BNNTs obtained in this work are stable for more than 12 months for a routine storage condition at 4 ^{o}C. Future studies involving cost effective dispersants

such as natural DNA and other polymers could be beneficial for the scale-up of the liquid phase processing of BNNTs, although the interactions of those polymers with nanotubes and the hybrid stability could be drastically different from that of DNA-BNNT hybrids created in this work using sequence specific $(GT)_n$ ssDNA. In addition, the salt concentration had little impact on the dispersion yield and quality of BNNTs as shown in Figure 3.1C for $(GT)_{20}$-BNNT dispersions with final concentrations of NaCl at 0, 50, and 100 mM.

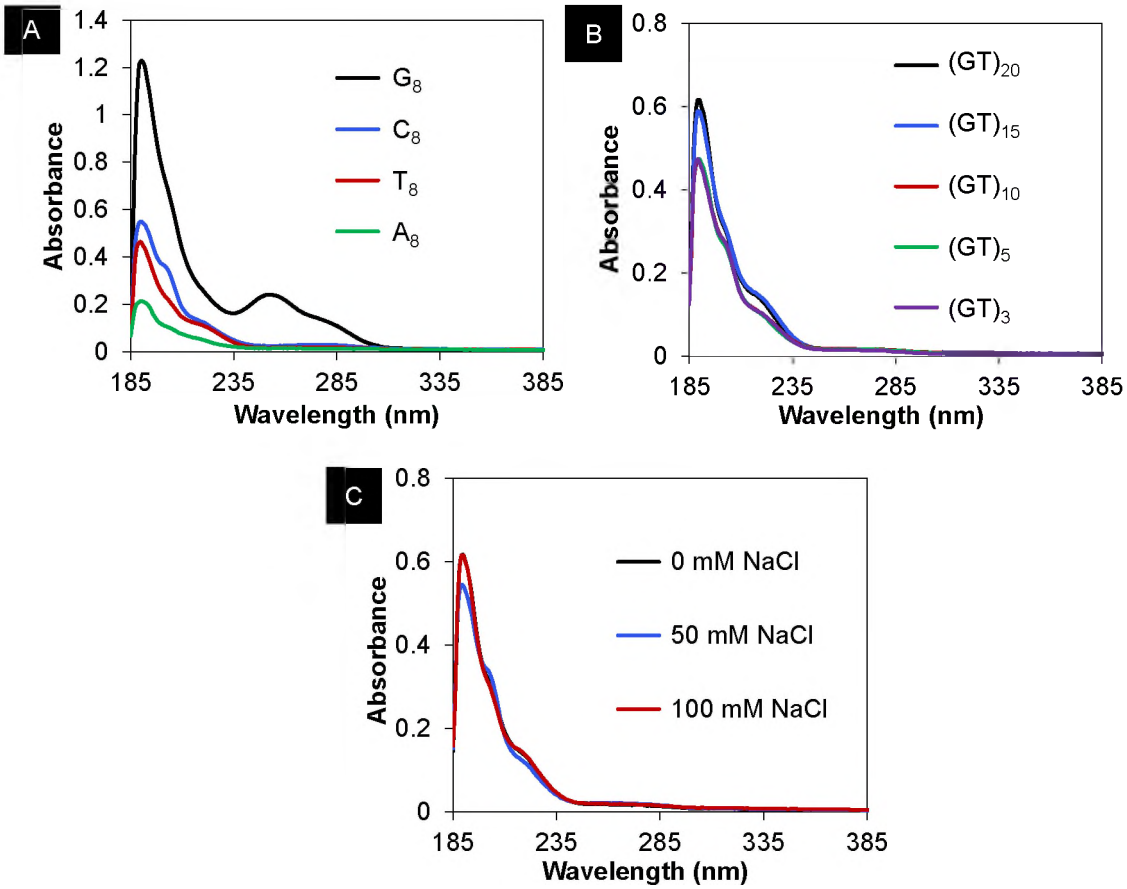

Figure 3.1. Absorbance spectra of BNNTs dispersed by (A) 8-mer single-mononucleotide repeats with 0.1 mol/L NaCl, (B) $(GT)_n$ sequences of varied lengths with 0.1 mol/L NaCl, and (C) $(GT)_{20}$ with final NaCl concentrations of 0, 50, and 100 mM. All spectra were measured after dilution of each DNA-BNNT sample by a factor of 100x in DI water. Only one set of spectra are shown here. Each dispersion and its corresponding absorbance measurements were repeated 6 times and the results were consistent and reproducible.

Figure 3.2A compares aqueous dispersions of DNA-BNNTs prepared by three different methods: BNNTs:DNA = 1:0 without adding DNA, a bulk dispersion of BNNTs:DNA = 1:1 without centrifugation, and a supernatant of BNNTs:DNA = 1:1 collected after centrifugation. All BNNTs/DNA ratios of various nanotube dispersions are reported in mass ratios. The uniform dispersion of BNNTs in an aqueous environment was obtained only with the assistance of DNA. The centrifugation step enabled the further removal of the majority of bundled BNNTs, and certain impurities (Appendix A1) as indicated by overall decreases in absorption peaks of DNA-BNNT dispersions. Specifically, we observed three characteristic peaks at 190, 205, and 220 nm wavelengths in the UV-region (Figure 3.2B). For a sample of BNNTs:DNA = 1:0 without the addition of DNA, particles of (22 ± 8) nm size were observed without obvious traces of nanotubes (Figure 3.3A). The existence of non-nanotube particles could lead to the absorption peak at 190 nm observed in absorbance spectra of BNNT dispersions with and without DNA. For a supernatant of BNNTs:DNA = 1:1, individually dispersed BNNTs were clearly observed along with non-nanotube impurities indicating that DNA is an efficient dispersing agent of BNNTs in an aqueous environment (Figure 3.3B).[47] The absorption of a DNA-BNNT hybrid is corresponded to the 205 nm peak, which is in good agreement with a band gap of ≈ 6 eV for BNNTs.[37] In general, an absorbance spectrum of a bulk dispersion showed increased background and broader peaks compared to that a supernatant dispersion (Appendix A2). Significant decreases in absorbance values were observed for supernatant dispersions of BNNTs:DNA = 1:1 indicating the removal of the majority of BNNT bundles and other impurities with centrifugation. Here, the concentration of nanotubes after precipitation and re-suspension of a supernatant dispersion of BNNTs:DNA = 1:1 in

deionized (DI) water is determined to be $\approx 0.382\, mg \cdot mL^{-1}$ using an extinction coefficient of 0.0926 $L \cdot mg^{-1} \cdot cm^{-1}$ at 205 nm for a DNA-BNNT hybrid (Appendix A3). Similar to the interactions of DNA and graphene, the hydrophobic DNA nucleotide bases can be potentially noncovalently complexed with *h*-BN structures, which likely gave rise to an absorption peak at 220 nm.[159] Figure 3.2C shows the length distribution of DNA-BNNT hybrids from a supernatant BNNTs:DNA = 1:1 sample by SEM and the number average length of hybrids was estimated to be $(268 \pm 110)\, nm$. High localized shear during ultrasonication process likely resulted in the cutting of as-synthesized nanotubes, which can be up to ≈ 200 μm long.[26] In addition, it has been reported recently that short $(GT)_{30}$-SWCNT hybrids bind preferentially to the imaging substrate (freshly cleaved mica) compared to long $(GT)_{30}$-SWCNTs due to their larger diffusion coefficients, resulting in a length distribution of nanotubes that is significantly smaller than the parent sample.[160] It could be possible that the length distribution of $(GT)_{20}$-BNNT hybrids determined in this work is smaller than the parent BNNT dispersion potentially due to the differential binding of hybrids to the silicon substrate. Although the accurate measurement of nanotube lengths and the production of long DNA-BNNT hybrids that are desirable for certain applications such as nanocomposites and fiber spinning can be rationalized by future studies, the ability to produce stable DNA-BNNT hybrids can nonetheless be exploited for purification and assembly of nanotubes, as shown in this work.

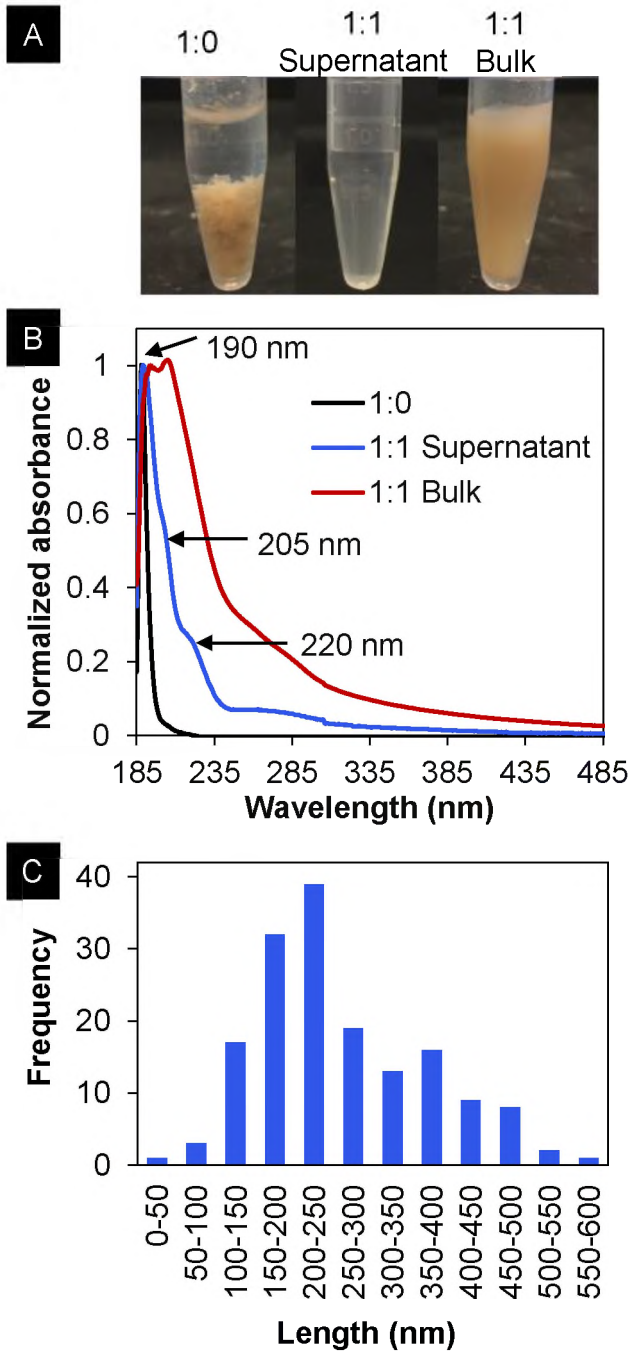

Figure 3.2. Aqueous dispersions of a synthetic BNNT material that are noncovalently complexed with $(GT)_{20}$ ssDNA. (A) Photographs of three different dispersions with BNNTs/DNA mass ratios of 1:0 and 1:1 before (*i.e.*, bulk) and after (*i.e.*, supernatant) centrifugation. (B) Corresponding absorbance spectra of DNA-BNNT dispersions. Arrows indicate characteristic absorption peaks at 190, 205, and 220 *nm* wavelengths, respectively. (C) Histogram of the length distribution of DNA-BNNT hybrids by measuring lengths of 200 nanotubes imaged by SEM.

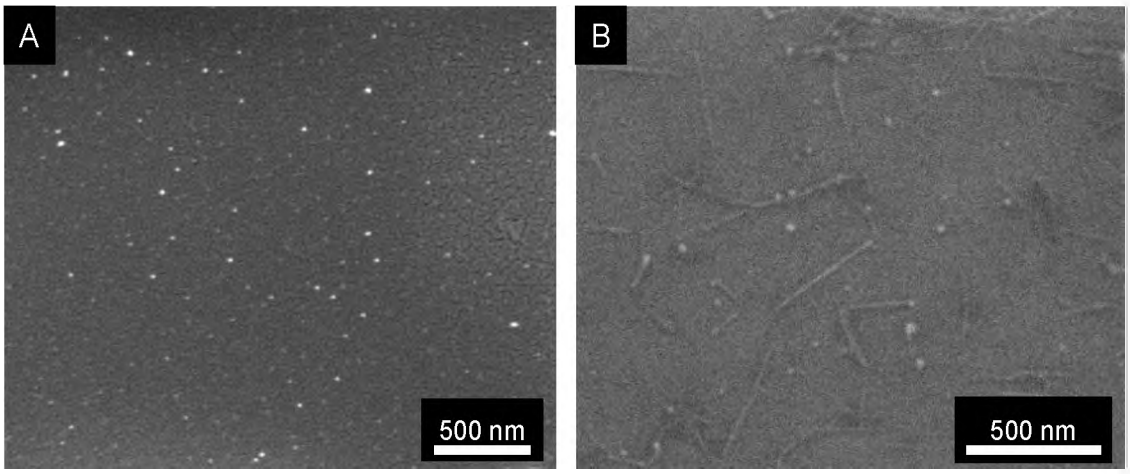

Figure 3.3. SEM images of BNNT dispersions with and without adding $(GT)_{20}$ DNA. (A) BNNTs:DNA = 1:0 showing no evidence of nanotube dispersion and (B) a supernatant BNNTs:DNA = 1:1 showing individually dispersed nanotubes. Both samples were imaged without further dilution.

In order to determine the effective BNNTs/DNA mass ratio for dispersing as-synthesized BNNTs, we compared absorbance values of three characteristic peaks of supernatant dispersions with increasing concentrations of DNA (Figure 3.4A). The absorption of DNA-BNNT hybrids at 205 *nm* increased for dispersions roughly up to a BNNTs/DNA mass ratio of 1:0.5 indicating an improved dispersion yield of nanotubes, followed by a plateau with further increase in DNA concentrations. The overall trend of absorption at 220 *nm* for *h*-BN structures with increasing DNA concentrations was similar to that of DNA-BNNT hybrids, however at lower absorbance values compared to that of DNA-BNNT hybrids (Figure 3.4A). It was reported previously that ssDNA can bind to flat graphite, however, at a much weaker binding strength compared to that of curved SWCNTs due to the spontaneous curvature of ssDNA.[159] Similarly, ssDNA is likely to stabilize *h*-BN impurities in a synthetic BNNT material through binding to the hydrophobic surface of *h-BN* structures. In addition, absorbance values of elemental boron at 190 *nm* remained relatively invariable at all BNNTs/DNA mass ratios tested indicating that the

dispersion yield of elemental boron is independent of the presence of DNA in an aqueous dispersion.

Our results show the fraction of DNA-stabilized BNNTs in an aqueous dispersion of synthetic BNNT mixture depended on the mass ratio of BNNTs/DNA. The change in absorbance values of a DNA-BNNT hybrid obtained in Figure 3.4A enables determining the fraction of nanotubes dispersed by DNA. The rapid increase in the fraction of DNA-BNNTs with increasing DNA concentration indicates that sufficient DNA molecules are needed to stabilize BNNTs in dispersions by overcoming strong van der Waals forces of attraction between nanotubes. However, the amount of DNA needed saturates at a certain point which is identified to be near 0.040 mM in this work. This corresponds to an initial dispersion of BNNTs:DNA= 1:0.5 mass ratio. The binding behavior of DNA on the sidewall of BNNTs in a stock DNA-BNNT dispersion can be described using a curve fitting approach of the Hill equation. Previously, the Hill equation arising from chemical kinetics was utilized to evaluate interactions of SWCNTs with biomolecules including DNA and dopamine.[161], [162] Here, we treat it as an empirical equation to describe the interactions between nanotubes and DNA at equilibrium due to the structural polydispersity of the synthetic BNNT material. We consider the following equation to describe our system:

$$\text{DNA} + \text{BNNTs} \leftrightarrows \text{DNA-BNNTs} \quad (5)$$

The total concentration of BNNTs in a dispersion, $[\text{BNNTs}]_{tot}$, is the sum of the concentrations of bare BNNTs and nanotubes coated by DNA:

$$[\text{BNNTs}]_{tot} = [\text{BNNTs}] + [\text{DNA-BNNTs}] \quad (6)$$

We assume the fraction of the DNA-bound BNNTs in a supernatant dispersion can be determined as a ratio between the concentration [DNA-BNNTs] of the bound BNNTs and the total concentration $[\text{BNNTs}]_{tot}$ of the synthetic material and described by the Hill equation:

$$\frac{[\text{DNA}-\text{BNNTs}]}{[\text{BNNTs}]_{tot}} = \alpha \frac{[\text{DNA}]^n}{K_D+[\text{DNA}]^n} + B \quad (7)$$

where the parameter α is a proportionality factor, B accounts for background due to impurities, and K_D and n are empirical parameters. Fitting the curve in Figure 3.4B results in $\alpha = 0.56$ with $B = 0.11$, $K_D = 1.36 \times 10^{-9}$, and the Hill coefficient $n = 4.7$, reflecting positive cooperativity of the interactions ($R^2 = 0.97$). In other words, binding becomes progressively easier as the BNNT surface gets populated with DNA molecules. Furthermore, the sigmoidal (*S*-shaped) curve in Figure 3.4B can be considered as an indicative of the positive cooperativity of interactions. For instance, a similar method was reported to understand the kinetics of fluorescent based SWCNTs-based dopamine sensors, resulting in the Hill coefficient $n = 0.66$ indicating negative cooperativity of interactions, which is in contrast with the n value obtained in this work.[162] This could be attributed due to the decrease in affinity of other dopamine molecules, once one dopamine molecule is bound to the available recognition site on the SWCNT sensor. Earlier, the Hill equation was used to determine an important parameter K_D, also referred as dissociation constant, to understand the strength of nanoparticle-biomolecule interactions, which is useful for comparisons of different nanoparticle-ligand interactions.[162],[163] For instance, by fitting the experimental data of different nanoparticle-ligand interactions to the Hill model, resulted in $K_D = 283 \times 10^{-9}$ for gold nanoparticle-protein complexes [163] and $K_D = 433 \times 10^{-9}$ for dopamine-SWCNTs hybrids,[162] which are significantly higher

compared to K_D value reported in this work. The estimated K_D in this work was observed to be lower by two orders of magnitude relatively when compared to other previously reported systems, [162],[163] implying the strong binding affinity and cooperativity of DNA molecules to the available binding sites of BNNTs. The constant K_D value also signifies the amount of ligand required to occupy half of the available binding sites on surface of nanoparticles. However, researchers working in different fields may have different considerations. In some studies, a similar model was utilized but the constant K_D is replaced by EC_{50} to quantify drug concentration to produce 50% maximal response.[164] Even more recently, a Hill type model was used to predict the total number of cases and deaths due to COVID-19 pandemic.[165] The parameter K_D was used to estimate the time (in days) at which cases attain half of its projected maximum value.[165]

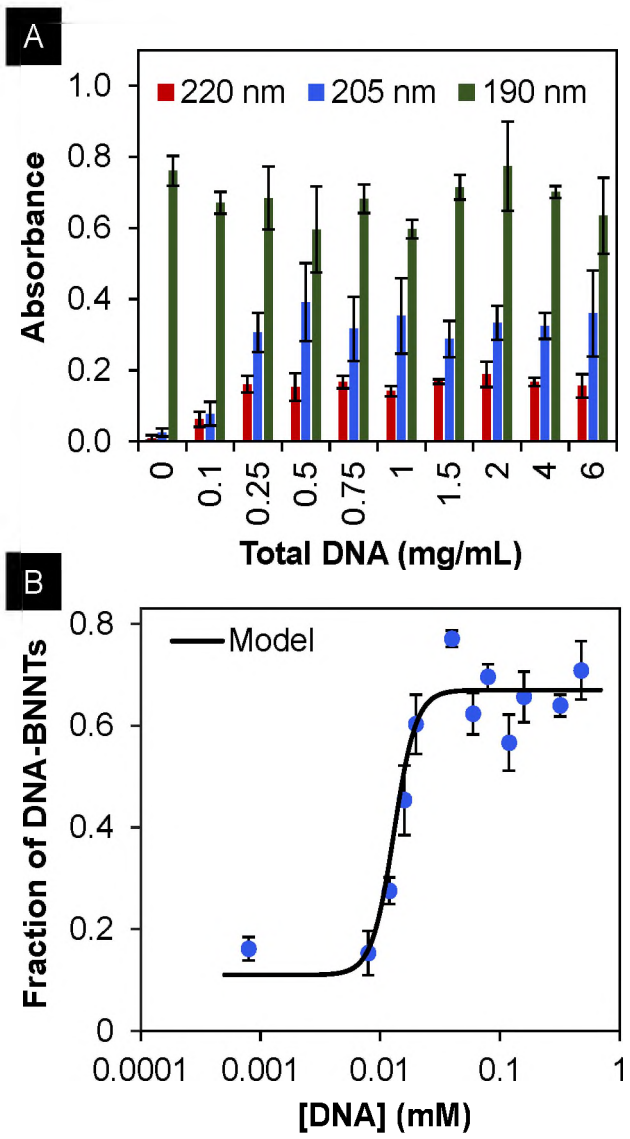

Figure 3.4. The dependence of $(GT)_{20}$-BNNT dispersion efficiency on the mass ratio of BNNTs/DNA. (A) Absorbance values of characteristic peaks observed at 190, 205, and 220 *nm* for supernatant dispersions of DNA-BNNTs at BNNTs/DNA mass ratios from 1:0 to 1:6. (B) Fraction of DNA-BNNT hybrids in supernatant dispersions as a function of DNA molar concentration. All samples were diluted by a factor of 100x in DI water for UV-vis absorbance measurements. The error bars were obtained from the standard deviation of a minimum of three repeats.

Generally, stock DNA-BNNT dispersions undergo a precipitation procedure to remove unbound DNA from the DNA-BNNTs. Here, we measured absorbance spectra of un-precipitated dispersions at various BNNTs/DNA mass ratios to determine the amount of free DNA as well as DNA bound to nanotubes (Figure 3.5A). The peak at 260 nm

corresponds to the free DNA absorption. The concentration of free DNA was calculated using the extinction coefficient of $(GT)_{20}$ DNA = 377200 $L \cdot mole^{-1} \cdot cm^{-1}$. The concentration of bound DNA was calculated from the difference between the amount of total DNA added and that of free DNA in the aqueous dispersion. An overall trend of exponential increases in concentrations of free DNA was observed up to BNNTs:DNA = 1:6 in Figure 3.5B. On the other hand, concentrations of bound DNA remained relatively stable up to BNNTs/DNA ratios of 1:2 and increased gradually from 1:4, indicating the potential binding of DNA to BN polymorphs like hexagonal boron nitride (*h*-BN). Similar to the interaction mechanism of single-stranded DNA to carbon nanotubes, DNA could possibly bind to curved BNNT surfaces preferably over flat *h*-BN due to the spontaneous curvature of DNA.[159]

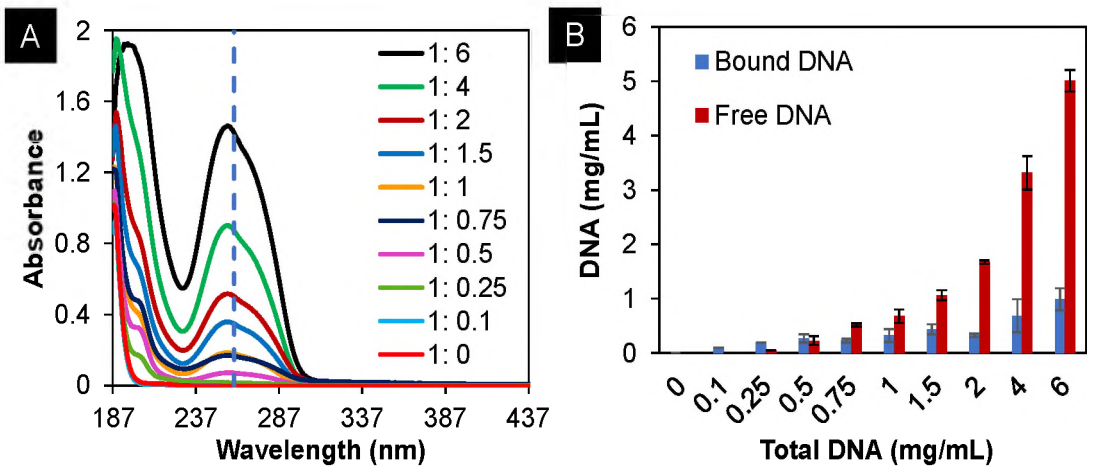

Figure 3.5. (A) Absorbance spectra of un-precipitated $(GT)_{20}$-BNNT dispersions at BNNTs/ DNA mass ratios of 1:0, 1:0.1, 1:0.25, 1:0.5, 1:0.75, 1:1, 1:1.5, 1:2, 1:4, 1:6. The dotted line indicates the absorption peak of free DNA at 260 nm. All samples were diluted by a factor of 100x in DI water for measurements. (B) A bar chart representing concentrations of free DNA and bound DNA in DNA-BNNT dispersions. Error bars were generated from the standard deviation of three repeats.

We attempted to use a previously reported heat treatment method[45] to purify as-synthesized BNNT materials. Specifically, synthetic BNNTs were baked up to 425 °C in

an oven for three days and the baked sample was washed with methanol to remove boron oxide (B_2O_3). The supernatant which contains B_2O_3 was discarded after centrifugation at 17000 g for 1 h at 19 °C. The TGA analysis of BNNT synthetic materials before and after heat treatment were shown in Figure 3.6A. Before heat treatment, a continuous weight loss of 6.2 % was observed up to 425 °C. The weight gain starting from 425 °C up to 1000 °C was likely due to the oxidation of elemental boron.[45] For the heat treated sample, a gradual weight loss of 4.21 % was observed up to 425 °C followed by a relatively stable sample amount indicating the possible elimination of elemental boron and B_2O_3 from the synthetic BNNT material.[45], [116], [153] The slight weight gain of 0.83 % for the heat treated sample between 800 °C and 1000 °C could be potentially due to the oxidation of BNNT outer layers.[46] In addition, a change in color from brown to milky white for bulk dispersions of DNA-BNNTs was observed for heated treated BNNTs (Figure 3.6C). However, absorbance spectra of supernatant dispersions of DNT-BNNTs using BNNT materials before and after heat treatment did not show significant differences, indicating that the heat treatment is not an effective way of purifying synthetic BNNT materials (Figure 3.6B).

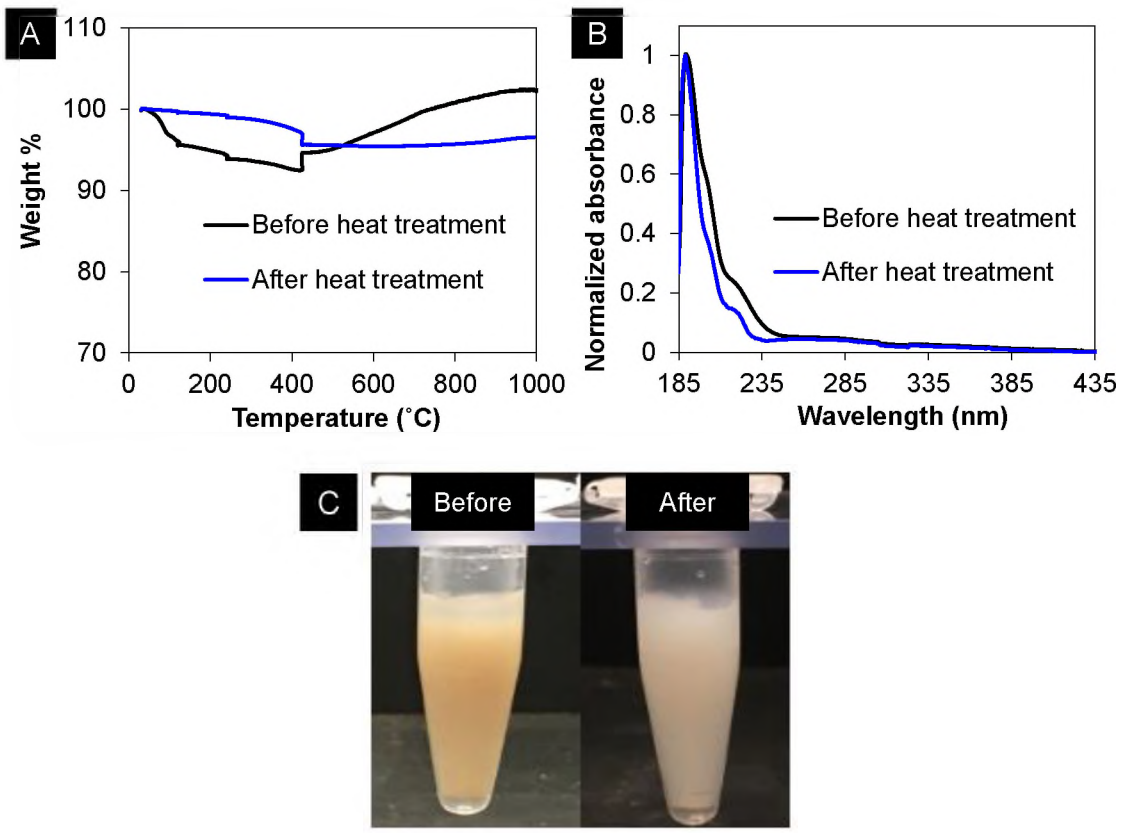

Figure 3.6. Comparison of BNNT materials before and after heat treatment including (A) TGA analysis of synthetic BNNT materials, (B) absorbance spectra of supernatant dispersions of DNA: BNNT = 1:1 mass ratio using $(GT)_{20}$, and (C) photographs of bulk dispersions of DNA-BNNTs. All samples were diluted by a factor of 100x in DI water for absorbance measurements.

The post-synthesis purification of an as-grown BNNT material is important for producing aligned solid materials such as films and fibers with outstanding properties.[47], [116] Here, we demonstrate the purification of aqueous dispersions of DNA-BNNTs *via* a membrane filtration method and self-assembly of aligned BNNT films from a concentrated dispersion of purified DNA-BNNTs. After filtration, BNNTs can be easily re-suspended in DI water by vortex mixing due to the DNA coating on the nanotube surface. Figure 3.7 compares absorbance spectra of a purified DNA-BNNT dispersion by membrane filtration with that of a stock dispersion. A dominant absorption peak at 205 *nm* corresponding to that of a DNA-BNNT hybrid was clearly observed for purified DNA-

BNNTs collected in the retentate after membrane filtration. We speculate that the manifestation of a sideband near 260 nm in the purified sample is intrinsic to BNNTs and may provide valuable information about phonon bands and optical activities relating to BNNT structures in future work.[163] In addition, the decrease in characteristic peaks at 190 and 220 *nm* corresponding to that of non-nanotube impurities such as elemental boron and *h*-BN structures for purified DNA-BNNT dispersions as well as the maintenance of those peaks in the permeate indicate the effective removal of the majority of impurities by filtration. Our purification approach produced DNA-BNNT dispersions that are highly enriched in individually dispersed nanotubes compared to those obtained from heat treated BNNT material, which was aimed primarily for eliminating elemental boron from an as-synthesized BNNT material (Figure 3.6).[153]

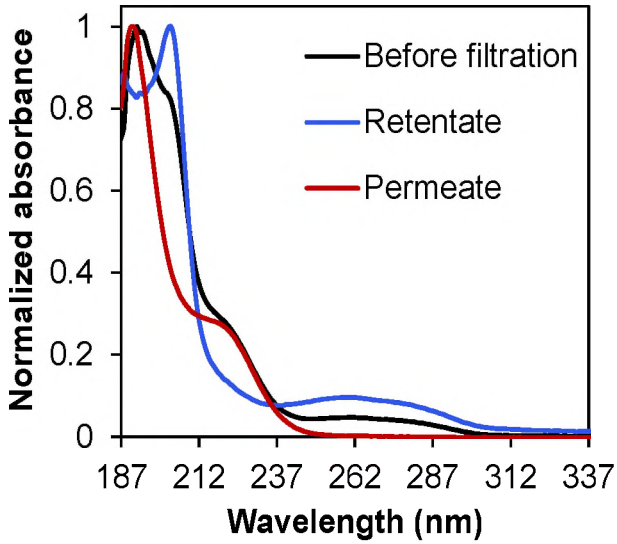

Figure 3.7. Absorbance spectra of $(GT)_{20}$-BNNT aqueous dispersions before and after membrane filtration of a stock dispersion of BNNTs:DNA = 1:1 (mass basis) using a centrifugal filter with a molecular weight cutoff of 30 kDa.

The microstructure of purified DNA-BNNT dispersions at increasing concentrations of nanotubes was characterized by optical microscopy. Notably, uniform dispersions of nanotubes were maintained when evaporating a low concentration

dispersion of purified $(GT)_{20}$-BNNTs containing an excess of DNA to as high as ≈ 11.5 mass % of DNA-BNNT hybrids (Figure 3.8). We tested membrane filtered BNNTs:DNA = 1:0.75 supernatant at various concentrations. A uniform dispersion of DNA-BNNTs with no nanotube aggregations were observed for a dilute dispersion of 0.15 mass % of DNA-BNNT hybrids as shown in Figure 3.8A. For a concentrated dispersion of 11.5 mass % of DNA-BNNTs, a texture resembling that of wavy sand was observed indicating possible self-assemblies of nanotubes at high concentrations (Figure 3.8B). More importantly, nanotube aggregations were not observed as the concentration of nanotubes was increased up to 11.5 mass % DNA-BNNT hybrids by evaporating the solvent water.

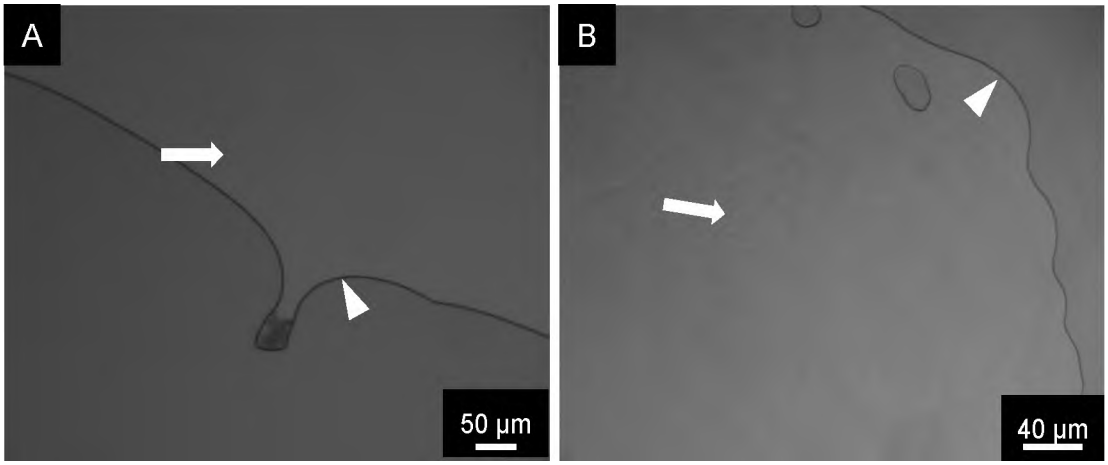

Figure 3.8. Optical microscopy of membrane filtered DNA-BNNT dispersions at (A) 0.15 mass % of DNA-BNNT hybrids and (B) 11.5 mass % of DNA-BNNTs. Arrows point to the region of aqueous DNA-BNNT dispersions and arrowheads indicate the boundary of DNA-BNNT dispersions.

Solid BNNT films were fabricated by allowing concentrated and purified dispersions (≈ 11.5 mass % of DNA-BNNT hybrids) to dry on a plasma treated silicon substrate without applied shear at ambient conditions. SEM of these films (Figure 3.9) revealed an aligned, densely packed structure composed of DNA/BNNT bundles after solvent removal. Bundles size was measured to be (143 ± 30) nm in diameter. To our

knowledge, this is the first demonstration of solid BNNT films produced by spontaneous alignment of DNA-BNNT hybrids. The spontaneous alignment of BNNTs obtained in dried solid films may be driven primarily by an increase in BNNT translational entropy with the reduction in BNNT excluded volumes as the nanotube concentration increases with solvent evaporation. This phenomenon has been the subject of many current studies involving self-assembly of anisotropic building blocks where the ordering is driven by maximizing entropy.[164], [165] In addition, emerging advances in the self-assembly of mesogenic nanomaterial dispersions,[166] including SWCNTs,[142], [144], [167] provide a foundation to better understand relationships between the phase behavior of DNA-BNNT dispersions, properties of solid assembled materials, and their processing conditions in future work. These important parameters will include the concentration and alignment of nanotubes in the dispersion precursor, substrate conditions, and shear and temperature during processing of solid films. Interestingly, the microstructure of aligned BNNT films resembles that obtained previously for solid films produced from a cholesteric liquid crystalline phase of SWCNTs stabilized by double-stranded DNA (dsDNA).[144] In addition, smooth surface morphology similar to that of dsDNA-SWCNT films was obtained due to uniform DNA coating of dried films while the alignment of nanotubes was observed beneath the outer thin layer of films. Relative to the DNA-stabilized BNNT films, the films without nanotubes exhibit high brittleness and break in glassy pieces when scribing to reveal the smooth underside of the films (Appendix A4). Our results indicate that DNA can effectively stabilize BNNTs in an aqueous environment and the removal of solvent by evaporating aqueous dispersions that are highly enriched in individually dispersed DNA-BNNT hybrids promotes the self-assembly of nanotubes into aligned

films. This work could potentially provide a foundation to develop large area assemblies of BNNTs such as films and fibers with improved morphology and properties.

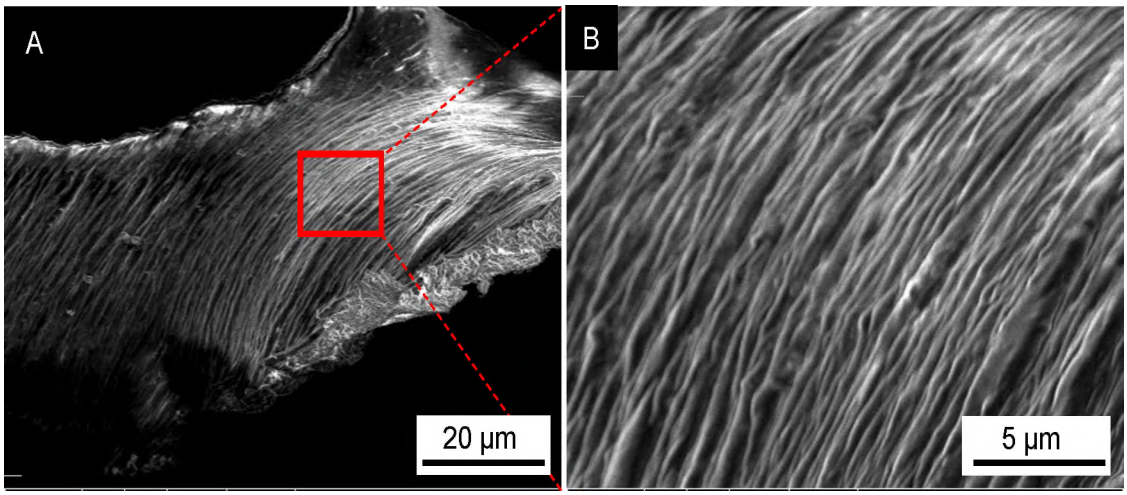

Figure 3.9. (A) SEM image of an aligned DNA-BNNT film formed by solvent evaporation of purified dispersions of BNNTs:DNA = 1: 0.75 mass ratio (≈ 11.5 mass % of DNA-BNNT hybrids) without applied shear. (B) Surface morphology of the film showing the alignment of densely packed nanotube bundles.

3.4. Conclusion

In summary, we have demonstrated a highly effective dispersion methodology of BNNTs in an aqueous environment using DNA and produced assembled solid films with improved nanotube alignment and purity. Similar to the binding of DNA to SWCNTs, our results showing the aqueous dispersion of DNA-BNNTs suggests the surface coating of nanotubes by DNA and the fraction of DNA-BNNT hybrids in dispersions depended on the BNNTs/DNA mass ratios. Purification of DNA-BNNT dispersions by membrane filtration resulted in the enrichment of dispersed nanotubes. Evaporation of concentrated, purified dispersions led to the formation of films comprising aligned DNA/BNNT bundles that has not been previously achieved. Our work establishes a method for the effective dispersion of BNNTs using biopolymer DNA, which may help guide the controlled and tailored liquid phase processing of BNNTs for applications in multifunctional materials,

such as films and fibers with enhanced properties for thermal interface material, protective fabrics, and electronic and optoelectronic applications.

CHAPTER IV

COSOLVENT-ASSISTED COMPLEXATION OF BORON NITRIDE NANOTUBES WITH DNA

4.1. Introduction

Stable dispersions of boron nitride nanotubes (BNNTs) enable the effective translation of unique properties of individual nanotubes into macroscopic assemblies using industrially viable, liquid phase processing techniques. A broad range of applications has been envisioned for BNNTs, such as thermal management materials,[150], [168], [169] water purification and desalination,[170]–[172] protective coatings,[173], [174] and nanomedicine,[175], [176] due to the promising mechanical, electrically insulating, thermal, and physiochemical properties of nanotubes. BNNT-enabled applications require versatile processing approaches, where nanotubes are generally integrated with other nanomaterials and polymer solutions in various solvents to achieve property control and enhancement. A main challenge in this process is to uncover the triangular effect of nanotube-solvent-dispersant interactions to obtain scalable dispersions of BNNTs with minimal energetic cost of debundling nanotubes in a solvent. To date, covalent modification has been explored for BNNT dispersions; however, this approach often

causes permanent change in the B-N lattice structure from sp^2 to sp^3 orbital hybridization that may deteriorate nanotube properties.[90], [94] In comparison, noncovalent complexation of BNNTs with surfactants, polymers, small molecules, and biomolecules assisted by sonication has been found to be a simple way of dispersing BNNTs in various solvents, including water – a useful solvent for many applications, particularly in biology.[103], [112], [177]–[179] Additionally, solvent-nanotube interaction has been optimized to disperse BNNTs without adding dispersants using chlorosulfonic acid,[44], [117] a true solvent for BNNTs, that does not require sonication as well as using good solvents[180] for BNNTs, such as dimethyl formamide (DMF), ethanol (EtOH) and isopropyl alcohol (IPA), with the assistance of sonication. Solvents containing amide or hydroxyl groups induce hydrogen bonding interactions with BNNTs, which exhibit an electron deficiency of B atoms due to partially ionic B-N bonds, thereby leading to dispersion of a low concentration of BNNTs.[37], [180] Various cosolvents of tunable solubility parameters have been exploited to disperse BNNTs as well, however, this method generally resulted in low concentration dispersions with poor stability.[181]

In comparison, alcohol/water cosolvents have been successfully utilized for achieving dispersions of carbon nanotubes and boron nitride nanosheets, that are one-dimensional (1D) and 2D counterparts of BNNTs, with improved stability and yield.[182]–[185] Molecular dynamics simulations have revealed the pseudosurfactant role of alcohols, such as EtOH and t-butanol, in solvating these nanomaterials in alcohol/water mixtures.[182], [183] Specifically, alkyl groups of alcohol molecules interact with nanomaterials, shielding them from the unfavorable interactions with polar water solvent with high dielectric constant (≈ 80), and the hydroxyl group of alcohols exposed to water

with hydrogen bonding to stabilize nanomaterials in alcohol/water cosolvents. Streit et al. further exploited a methanol (MeOH)/water cosolvent to disperse DNA-wrapped single-wall carbon nanotubes (DNA-SWCNTs) under mild bath sonication as well as displacing a strong surfactant (i.e., sodium deoxycholate) coating for SWCNTs by arbitrary DNA sequences with simple mixing.[156] These arbitrary DNA-SWCNT complexes are stable in both water and MeOH/water mixture and further enable purification of single-chirality SWCNTs using recognition DNA sequences by a polymer aqueous two-phase separation method.[22], [156] Additional alcohol/water cosolvents composed of EtOH and IPA were tested, however, they did not disperse DNA-SWCNTs.[156]

Exploiting the solvation behavior of BNNTs assisted by dispersants (i.e., DNA) in solvents or cosolvents is important to minimize energetic cost of producing dispersant-BNNT complexes, that are highly stable for versatile processing, such as dispersion, assembly, and characterization. Dispersion process that does not rely on harsh sonication is also beneficial for preserving intrinsic properties of BNNTs by attenuating defect generation and cutting of tubes as well as preventing damage to dispersants (i.e., DNA).[119], [186] Maintaining longer nanotubes during processing is required for producing mechanically strong fibers and nanocomposites.[142] Consequently, it is desirable to develop a rapid method for length determination of bulk BNNT samples in liquid media as compared to imaging of a small quantity of nanotubes (thousands of tubes) that are deposited on a substrate. In addition, microcopy-based method is time consuming, less sensitive toward distinguishing individual and bundled tubes, and prone to artifacts caused by differential binding of nanotubes to a substrate due to different surface coatings.[123], [160], [187] Parra-Vasquez et al. developed a reliable rheological method

to assess the length distribution of SWCNTs (≈ 10^{15} tubes) from dilute dispersions based on the rheological behavior of Brownian rigid rods in dilute regime.[123], [133], [187] Most recently, BNNTs have been demonstrated to behave like model rigid rods undergoing Brownian motion.[125]

We have previously demonstrated that DNA-BNNT complexes prepared by probe tip sonication in water are highly stable up to ≈ 11.5 % (mass basis) and allow purification and assembly of BNNT dispersions into solid aligned films.[178] Here, we report a comprehensive work on producing stable DNA-BNNT complexes with improved dispersion yield at a reduced energetic cost under mild bath sonication by exploiting alcohol/water cosolvents as well as determining length of dispersed tubes by rheology. The resulting DNA-BNNT complexes are stable in both water and alcohol/water mixture, enabling various processing and characterization of samples, such as purification, solvent exchange, and subsequent rheology measurements of aqueous dispersions of DNA-BNNTs. In addition, molecular dynamics simulations were used to examine the solvation behavior of BNNTs in IPA/water mixture, revealing the pseudosurfactant role of IPA in dispersing BNNTs.

4.2. Experimental section

4.2.1. *Materials*

Synthetic few-wall BNNT material (puff ball, lot no: 719171) was purchased from BNNT, LLC (Newport News, VA). DNA from herring sperm (crude oligonucleotides, bp <50, lot no: SLBW1026, Sigma-Aldrich), Sodium deoxycholate (SDC, ≥98% BioXtra, Sigma-Aldrich), sodium dodecyl sulfate (SDS, ≥99% BioXtra, Sigma-Aldrich), methanol

(MeOH, ≥99.9%, Sigma-Aldrich), ethanol (EtOH, 100%, Decon Labs, Inc.) and isopropyl alcohol (IPA, ≥99.5%, Sigma-Aldrich) were used as received.

4.2.2. *Dispersion of BNNTs*

Synthetic few-wall BNNT material (puff ball, lot no: 719171) was purchased from BNNT, LLC (Newport News, VA). DNA from herring sperm (crude oligonucleotides, bp <50, lot no: SLBW1026, Sigma-Aldrich), Sodium deoxycholate (SDC, ≥98% BioXtra, Sigma-Aldrich), sodium dodecyl sulfate (SDS, ≥99% BioXtra, Sigma-Aldrich), methanol (MeOH, ≥99.9%, Sigma-Aldrich), ethanol (EtOH, 100%, Decon Labs, Inc.) and isopropyl alcohol (IPA, ≥99.5%, Sigma-Aldrich) were used as received. Dispersions of DNA-wrapped BNNTs (i.e., 1mg/mL BNNTs-1 mg/mL DNA) were prepared in a total volume of 1 mL mixed solvents of deionized (DI) water and alcohols including MeOH, EtOH, and IPA, respectively, by bath sonication (Fisher Scientific, Model no: 15337418, 5.7 Liter capacity) at room temperature for 24 hours, unless indicated otherwise. The alcohol contents in mixed alcohol/water solvents were varied from 0 to 100 vol%. Supernatant dispersions were collected after 90 min centrifugation at 17,000 g and 19 ^{o}C and were used as stock DNA-BNNT dispersions. Additionally, dispersions of 1 mg/mL BNNTs by surfactants (i.e., SDS and SDC) at a final concentration of 1 mass% surfactant were prepared by bath sonication for 24 hours in a total volume of 1 mL solvents including DI water and a IPA/water mixture with 50 % (v/v) IPA, followed by centrifugation at 17,000 g for 90 min at 19 ^{o}C to collect supernatant samples. Comparative study of BNNT dispersions prepared by probe tip sonication was performed based on our previously reported method.[178] Briefly, 1mg/mL BNNTs were mixed with a total volume of 1 mL aqueous solution of either 1 mg/mL DNA or 1 mass% surfactant (i.e., SDC or SDS), and

sonicated (model VCX 130, Sonics and Materials, Inc.) in an ice bath for 1 hour at a power level of 8 W using a 2 mm diameter probe. The subsequent steps for collecting supernatant samples were the same as above described procedures.

4.2.3. *Displacing DNA coatings of BNNTs by surfactant*

Stock solution of 10 mass% SDC in DI water was prepared for DNA/surfactant exchange reaction of BNNTs. First, solvent exchange was performed by membrane filtration for the stock sample prepared from DNA-BNNT dispersions in IPA/water mixture with 50 % (v/v) IPA using a Microcon® centrifugal filter with a molecular weight cutoff (MWCO) of 30 kDa according to our previously reported procedure.[178] After membrane filtration, DNA-BNNT complexes were re-dispersed in DI water, while impurities being removed with this treatment as well. Then, 5 μL of stock SDC solution was mixed with 500 μL of DNA-BNNT sample in water to obtain a final concentration of 0.1 mass % SDC. The mixture was incubated in a water bath at 30 ˚C for 30 min to facilitate the surfactant exchange.

4.2.4. *BNNT characterization*

UV-vis absorbance measurements were performed using a Jasco V-760 spectrophotometer over the wavelength range 190-800 nm using a 10 mm path length quartz cuvette. All BNNT dispersions were diluted by a factor of 100 × in DI water for UV-vis absorbance measurements unless indicated otherwise. The concentration of DNA-BNNT complexes was determined using an extinction coefficient of 0.0926 L mg^{-1} cm^{-1} at 205 nm wavelength based on our prior work.[178] For peak fitting using Python 3.8.0, the deconvoluted absorption peak of BNNTs at 205 nm was obtained by performing a linear regression of absorption peaks of each component (i.e., free DNA and BNNTs,

respectively) to obtain a global fitting of the measured absorbance spectra of DNA-BNNT samples.

Imaging of BNNT samples were performed using a high-resolution field emission scanning electron microscope (SEM), Inspect F50 by FEI, equipped with an Everhart-Thornley detector with variable grid bias. Particularly, dried samples of aqueous dispersions of DNA- and SDC-coated BNNTs from surfactant exchange were imaged for nanotube length distribution analysis. BNNT samples were deposited and dried on a plasma treated silicon substrate followed by gold sputtering for SEM imaging at 5 kV. ImageJ software was used to record the lengths of DNA-BNNT and SDC-BNNT complexes obtained from SEM images. The significance in the shift of number-average lengths of BNNTs was statistically addressed using the nonparametric Mann-Whitney U-test at 95% confidence level. Statistical analyses were performed using R statistical tool.[188]

4.2.5. *Rheology of dilute DNA-BNNT dispersions*

The length distribution of nanotubes was determined by rheology of dilute, aqueous dispersions of DNA-BNNTs. Solvent exchange of BNNT samples from IPA/water mixture to water only was performed for stock samples prepared from DNA-BNNTs in IPA/water mixture containing 50 % (v/v) IPA by membrane filtration using a 50 mL Amicon® stirred cell with a 30 kDa Regenerated Cellulose membrane (operating pressure < 5 bar). This process removes impurities and excess, unbound DNA (i.e., free DNA) as well. After membrane filtration, purified DNA-BNNT complexes were re-suspended in DI water and bath sonicated for 1 hour at room temperature. Aqueous dispersions of DNA-BNNTs were further diluted in DI water to obtain various samples of different BNNT

concentrations in the dilute regime for rheological characterization using Anton Paar (GmbH) Physica MCR 301 rotational rheometer. Steady shear viscosities (η) of DNA-BNNT samples were measured in the shear rate range from 1 to 100 s^{-1} using a double gap geometry (I.D. = 24.655 mm, O.D. = 26.668 mm) at 10 °C. A step rate test was performed to determine the time required to achieve a steady-state flow. Error bars were obtained from four replicates consisting of two separate loads of samples with two measurements for each load. The volume fractions (ϕ) of nanotubes of DNA-BNNT dispersions were determined using a BNNT density of 1.50 g cm^{-3} by taking the average of previously reported values.[189], [190] DNA-BNNT dispersions with viscosities roughly below twice the solvent viscosity η_s (i.e., water) were considered as samples in the dilute regime.[187], [191]

4.2.6. *Simulation method*

The simulated system consisted of a single BNNT of chirality (6,5) 1 unit-cell in length (4.8302 nm). The BNNT is periodic in the z-dimension creating an infinitely long nanoparticle that was solvated with the appropriate number of solvent molecules to achieve alcohol concentrations of 0, 20, 40, 60, 80, and 100 mol % (Table B1). All simulations were performed using GROMACS (ver. 2018.2)[192] applying the TIP4P model for water[193] and the CHARMM36 forcefield[194] for treatment of all alcohols. The forcefield for the BNNTs was taken from Wu et al.[195] A simulation timestep of 2 fs was achieved by utilizing the LINCS constraint algorithm[196] to prevent high frequency oscillation of all hydrogen-containing bonds. Equilibration was carried out first for 200 ps in the NVT ensemble using a velocity rescaling thermostat[197] to maintain the temperature at 300 K, followed by 200 ps in the NPT ensemble making use of the

Parrinello-Rahman barostat[198] to maintain a pressure of 1 atm. The barostat was applied in a semi-isotropic manner in order to maintain the correct box-size in the z-dimension which corresponds to the length of the periodic BNNT unit cell. Following these equilibration steps, data was collected over production runs of 100 ns. The change in Gibbs free energies of solvation, ΔG_{solv}, of the BNNTs were calculated using the free energy perturbation (FEP)[199] approach used previously to measure the solvation energies of single-wall carbon nanotubes.[182] This allows for the BNNT to be decoupled from the solution by effectively turning off the pair interactions. The end-points of this decoupling procedure thereby represent a solvated BNNT and a BNNT in vacuum. The intermediate "ghost states" exist only *in silico* and use soft-core Lennard-Jones type potentials to avoid singularities. For each system, 60 intermediate decoupling states were used (20 for the Coulombic interactions and 40 for the van der Waals interactions). Results of this method were analyzed using Bennet Acceptance Ratios (via the *gmx bar* module) to yield free energy differences.[200], [201]

The decoupling procedure above yields a change in the system size due to the removal of the BNNT. Shirts et al.[199] have developed a method to correct for this volume change in the final free energy result by using the ratio of the initial and final system volumes (equation 8).

$$\Delta G_{solv} = \Delta G_{sim} - kTln\left(\frac{V_i}{V_f}\right) \tag{8}$$

Here V_i denotes the initial system volume with full solute/solvent interaction and V_f is the final volume of a box of pure solvent with the same number of molecules. In our simulations, the largest observed volume change was roughly 3%, yielding a correction

factor on the order of ~80 J/mol. This correction value is much lower than the statistical uncertainty of our simulations and can therefore be neglected in all cases.

4.3. Results and Discussion

We show that alcohol/water cosolvents, particularly isopropyl alcohol (IPA), are essential for the complexation of BNNTs with DNA under mild bath sonication. The resulting DNA-wrapped BNNT complexes are highly stable during purification and solvent exchange from cosolvents to water, providing potential for the versatile liquid-phase processing of BNNTs. Via molecular dynamics simulations we demonstrate that IPA assists in the solvation of BNNTs due to its pseudosurfactant nature by verifying that water is replaced in the solvation layer as IPA is added. Additionally, we quantify the solvation free energy of BNNTs in various IPA/water mixtures and observe a non-monotonic trend, highlighting the importance of utilizing solvent-nanotube interactions in nanomaterial dispersions. Additionally, we show that nanotube lengths can be characterized using rheology *via* measurement of the viscosity of dilute dispersions of DNA-BNNTs. This represents the bulk sample property in the liquid state, as compared to the conventional surface deposition method of imaging dried samples. Our results also demonstrate that BNNT dispersions exhibit the rheological behavior of dilute Brownian rigid rods, which can be further exploited for the controlled processing and property enhancement of BNNT-enabled assemblies such as films and fibers.

Noncovalent complexation of nanomaterials with dispersants, such as surfactants, polymers, and biomolecules, has been widely utilized for achieving stable dispersions of nanomaterials in various solvents, while preserving the chemical structures and intrinsic properties of nanomaterials. It also offers vast potential for designing dispersant-

nanomaterial complexes with added functionalities through introducing tailored functional groups for biological sensing and imaging, directed assembly, and overall property enhancement.[154] DNA-wrapped SWCNTs have been considered as a model system to study the solvation energy of macromolecular objects with unique surface functionalities and to develop applications, particularly separation of pure-chirality SWCNT species for biomedical sensing, imaging, and therapeutic applications.[22], [202]–[205] Surfactants, such as sodium deoxycholate (SDC) and sodium dodecyl sulfate (SDS), are known to produce stable dispersions of SWCNTs in water by forming a bound interfacial layer of surfactants around SWCNTs.[206]–[208] In addition, various surfactants, including SDS, have been utilized for aqueous dispersions of BNNTs.[112] We previously demonstrated the effective dispersion of BNNTs in water using sequence controlled DNA, which form DNA-wrapped BNNT complexes *via* π-π stacking of hydrophobic DNA nucleotide bases and the hydrophobic surface of aromatic BNNTs.[120], [178] Here, we aim to produce stable BNNT dispersions with minimal energetic cost using mild bath sonication by exploiting the solvent-nanotube interactions.

We tested three dispersants including natural DNA (<50 base pairs), SDC, and SDS for stabilizing BNNTs in water and various alcohol/water mixtures (i.e., MeOH, EtOH, and IPA). Stable BNNT dispersions can be formed with DNA and surfactants (i.e., SDC and SDS) in water under probe tip sonication showing the characteristic BNNT absorption peak at 205 nm wavelength (Appendix B1). However, when using mild bath sonication, the dispersion yield of BNNTs in water decreased significantly for all three dispersants with less-resolved absorption peak of nanotubes (Appendix B1). We then changed the solvent to alcohol/water mixtures containing 50 % alcohol and found that

DNA can disperse BNNTs better in cosolvents of IPA, followed by EtOH, under mild bath sonication as compared to using water only, while MeOH/water mixture did not result in improved dispersions of BNNTs (Figure 4.1). In fact, IPA/water cosolvents enabled the stabilization of DNA-BNNT complexes at a higher dispersion yield with mild bath sonication as evidenced by the increased absorbance value at the 205 nm peak, compared to that of DNA-BNNT dispersions obtained by harsh tip sonication in water based on our previous work (Appendix B2).[178] The discrepancy of a poor dispersion of BNNTs in MeOH/water mixture as compared to that of SWCNTs reported by Streit et al. is likely due to different lattice structures of nanotubes, namely the partially ionic B-N bonds in BNNTs exhibiting a polar behavior versus the nonpolar carbon bonds in SWCNTs.[156]

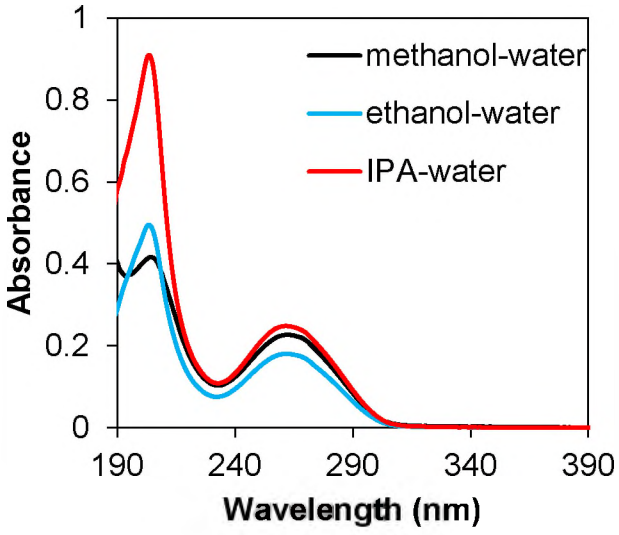

Figure 4.1. Absorbance spectra of supernatant dispersions of DNA-BNNT complexes prepared in alcohol/water mixtures containing 50 % (v/v) MeOH, EtOH, and IPA, respectively.

We then selected IPA/water cosolvents with 50 % IPA to disperse BNNTs using SDC and SDS, however, both did not disperse nanotubes (Figure 4.2). The absorption observed in the UV region (< 220 nm) for SDC-BNNT sample is caused by the intrinsic absorption of SDC itself (Appendix B1). Although surfactants can stabilize BNNTs in

water, interactions between surfactants and nanotubes become weak in a less polar solvent, as individual surfactant molecules interact stronger with solvent molecules and become better solubilized.[156] Therefore, we selected IPA/water cosolvent for DNA-BNNT dispersions in the following work and kept the bath sonication time for 24 hours to ensure sufficient dispersions of nanotubes in cosolvents with various alcohol contents. However, the bath sonication time can be further reduced to 8 hours as demonstrated by DNA-BNNT dispersions in IPA/water mixture with 50 % IPA (Appendix B3).

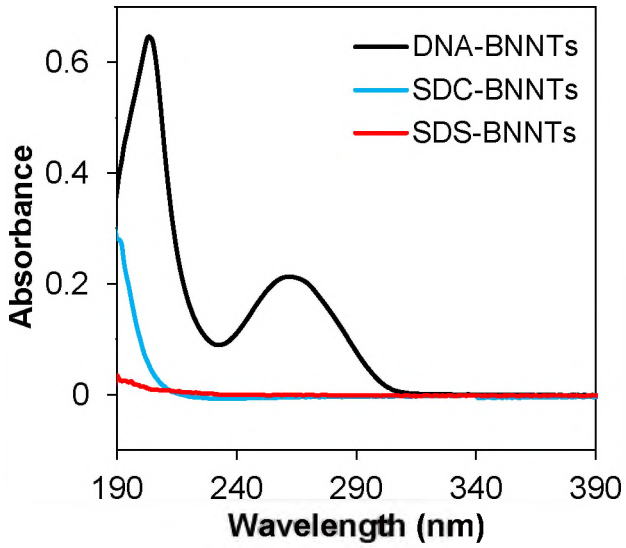

Figure 4.2. Absorbance spectra of supernatant dispersions of BNNTs coated by DNA, SDC, and SDS prepared in IPA/water mixture of 50 % IPA with 24 hr bath sonication.

We then tested how the alcohol content in IPA/water mixture affect the dispersion quality and yield of DNA-BNNT complexes. We found that the absorption at 205 nm peak corresponding to that of BNNTs barely increased up to 20 % IPA, then became much stronger with increasing IPA content up to 60 %, followed by a drastic decrease with further increase in IPA showing no sign of nanotube dispersions in IPA alone (Figure 4.3a, Appendix B4). The increase in IPA content leads to a decrease in the dielectric constant of the solvent reaching a value of ≈ 36 at 60 % IPA.[209] In addition to behaving as pseudosurfactants, the lower dielectric constant and polarity of IPA likely plays a role in

increasing the solvation of BNNTs.[182] IPA may also behave as a better solvent for DNA, assisting the wrapping conformation to occur on the surface of nanotubes. However, the solvation of DNA begins to decrease at 70 % IPA and DNA became insoluble in IPA alone (Figure 4.4). In fact, alcohols including EtOH and IPA have been frequently used for DNA precipitation and extraction.[156], [210] The precipitation of DNA at higher IPA content likely relates to the significant decrease in the stabilization of BNNTs in IPA/water mixtures at 70-100 % IPA due to lack of interactions between DNA and BNNTs (Appendix B4). Figure 4.3b shows the corresponding concentration of DNA-BNNT complexes stabilized in supernatant dispersions with increasing IPA content. At 60 % IPA, a nanotube dispersion yield of as high as ≈ 48 % was obtained based on the BNNT absorption peak from peak fitting and an extinction coefficient of 0.0926 L mg^{-1} cm^{-1} at 205 nm for BNNTs (Appendix B5).[178] Our results suggest that IPA/water cosolvent drastically promotes the DNA complexation with BNNTs under mild bath sonication in the range of ≈ 50-60 % IPA, however, DNA precipitation at higher IPA content (i.e., > 70 % IPA) leads to poor dispersions of DNA-BNNTs.

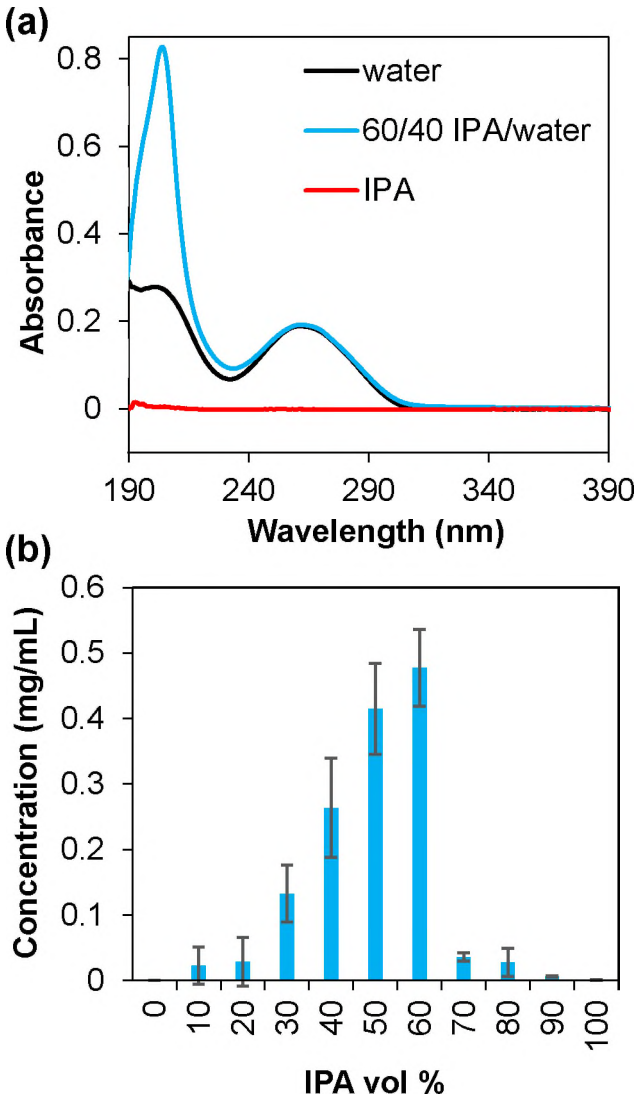

Figure 4.3. Dispersions of DNA-BNNTs in IPA/water mixtures. (a) Absorbance spectra of DNA-BNNT complexes in water, IPA/water mixture containing 60 % IPA, and IPA, respectively. (b) The concentration of DNA-BNNT complexes as a function of increasing volume fractions of IPA from 0 to 100 % in IPA/water mixture. The error bars were obtained from the standard deviation of a minimum of three repeats.

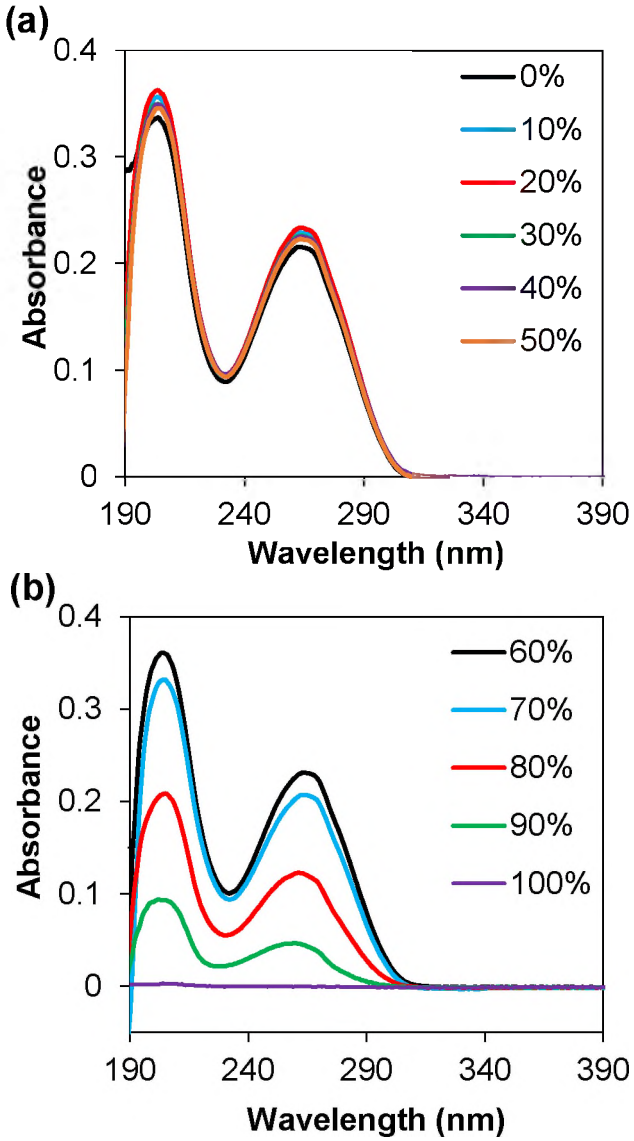

Figure 4.4. Absorbance spectra of DNA only solutions (without BNNTs) in IPA/water mixtures with increasing amount of IPA including (a) 0 - 50 % (v/v) IPA and (b) 60 - 100 % (v/v) IPA.

Additionally, we performed MD simulations to examine the solvation behavior of BNNTs in IPA/water cosolvents without adding DNA. Self-assembly of DNA on the surface of BNNTs in IPA/water mixtures is worthy of future studies, but it is first important to understand the mixed solvent behavior. Radial distribution functions (RDFs) yield information about solvent structure. RDFs of the water around the BNNT show that at concentrations as low as 20 mol% IPA (i.e., ≈ 51.5 vol %), nearly all water has been

displaced from the solvation shell confirming its behavior as a pseudosurfactant (Figure 4.5). Similar behavior has been previously reported for BNNSs and their interaction with t-butanol/water cosolvents.[183] This will have an effect on the single-stranded DNA adsorption as it will alter the ability to form hydrogen bonds.

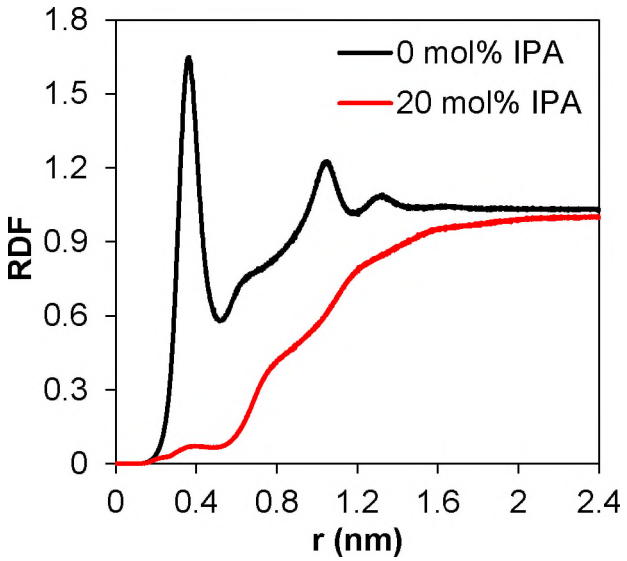

Figure 4.5. RDF of water molecules around the BNNT. Depletion of water in the solvation layer indicates replacement by IPA molecules.

Free energy perturbation (FEP) reveals a non-linear trend in the solvation free energy of the BNNT as the IPA concentration increases (Figure 4.6). This is different from the behavior previously reported for SWCNTs in mixed solvents which gave a monotonic decrease.[182] The difference in the solvation energy can be described by the strong columbic interactions with the charged boron-nitride lattice which leads to more favorable solvation than with SWCNTs.[182] The value obtained for water results in a surface energy of $0.99\, kJ/mol \cdot Å^2$ which compares well with the value of $0.84\, kJ/mol \cdot Å^2$ reported from previous simulations.[195] These complex interactions between the BNNT, cosolvents, and further dispersing agents such as DNA are part of ongoing characterization work and highlight the importance of utilizing solvent-nanotube interactions when seeking

novel nanomaterial processing techniques.

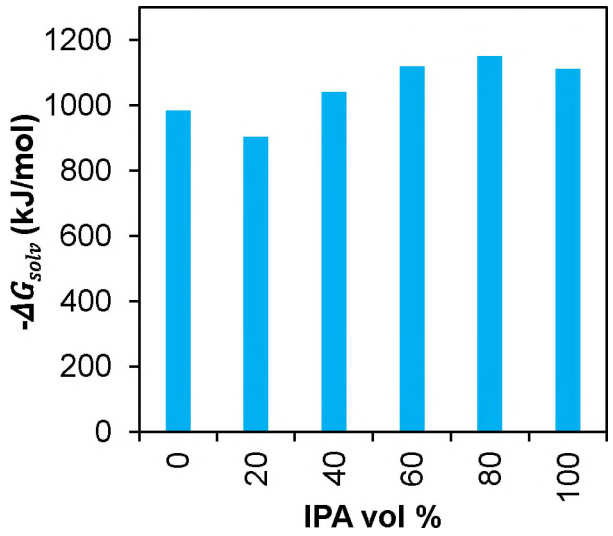

Figure 4.6. Solvation free energies of BNNTs in IPA/water mixture systems.

Stabilizing DNA-BNNTs in IPA/water cosolvent using mild bath sonication requires minimal energetic costs and offers improved dispersion yield and scalability. We then evaluated the length distribution of BNNTs from dispersions prepared in the IPA/water mixture containing 50 % IPA. Nanotube dispersion state, including nanotube length, directly relate to the overall property enhancement of the resulting products, such as composite materials and assembled fibers. Initially, we performed the length distribution analysis of BNNTs *via* the conventional imaging of dried nanotube samples that are deposited on a plasma treated silicone substrate. SEM images (Figure 4.7) revealed that the lengths of deposited DNA-BNNTs were smaller than that of DNA displaced SDC-BNNTs.

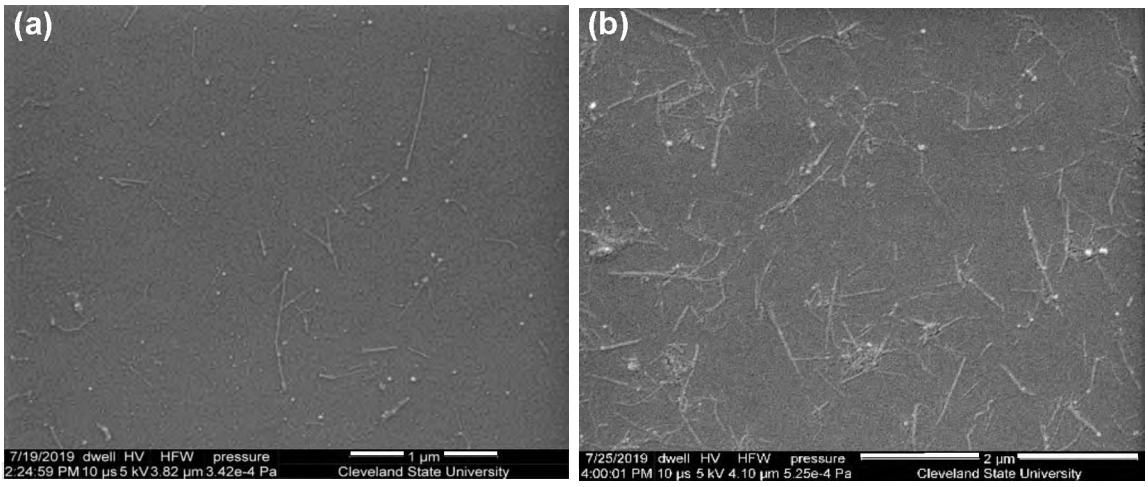

Figure 4.7. SEM images of (a) purified DNA-coated BNNTs and (b) SDC-coated BNNTs after displacing DNA with surfactant in water.

A manual counting of lengths of BNNTs was performed on SEM images of each explanatory variable, i.e., DNA-BNNTs and SDC-BNNTs. Figure 4.8a shows the histograms of lengths comparisons of BNNTs from each sample of ≈305 DNA-BNNT and ≈298 SDC-BNNT complexes. The distribution for SDC-BNNTs was shifted to longer BNNT lengths compared to that of DNA-BNNTs. The corresponding box and whisker plots for DNA-and SDC-coated samples are shown in Figure 4.8b. DNA- and SDC-coated BNNT samples were obtained from the same parent dispersion of DNA-BNNTs in IPA/water, which was later exchanged to water only using membrane filtration. Then, DNA coatings of aqueous dispersions of BNNTs were displaced by SDC and the corresponding absorbance spectra of BNNT dispersions remained essentially unchanged after DNA/surfactant exchange, indicating that the dispersion quality was maintained (Appendix B6). In addition, SDC is a strong surfactant known to displace DNA coatings on the surface of SWCNTs, and DNA/surfactant exchange reaction has been utilized previously to study the binding affinity of different DNA sequences to SWCNTs.[121], [211] After surfactant exchange, SDC-coated BNNTs resulted in a number-average length

of 372 ± 177 nm, which is roughly 21 % larger than that of DNA-coated BNNTs (i.e., 301 ± 177 nm). The detailed statistical analysis was performed on the response variable with respect to explanatory variables under the assumption that the samples were random and the distributions of the variable in the two populations were having the same shape.[188], [212] It affirms that the apparent length distributions of deposited BNNTs are affected by the wrapping type i.e., DNA vs. surfactant (Mann-Whitney U-test, $p < 0.001$). This discrepancy of BNNT length distribution is likely due to the differential binding of nanotubes to a substrate caused by different coating materials. Particularly, short and long SWCNTs coated by different DNA sequences tend to deposit on a substrate differently due to their differences in diffusion coefficients and electrostatic interactions with a substrate induced by sequence-dependent DNA density on the SWNT surface.[160], [213] This inherent bias of the surface deposition method can be mitigated by displacing DNA by a common surfactant (i.e., SDC), which tends to form a compact, uniform coating layer around the SWCNTs.[160], [208] Regardless, an alternative method for the length determination of BNNTs in their original liquid state from a bulk sample is necessary to accommodate the need of better characterizing BNNT dispersions.

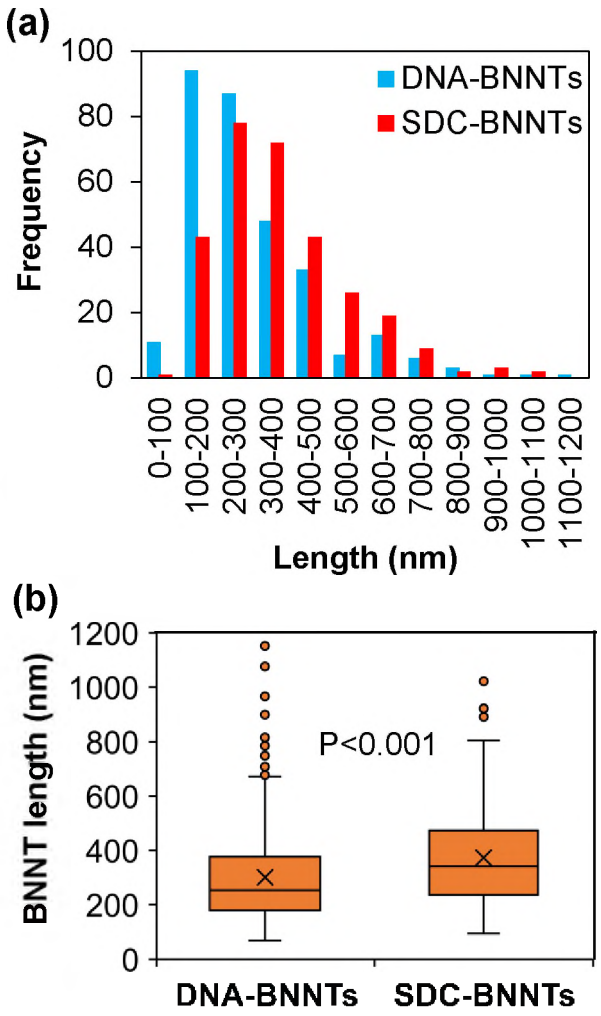

Figure 4.8. Length distributions of aqueous dispersions of DNA- and SDC-coated BNNTs in water. (a) Histograms of length distributions of BNNTs obtained from SEM imaging of ≈ 300 nanotubes coated by DNA and SDC, respectively. (b) The corresponding box and whisker plots comparing the number-average lengths of DNA-BNNT and SDC-BNNT samples (Mann-Whitney U-test, $p < 0.001$). The boxes represent the 25-75 percentile data and median values from imaging ≈ 300 tubes, while average values are indicated by the cross symbols. The whiskers represent minimum and maximum values while outliers are indicated by the solid circles.

Rheological measurements have long been an invaluable tool to study properties of polymers, providing important information such as molecular weight, crosslinked network, alignments, and phase transitions.[214] Later, the established field of rheology for rod-like polymers has been extended to rigid rod-like nanomaterial dispersions, which enabled

researchers to discover important behaviors of various nanomaterials – including SWCNTs – from flow-induced microstructures to liquid crystalline phase formation.[126], [127], [215] A simple rheological method was also developed to determine the SWCNT length by expanding the theory of the rheological behavior of Brownian rigid rods to nanotubes in dilute regime.[123], [133], [187] The suspension of Brownian rods behaves as Newtonian liquids at low shear rate $\dot{\gamma}$, because the rod orientational distribution is unaffected by the flow. With increasing shear rate, rods start aligning with the flow, accompanied by a decrease in viscosity. Recent work demonstrated that BNNTs of micron length can undergo Brownian motion and behave as ideal rigid rods.[125]

Similarly, we determined the viscosity average length of BNNTs by measuring the zero-shear viscosity of aqueous dispersions of DNA-BNNT complexes in the dilute regime. DNA-BNNT dispersions with viscosities roughly below twice the solvent viscosity η_s (i.e., water) were considered as samples in the dilute regime.[187], [191] We first removed excess, unbound DNA from aqueous dispersions of DNA-BNNTs by membrane filtration to eliminate the effect of free DNA on the overall viscosity measurements. Then, purified DNA-BNNT dispersions were diluted in water to obtain various nanotube concentrations ranging from 132 – 3453 ppm vol (i.e., 199 – 5180 mg/L), based on the extinction coefficient of 0.0926 L mg^{-1} cm^{-1} at 205 nm for BNNTs (Figure 4.9).[178]

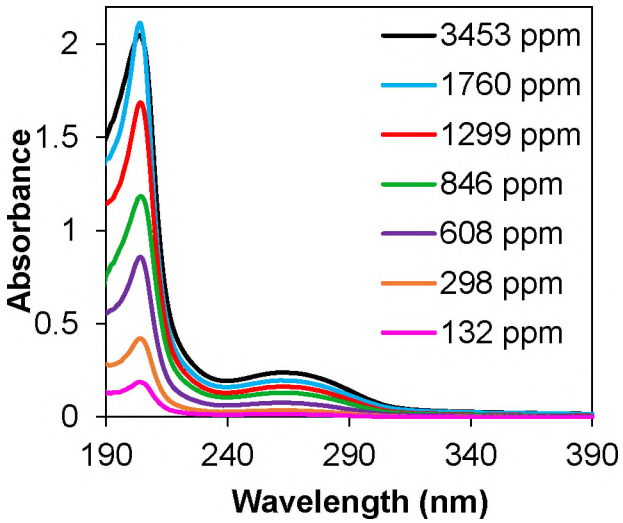

Figure 4.9. Absorbance spectra of aqueous dispersions of purified DNA-BNNTs in the dilute regime. Samples were diluted by a factor of 100x in DI water for UV-vis absorbance measurements, excepts for the dispersion with 3453 ppm BNNTs, which was diluted by a factor of 200x in DI water. Stock sample was prepared from DNA-BNNT dispersions in IPA/water mixture with 50 % IPA. Instrument errors for absorbance values above 1.5 and 2.0 were accounted to be 8 ± 2 % and 19 ± 2 %, respectively.

Figure 4.10a shows the steady-shear viscosity η of dilute dispersions of DNA-BNNTs as a function of shear rate from 1 to 100 s^{-1}. In general, we observed increase in viscosity when BNNT concentration increased and a shear thinning behavior was observed for samples at nanotube concentrations of 846 ppm vol and higher at higher shear rates. Particularly, the viscosity drastically increased from 1760 to 3453 ppm vol, clearly showing the shear thinning behavior starting at a shear rate of $\dot{\gamma} \approx 2.5$ s^{-1}. Based on the rheological theory for Brownian rigid rods in dilute region, as detailed in the section 2.5, the corresponding reduced viscosity $\eta_{red} \equiv \frac{\eta - \eta_s}{\eta_s \phi}$, where ϕ is the volume fraction of nanotubes, of aqueous dispersions of DNA-BNNTs overlaid at all shear rates, as expected for noninteracting rods in a dilute regime (Figure 4.10b).[123] By fitting the reduced viscosity of each DNA-BNNT dispersion using Carreau-Yasuda model, we can extract the intrinsic viscosity $[\eta] \equiv \lim_{\phi \to 0} \frac{\eta_0 - \eta_s}{\eta_s \phi}$, where η_o corresponds to the zero-shear viscosity in

the Newtonian regime below $\dot{\gamma} \approx 2.5\ s^{-1}$. This yielded $[\eta] = 360 \pm 65$, corresponding to an average aspect ratio of $L/D_e = 78 \pm 9$, where L is the nanotube length and $D_e = 2R_e$ is the effective diameter of the DNA-BNNT complex, based on the Kirkwood-Auer-Batchelor (KAB) relationship (equation 9) for a dilute dispersion of Brownian rods, as defined below.[123], [126], [133]

$$[\eta] \equiv \lim_{\phi \to 0} \frac{\eta_0 - \eta_s}{\eta_s \phi} = \frac{2\,(L/R_e)^2}{45\,[ln\ (L/R_e)]} \left[\left(\frac{1+\frac{0.64}{ln\ (L/R_e)}}{1-\frac{1.5}{ln\ (L/R_e)}} \right) + \frac{1.659}{(ln\ (L/R_e))^2} \right] \quad (9)$$

Here, $R_e = R + a$ refers to the effective radius of the DNA-BNNT complex, where R is taken as the radius of nanotubes plus the average van der Waals radius (i.e., ≈ 0.14 nm) of boron and nitrogen atoms (i.e., 1.485 A° for boron and 1.397 A° for nitrogen)[216] and $a \approx 0.5$ nm[160], [217] was estimated for the effect of DNA size coated on the surface of nanotubes. By taking the average of previously reported values for BNNT diameter (i.e., D = 4.9 nm),[94], [125], [218], [219] we estimated $D_e \approx 6.2$ nm in our sample. This leads to a viscosity average length of $L = 484 \pm 53$, which differs by ≈ 26 % as compared to that of SDC-coated BNNTs from the surface deposition method. While instrument sensitivity can account for 5-10 % error in viscosity measurements,[123] rheological characterization relying on bulk samples in a liquid state can be utilized as a simple, reliable method for determining nanotube length by mitigating artifacts introduced in sample preparation and analysis of dried samples on a substrate. Our results also demonstrate that BNNTs dispersed in water share the similar rheological behavior of Brownian rods, which can be potentially taken advantage of for self-assembly of macroscopic materials utilizing previously established liquid phase processing of rigid polymers and other nanomaterials.

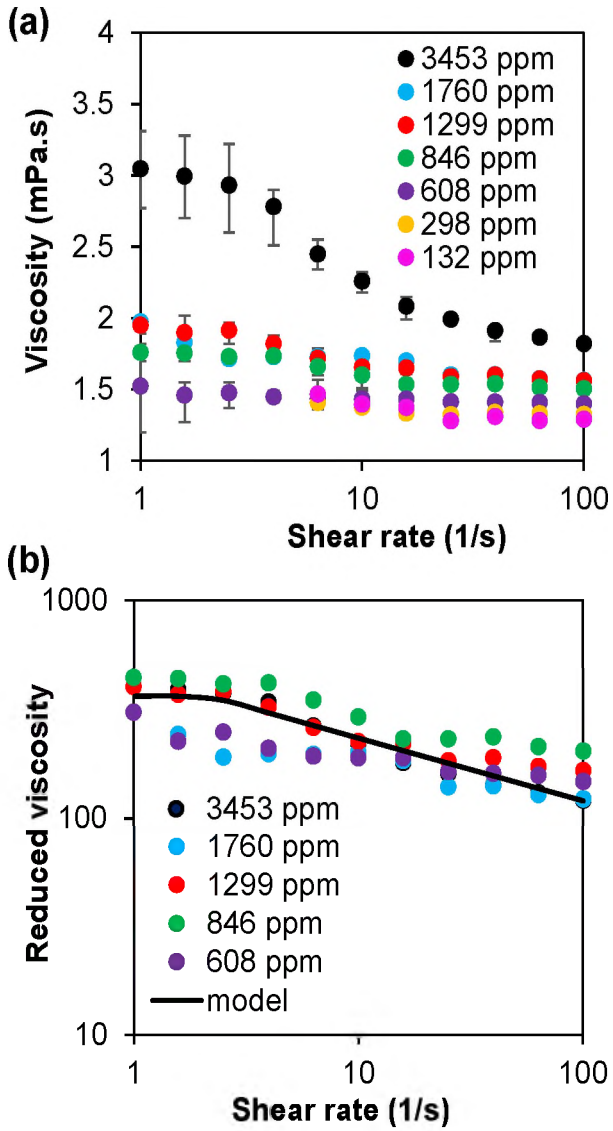

Figure 4.10. Rheology of aqueous dispersions of DNA-BNNTs in dilute regime. (a) Steady shear viscosity as a function of shear rate at BNNTs concentrations from 132 to 3453 ppm vol measured at 10°C. For samples at low concentrations of 132 and 298 ppm vol, viscosity measurements at lower shear rate were not obtained due to instrument limitations. (b) Reduced viscosity as a function of shear rate for DNA-BNNT dispersions at BNNT concentrations from 608 to 3453 ppm and the calculated average reduced viscosity (i.e., model) based on Carreau-Yasuda model to extract plateau to the zero-shear reduced viscosity. The slope in the shear thinning region is determined to be − 0.3.

4.4. Conclusion

In summary, we have demonstrated an effective method for the complexation of BNNTs with DNA by exploiting the alcohol/water cosolvents in dispersing nanotubes.

IPA with a lower dielectric constant and polarity significantly increased the dispersion yield of DNA-BNNT complexes at 60 % IPA with mild bath sonication up to ≈ 48 %, which is more effective than dispersing DNA-BNNTs in water by probe tip sonication. The resulting DNA-BNNT complexes obtained in IPA/water mixtures are highly stable in water as well after a solvent exchange process, providing potential for the versatile processing of BNNTs for applications, such as biomedical sensing and water-based coatings. In comparison, EtOH slightly improved the dispersion outcome of DNA-BNNTs, while MeOH did not result in an obvious dispersion of BNNTs. Results from our MD simulations showed that water is quickly removed from the solvation shell upon the addition of IPA. This pseudosurfactant behavior agrees with the experimentally observed improvement for dispersion in IPA/water solutions. Furthermore, we used FEP to calculate solvation energies and determined that the Columbic interactions (not present in SWCNTs) result in a non-monotonic relationship between ΔG_{solv} and IPA concentration. Upon addition of 20 vol% IPA the solvation energy decreases when compared to that in pure water. However, as more IPA is added the solvation energy increases (meaning a more favorable dispersion) to a maximum in the range of 60-80 vol% IPA. This has been shown to agree with our experimental observations. In addition, we showed that the nanotube length can be determined by rheology utilizing dilute dispersions of DNA-BNNTs, opening new possibilities for the controlled assembly and processing of BNNTs by exploiting the Brownian rigid rod behavior of nanotubes. Combined, our work provides insights for exploring the nanotube-dispersant-solvent interactions and the behavior of Brownian rigid rods to obtain scalable dispersions and controlled processing of BNNTs for applications.

CHAPTER V

LIQUID DISPERSIONS OF HEXAGONAL BORON NITRIDE NANOSHEETS STABILIZED BY DNA

5.1. Introduction

Since researchers reported the first isolated atomically thin hexagonal boron nitride hBN in 2008, they have been used in a wide range of applications due to their unique properties. More recently, they have started to gain significant attention in cosmetic industry applications, especially as sunscreen for protection to skin against solar radiation. Solar radiation that is mainly detrimental to the human body is composed of three types of UV light depending on the UV wavelength: UVC (200-290 nm), UVB (290-320 nm), and UVA (320-400 nm).[220] While UVC is mostly blocked by the ozone layer, high energy solar radiation including UVB and UVA however can damage human skin when exposed to over a period of time. This results in implications from a minor sunburn, to redness of skin, or even serious damage to DNA in an human body.[221] In addition, it results in degeneration of elastin and collagen in skin, leading to wrinkles formation on the skin.

It has been reported that many commercially available sunscreen products in the market consist of a high level of organic compounds to protect from solar UV light.

However, prolonged exposure of these organic substances on skin to UV result in implications such as phototoxic reactions.[63] On the other hand, several other inorganic sunscreen agents such as titanium dioxide, mica and boron nitride were also reported as effective UV blocking performers. This enables a fewer allergic reactions and less irritation on skin.[222] More recently, BN-coated CeO_2 particles were reported to have improved transparency and UV protection comparatively with conventional TiO_2 or ZnO-coated CeO_2 particles.[64], [223] However, attempts to modify these inorganic materials such as BN sheets have been less reported to improve their efficacy.

In this study, we reported our preliminary work on noncovalent complexation of hBN nanosheets assisted by DNA. A highly concentrated and stable dispersions of DNA-hBN nanosheets in PBS were prepared. To begin with, UV-vis spectrophotometer and SEM were used to characterize dispersions of hBN nanosheets stabilized by DNA. Our results provided important insights and laid a foundation to develop potential cosmetic applications such as sunscreen, in our future work.

5.2. Experimental section

5.2.1. *Materials*

Synthetic hBN material (Powder AC6004, batch no: 19BSTA001) and cosmetic grade hBN material (Softouch CC6004, lot no: 19JSTA010) were acquired from Momentive Performance Materials. DNA from herring sperm (crude oligonucleotides, bp<50, lot no: SLBW1026, Sigma-Aldrich), phosphate buffered saline solution (pH 7.43, lot no: SLCF6818, Sigma-Aldrich) were used as received. Sodium deoxycholate (SDC, ≥98%, BioXtra) and sodium dodecyl sulfate (SDS, ≥99%, BioXtra) were purchased from

Sigma-Aldrich. Dulbecco's Modified Eagle Medium (DMEM) was purchased from AddexBio Technologies.

5.2.2. *Dispersions of DNA-hBN complexes*

The synthetic hBN material was dispersed at an initial concentration of 3mg/mL in PBS (pH 7.43) using DNA by maintaining a mass ratio of hBN:DNA = 1:2. Suspensions were probe tip ultrasonicated with a 0.75 in. diameter probe in an ice bath for 1 h at a power level of 50 W (model 550, Fisher Scientific). Samples were centrifuged at 3,260 g at 19 °C for 30 min to eliminate majority of the undispersed nanosheets and impurities. The supernatant samples were precipitated to remove excess DNA by adding a final concentrations of 1.5 M NaSCN and 6 mass % PEG, and the mixture was incubated overnight at 4 °C followed by a centrifugation at 3,260 g for 30 min. After centrifugation, the supernatant was removed, and the pellet was re-dispersed in DMEM by bath sonicating for 30 min for cell cytotoxicity studies.

To determine the dispersion yield of hBN-DNA hybrids, we prepared hBN samples using both small scale and large-scale approaches. Briefly, for a large-scale dispersion methodology of hBN sheets, we prepared an initial mixture of cosmetic grade hBN at a concentration of 3mg/mL and 6 mg/mL DNA in 50 mL PBS (pH 7.43) buffer solution. This dispersion mixture was sonicated at 50 W for 1 h without pulse on/off. The bulk samples were centrifuged at 3260 G for 30 min to collect the supernatant samples. These supernatant samples were precipitated using 6% PEG and 1.5 M NaSCN and incubated overnight at 4 °C followed by a centrifugation at 3,260 G for 30 min. We discarded the supernatant and washed the pellet 4 times with water prior to concentrating each pellet to ~33 times to eliminate any traces of PEG and NaSCN on the surface of pellet. ~3 µL of

concentrated sample was separated to measure absorbance of excess DNA, which was later accounted into the dispersion yield calculation of hBN sheets (Appendix C1). The resulting sample volume was separated into four individual aluminum pans for drying over 24 hrs under sunlight followed by drying in an oven at 80°C for 24 hrs. The mass of empty pans was recorded. The amount of excess DNA was estimated using the extinction coefficient of DNA at 260 nm (Appendix C2) and was adjusted in a mass of dried sample. The total supernatant sample volume of ~290 mL was precipitated overnight with 6% PEG and 1.5M NaSCN and centrifuged at 3,260 G for 30 min and washed 4 times with PBS and resuspended in 2 mL of cell culture media (DMEM) for cytotoxicity studies.

The powder morphology of raw hBN material and supernatant samples of DNA-hBN complexes were imaged using a high-resolution field emission scanning electron microscope (SEM), Inspect F50 by FEI, equipped with an Everhart-Thornley detector with variable grid bias. hBN samples were deposited and dried on a plasma treated silicon substrate followed by gold sputtering for SEM imaging at 5 kV.

5.3. Results and Discussion

Our goal was to develop a high throughput and efficient dispersion methodology for hBN nanosheets for potential sunscreen application development. We used some of our previous knowledge from BNNT work to produce hBN dispersions assisted by DNA in PBS buffer saline solution. To start with, UV-vis spectrophotometer and SEM were utilized to characterize and determine the dispersion yield of hBN samples in PBS. Our results elucidated that DNA is not only an efficient dispersing agent to disperse hBN nanosheets through noncovalent complexation but also help stabilize the nanosheets as high concentrations as ≈ 8 mass % in DMEM for cytotoxicity studies.

For practical cosmetic applications, the powder morphology of starting material is an important issue. The powder morphology was initially examined using SEM. Figure 5.1A shows the starting hBN powder where plate-like particles can be observed. Higher magnification SEM image (Figure 5.1B) shows that plate-like particles stacked upon one another, with an average grain size of ≈12-13 μm and surface area of 2 m^2/g, as provided by the Momentive Performance Materials, Inc.

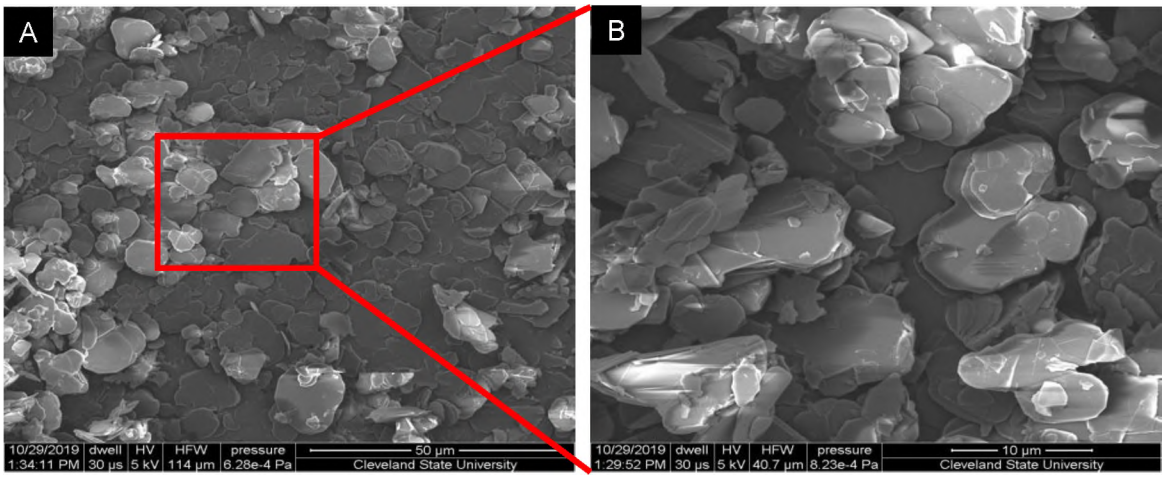

Figure 5.1. SEM images of powder morphology of hBN nanosheets.

Anionic surfactants including SDC and SDS were initially utilized to help disperse hBN in water. The hBN supernatant samples were prepared using 1 mass% SDS in water to check the characteristic peak of hBN in the UV region. Samples were tip sonicated for 1hr and centrifuged at 3,260 g for 30 min. I measured the absorbance spectra (Figure 5.2A) of 1 mass% SDS in water and hBN-1 mass% SDS supernatant samples. The concentration of hBN in supernatant sample was estimated to be 0.033 mg/mL using a reported extinction coefficient of 2367 mL mg^{-1} m^{-1} at 300 nm.[105] Although, we observed the absorbance of individually dispersed hBN-SDS in UV region, that is consistent with the previously reported studies,[52] the concentrations determined was significantly lower. On the other hand, UV-vis measurements of supernatant samples of 1 mass% SDC in water and hBN-1

mass% SDC were performed (Figure 5.2B). The absorbance spectra of SDC in water was analogous to the absorbance spectra of SDC-hBN itself in the UV region, indicating that SDC is not efficient in dispersing hBN in water. Moreover, we speculate that, it is likely that we will not be able to get a stable dispersion of SDS-hBN at 1 mass% hBN concentration, especially after removing excess SDS. Second, SDS-hBN will be most likely not stable in cell culture medium. Third, it is likely SDS-hBN will not be stable in PBS buffer as well. Surfactants, including SDS, are toxic to cells. We need potentially biocompatible dispersing agents, such as DNA and other biomolecules for studying cytotoxicity and developing sunscreen applications.

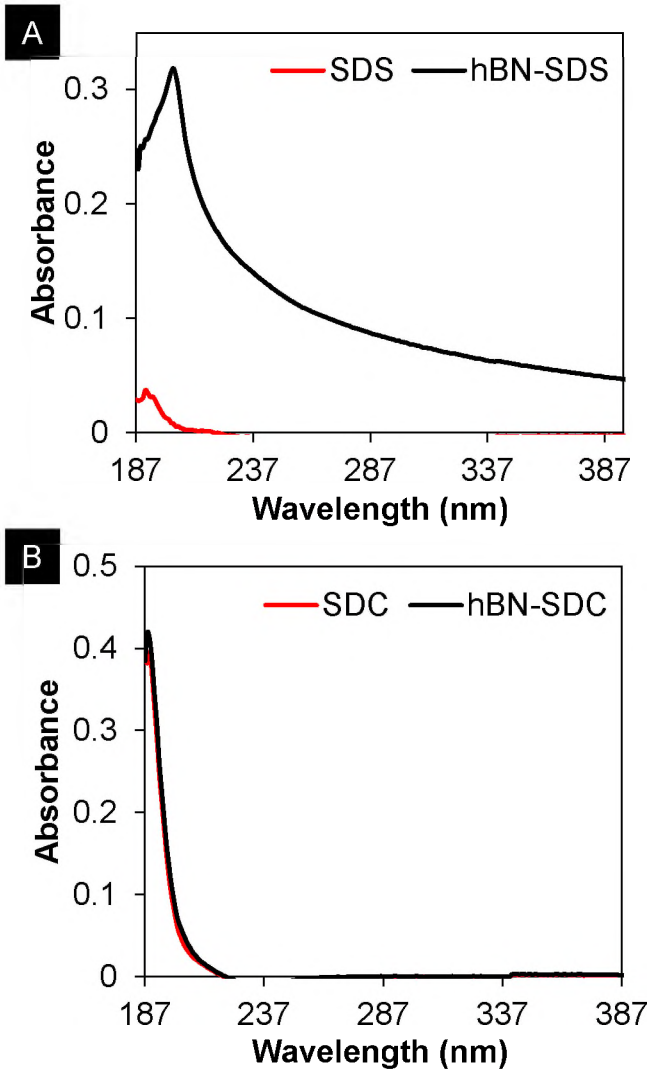

Figure 5.2. Absorbance spectra of aqueous dispersions of (A) hBN-SDS and 1 mass% SDS. (B) hBN-SDC and 1 mass% SDC.

We tested the dispersion capability of DNA via noncovalent complexation of hBN nanosheets in water and phosphate buffered saline solution (pH 7.43). Figure 5.3A compares the bulk (non-centrifuged) and supernatant sample of hBN in PBS. The dispersion color was observed to be whitish for bulk sample and clear for supernatant sample of DNA-hBN hybrids. The bulk sample consists of individually dispersed hBN-DNA hybrids, aggregates, and impurities. These samples are centrifuged to remove the undissolved hBN and impurities. Later, samples were precipitated with 1.5 M NaSCN and

6 mass % PEG to better resolve the absorption peak of individual peak at 260 nm by removing the excess DNA through a centrifugation step. However, we noticed (Figure 5.3B) a clear pellet at the bottom of the vial after centrifugation solely for hBN-DNA precipitated sample in PBS, unlike the precipitated sample of hBN-DNA sample in water, indicating hBN was precipitated in PBS solvent. UV-vis measurements (Figure 5.3C) of supernatant samples revealed the strong absorbance of hBN-DNA in UV-region, where peak at 205 nm corresponds mainly to the DNA-hBN hybrids and 260 nm corresponds to the excess DNA in the supernatant sample of hBN dispersions. The average dispersion yield of hBN in PBS was estimated as 19.04 ± 5.10 % (Table C.1). SEM imaging of supernatant samples (Figure 5.4) further revealed the exfoliated DNA-coated hBN nanosheets in PBS. However, it is noted that SEM revealed the presence of a very few sheets of SDC-assisted hBN hybrids of supernatant samples on an imaging substrate unlike the hBN supernatant samples by DNA. This indicates that DNA is an efficient dispersing agent and resulted in higher concentrations of hBN sheets in PBS.

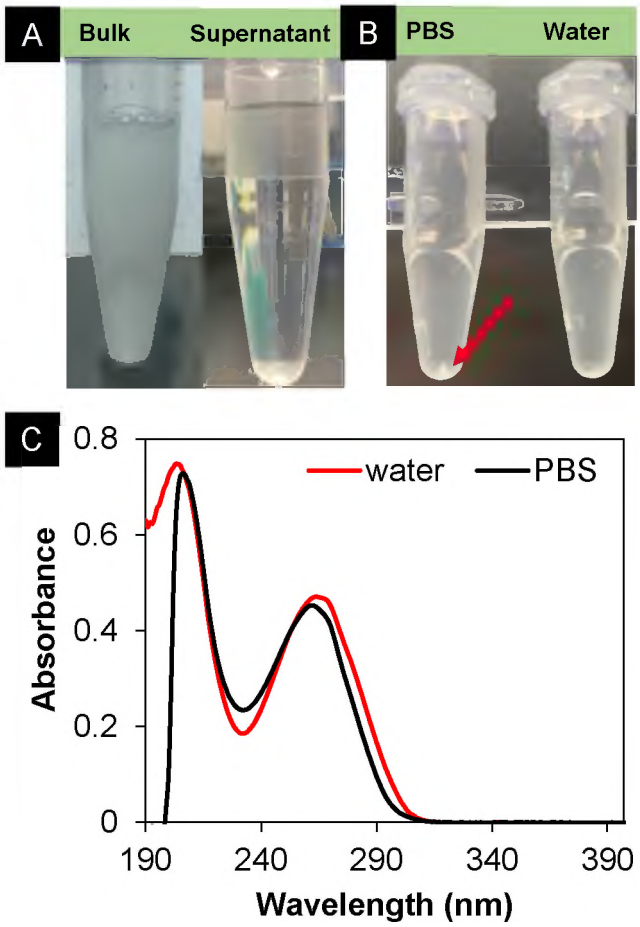

Figure 5.3. Photographs of two different dispersions of hBN-DNA complexes comparing (A) before (non-centrifuged) and after (supernatant) centrifugation (B) precipitated samples in water and PBS (C) Absorbance spectra of supernatant dispersions of DNA-hBN complexes in DI water and PBS.

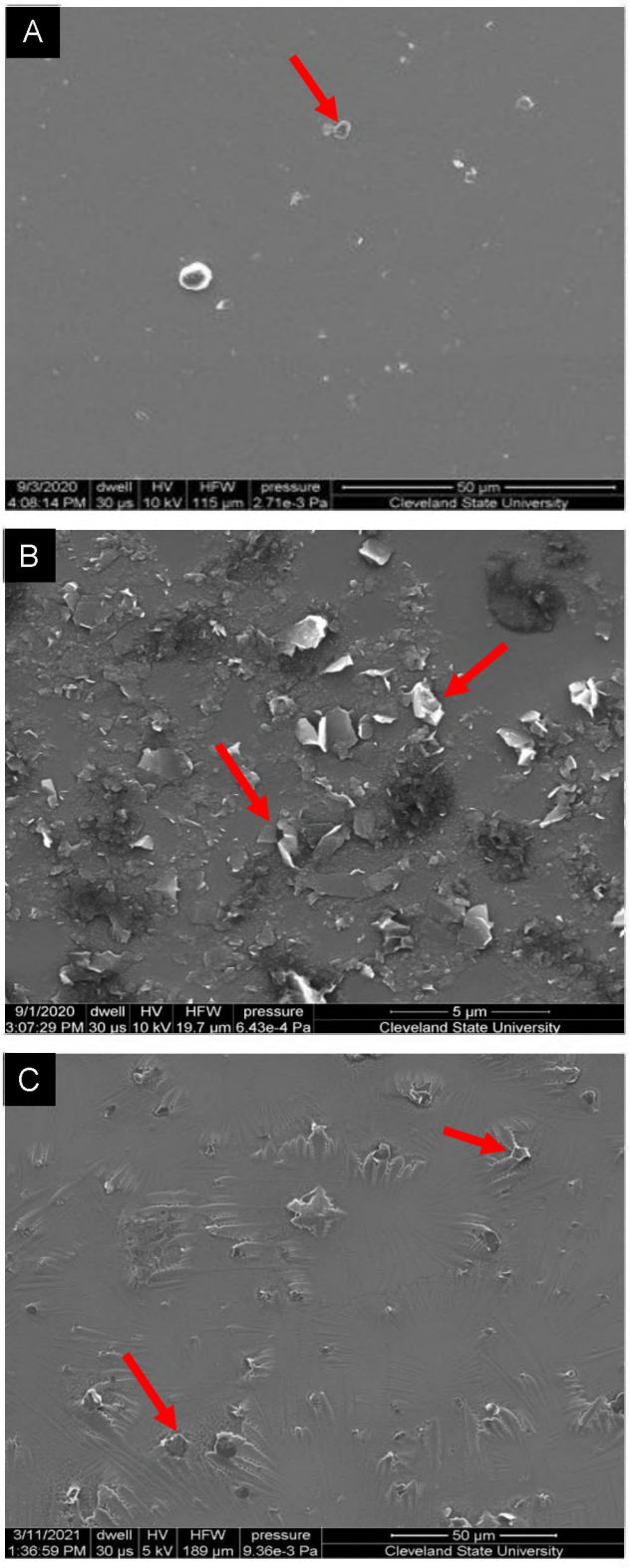

Figure 5.4. SEM images of supernatant samples of (A) SDC-coated hBN hybrids dispersed in water (B) DNA-coated hBN in PBS and (C) precipitated samples of DNA-hBN complexes in PBS.

5.4. Conclusion

In conclusion, we reported our work on developing dispersion methodology of hBN nanosheets using DNA. Our SEM and UV-vis measurements revealed the presence of individually dispersed hBN nanosheets in PBS. The extinction coefficient of crude DNA was estimated to be 16.14 $L \cdot mg^{-1} \cdot cm^{-1}$, which was further utilized to determine the average dispersion yield of cosmetic grade hBN sheets in PBS to be 19.04 ± 5.10 %. Our results elucidated that DNA is not only an efficient dispersing agent to disperse hBN nanosheets through noncovalent complexation but also help stabilize the nanosheets at high concentrations up to 8 mass %. Successful completion of work can lead to the development of potential hBN cosmetic and sunscreen applications with enhanced biocompatibility and multifunctionality.

CHAPTER VI

CONCLUSIONS AND RECOMMENDATIONS

In a nutshell, developing and understanding an efficient BN dispersion system stabilized by DNA, purification methodologies, self-assembly, and rheological characterization is essential to better maneuver the characteristics of a final applications. Since many biopolymers, especially DNA, being a strong dispersing agent for nanotubes like CNTs, incorporating the characteristics of DNA with added benefits including biocompatibility, green chemistry and multifunctionality to BN nanomaterials have broadened the wide range of potential applications. Our work on dispersion methodology and self-assembly of BN nanosystems using biomolecules like DNA provided a strong basis for BN-directed controlled architectures including films, fibers and composites while offering green chemistry, multifunctionality and enhanced biocompatibility.

6.1. Boron nitride nanotubes

In this thesis, the highly efficient dispersions of BNNTs were achieved in an aqueous environment using DNA and produced assembled solid films with improved nanotube alignment and purity. The aqueous dispersion of DNA-BNNTs suggests the surface coating of nanotubes by DNA and the fraction of DNA-BNNT hybrids in

dispersions depended on the BNNTs/DNA mass ratios. Purification of DNA-BNNT dispersions by membrane filtration resulted in the enrichment of dispersed nanotubes. Evaporation of concentrated, purified dispersions led to the formation of films comprising aligned DNA/BNNT bundles that has not been previously achieved. Thus, the results including the effective dispersion of BNNTs using DNA, purification and self-aligned solid BNNT films resulted in improved understanding of potential phase behavior and broadened the feasibility of bottom-up assembly studies.

We reported a simple yet highly efficient dispersions of boron nitride nanotubes by DNA in alcohol/water cosolvents via noncovalent complexation using a gentle bath sonication. Our results showed that the bath sonication not only unleashes the production of long pristine boron nitride nanotubes surface coated by DNA but also produces stable dispersions in IPA/water. Here, IPA played a pseudosurfactant role while solvating nanotubes in alcohol/water cosolvents, enabling the dispersion yield of boron nitride nanotubes as high as ≈ 48 % in the mixture of IPA/water with 60 % IPA. SEM imaging of solvent exchanged purified stable dispersions of boron nitride nanotubes in DI water revealed the inconsistencies in observed average lengths of DNA-coated boron nitride nanotubes and surfactant-coated boron nitride nanotubes by ≈ 21 %. While the average lengths of surfactant-coated boron nitride nanotubes differed by ≈ 26 % with viscosity average length of DNA-coated boron nitride nanotubes determined by rheology.

The DNA-BNNT liquid crystalline dispersions can be a favorable starting material for subsequent fabrication of BNNTs into films with improved alignment and morphologies for application developments. Our results provided a basis for the future work to study the phase behavior and microstructure of aqueous dispersions of DNA-

BNNT hybrids from dilute to possible lyotropic liquid crystalline phases using rheology and optical microscopy. However, further studies need to be conducted to accomplish the potential BNNT liquid crystalline formation. I propose the following recommendations:

Recent developments on the as-synthesized BNNTs by BNNT LLC., have been made to help improve the quality of a raw material, which are currently available in different forms including SP10-R, SP10-R-P and SP11-R and SP11-R-P. It is noted that the synthetic BNNT materials (P1-Beta) has ≈ 45.2 mass% of non-nanotube impurities as determined in this work Therefore, I propose to use the latest grade of raw material, which is the refined powder form to help accomplish the liquid phase behavior of BNNTs and their DNA-directed assembly.

The exact wrapping pattern of DNA (both ssDNA and dsDNA) on BNNTs is not clear, although the interaction would originate from the π-stacking interactions between BNNTs and DNA bases. Notably, the ionic nature of the BN bond,[7,9] wall number of BNNTs and different solvent conditions could lead to a different DNA conformation on the surface of few-wall BNNTs used in this study. More efforts should be made to better understand the DNA molecular interactions and conformations on the side wall of BNNT surface using high-resolution imaging techniques such as cryo-EM and molecular dynamic simulations potentially with a collaboration work to help further understand and optimize the dispersions of BNNTs.

SEM imaging has been extensively used in this work for characterizing length distributions of DNA-BNNTs complexes. However, SEM cannot distinguish individualization vs. bundles of parallel aligned nanotubes that will appear as individualized nanotubes especially at nanoscale. Therefore, I propose to use the following

two methods: 1) AFM where it will not only allow a precise measurement of the nanotube height in a horizontal surface (its diameter) but also, hundreds of nanotubes can be counted allowing for an appropriate statistical analysis of bundle size. 2) rheology, which is the representative of bulk sample ($\approx 10^{15}$ tubes), reproducible and less-time consuming.

The results including aqueous dispersion, purification and self-assembly of DNA-BNNTs resulted in improved understanding of the dispersion behavior of the ternary system (BNNT, DNA, water) as well as the feasibility of bottom-up assembly of BNNTs. However, it has also resulted in new questions on how the dispersion microstructure, phase behavior and rheology of BNNT dispersions behaves as a function of shear, temperature and concentration. Theoretically, BNNTs being rodlike 1-D nanostructures with a superior structural[46] and mechanical properties[224]–[226] including bending and shear moduli compared with other mesogenic nanocylinders like CNTs,[148] we hypothesize that BNNTs should form lyotropic liquid crystalline phases at sufficiently high concentrations. Although our previous work on self-assembly of BNNTs using DNA in water did not exhibit the birefringence characteristics that is pertinent to their potential liquid crystalline behavior, further experiments should be investigated to test for birefringence characteristics using optical microscopy. In addition, the critical phase transitions of potential liquid crystalline phases of DNA-BNNT hybrids will be determined using optical microscopy. I recommend using the magnification objectives of 10X, 20X, 40X and 60X for microscopy experiments with and without cross polarizers.

Understanding the phase behavior of potential lyotropic DNA-BNNT dispersions with shear flow and texture effects is required to improve the properties like nanotube alignment of their macroscopic assemblies such as films. The effect of shear and

temperature on liquid crystalline phases of DNA-BNNTs will be tested using rheometer, a powerful tool that can predict the critical phase boundaries and texture evolution of dispersions under the shear field. The samples will be characterized rheologically through amplitude sweep, frequency sweep, step rate and steady shear rate tests. The evolution of dispersion microstructure and the phase diagram of viscosity against BNNT concentrations at a shear rate of 0.1 s^{-1} will be developed which will help determine the critical phase transitions. All data will be acquired within linear viscoelastic (LVE) regions which can be obtained from the amplitude sweep test. The start-up of a shear flow indicated by viscosity vs. time will be conducted for BNNT dispersions over a wide range of concentrations at a constant shear rate. More importantly, at even higher concentrations, the key rheological characteristics will be compared to the well-known liquid crystalline dispersions of high molecular weight rod-like polymers and nanocylinders. It would be interesting to see the sensitivity of preparation method of DNA-BNNT dispersions including bulk and supernatant samples on the critical phase transitions and dispersion morphologies at different concentrations.

The potential liquid crystalline DNA-BNNT dispersions will be processed into macroscopic artifacts such as films using drop drying techniques (Section 2.6). The macroscopic BNNT films can be obtained by simple drop drying approach of sufficiently concentrated DNA-BNNT samples under the ambient conditions or vacuum oven. Here, the parameters including the type of substrate (e.g., glass slides, clean silicon wafer chips and copper tape), precursor concentration of DNA-BNNT hybrids will be optimized. It would be interesting to see the difference in alignment of BNNTs drop casted from dispersions of biphasic and LC phases. The temperature and pressure of the drying system

i.e., evaporation rate can be controlled using an enclosed cell with a small aperture. More importantly, DNA-BNNTs LC dispersions will be manually sheared by roller coating on a sample drying substrate to test the degree of nanotubes alignment and shear induced transitions in textures. The results from the recommended work will provide key insights to better improve the properties of aligned bulk materials consisting of nanocylinder building blocks.

6.2. Hexagonal-boron nitride nanosheets

In this thesis, we used natural DNA to help disperse hBN in PBS via sonication and centrifugation. We initially attempted to use mild sonication to disperse hBN sheets in PBS, but due to relatively high density of hBN compared to BNNTs, hBN sheets tend to settle at the bottom of the vial while bath sonication. As a result, an inefficient dispersion was observed visually. To overcome this, we used a probe tip sonication that utilize the acoustic energy that induces cavitation; the resulting flow fields exfoliate nanosheets from the parent material. Also, long sonication times lead to more exfoliation. In our work, probe tip sonication resulted in the increase in the dispersion yield of hBN nanosheets when compared to the dispersion prepared using solely bath sonication. The DNA-hBN complexes were characterized spectroscopically. Although, we used different solvents MeOH/water, EtOH/water, IPA/water, and water to disperse hBN using DNA and other dispersant molecules such as SDC and SDS surfactants. Unfortunately, the ultraviolet absorption and emission of hBN overlaps considerably with DNA, PEG, NaSCN, and mixtures of alcohol and DI water solvents by itself, making their study cumbersome. Additionally, we found that alcohols used in this study contributes to spectroscopic errors, especially while diluting samples for measurements. Therefore, a detailed investigation

should be conducted on a set of control experiments to better resolve the absorbance peak of DNA-hBN complexes from other components in the dispersion system. In addition, it is likely that hBN dispersions might require relatively more DNA molecules to stabilize high surface area hBN sheets compared to BNNTs, which was found to be optimum at BNNTs:DNA = 1:1 mass ratio. Therefore, further tests need to be conducted to determine the optimum mass ratio of hBN:DNA in the initial dispersion mixture.

The dispersions of hBN nanosheets stabilized by DNA were characterized by SEM in our preliminary work. Additional work on determining lateral size and thickness will be recommended using other imaging techniques such as AFM. In fact, more recently, the lateral size of 2D graphene oxide mono layered sheets was characterized using optical microscopy,[227] perhaps, could be a potential method to characterize the size distribution of hBN nanosheets. Moreover, it would be interesting to understand the surface wrapping/attachment conformation of DNA molecules on the surface of hBN sheets. This could be achieved using molecular dynamic simulations along with an experimental work of high-resolution imaging techniques such as cryo-EM. The thermogravimetric analysis can be further utilized to estimate the amount of DNA attached on the surface of hBN to help optimize the experimental conditions of hBN dispersions for improved stability and yield.

REFERENCES

[1] L. F. Dobrzhinetskaya *et al.*, "Qingsongite, natural cubic boron nitride: The first boron mineral from the Earth's mantle," *Am. Mineral.*, 2014.

[2] N. G. Chopra *et al.*, "Boron Nitride Nanotubes," *Science (80-.).*, vol. 269, no. 5226, pp. 966–967, 1995.

[3] Z. G. Chen *et al.*, "Novel boron nitride hollow nanoribbons," *ACS Nano*, 2008.

[4] Y. Qiu *et al.*, "Synthesis of continuous boron nitride nanofibers by solution coating electrospun template fibers," *Nanotechnology*, 2009.

[5] H. Zhang, J. Yu, Y. Chen, and J. F. Gerald, "Conical boron nitride nanorods synthesized via the ball-milling and annealing method," *J. Am. Ceram. Soc.*, 2006.

[6] O. Stéphan *et al.*, "Formation of small single-layer and nested BN cages under electron irradiation of nanotubes and bulk material," *Appl. Phys. A Mater. Sci. Process.*, 1998.

[7] C. Li *et al.*, "Magnesium-induced preparation of boron nitride nanotubes and their application in thermal interface materials," *Nanoscale*, 2019.

[8] H. Jiang, Z. Wang, H. Geng, X. Song, H. Zeng, and C. Zhi, "Highly Flexible and Self-Healable Thermal Interface Material Based on Boron Nitride Nanosheets and a Dual Cross-Linked Hydrogel," *ACS Appl. Mater. Interfaces*, 2017.

[9] J. Li *et al.*, "Porous boron nitride with a high surface area: Hydrogen storage and water treatment," *Nanotechnology*, 2013.

[10] S. Yu *et al.*, "Boron nitride-based materials for the removal of pollutants from aqueous solutions: A review," *Chemical Engineering Journal*. 2018.

[11] G. Lian, X. Zhang, H. Si, J. Wang, D. Cui, and Q. Wang, "Boron nitride ultrathin

fibrous nanonets: One-step synthesis and applications for ultrafast adsorption for water treatment and selective filtration of nanoparticles," *ACS Appl. Mater. Interfaces*, 2013.

[12] Q. Wang *et al.*, "Hexagonal boron nitride nanosheets doped pyroelectric ceramic composite for high-performance thermal energy harvesting," *Nano Energy*, 2019.

[13] G. J. Lee, M. K. Lee, J. J. Park, D. Y. Hyeon, C. K. Jeong, and K. Il Park, "Piezoelectric Energy Harvesting from Two-Dimensional Boron Nitride Nanoflakes," *ACS Appl. Mater. Interfaces*, 2019.

[14] M. M. Fiume *et al.*, "Safety Assessment of Boron Nitride as Used in Cosmetics," *International Journal of Toxicology*. 2015.

[15] L. M. S. Ansaloni and E. M. B. de Sousa, "Boron Nitride Nanostructured: Synthesis, Characterization and Potential Use in Cosmetics," *Mater. Sci. Appl.*, 2013.

[16] G. Elumalai, H. Noguchi, and K. Uosaki, "Electrocatalytic activity of various types of h-BN for the oxygen reduction reaction," *Phys. Chem. Chem. Phys.*, 2014.

[17] H. B. Cho *et al.*, "Modification of BN nanosheets and their thermal conducting properties in nanocomposite film with polysiloxane according to the orientation of BN," *Compos. Sci. Technol.*, 2011.

[18] J. Yu, X. Huang, C. Wu, X. Wu, G. Wang, and P. Jiang, "Interfacial modification of boron nitride nanoplatelets for epoxy composites with improved thermal properties," *Polymer (Guildf).*, 2012.

[19] Y. L. Zhou *et al.*, "Surface functionalization of cubic boron nitride films for biological sensing applications," *Appl. Phys. Lett.*, 2008.

[20] V. Raffa, G. Ciofani, and A. Cuschieri, "Enhanced low voltage cell electropermeabilization by boron nitride nanotubes," *Nanotechnology*, 2009.

[21] Q. Weng *et al.*, "Highly water-soluble, porous, and biocompatible boron nitrides for anticancer drug delivery," *ACS Nano*, 2014.

[22] G. Ao, J. K. Streit, J. A. Fagan, and M. Zheng, "Differentiating Left- and Right-Handed Carbon Nanotubes by DNA," *J. Am. Chem. Soc.*, 2016.

[23] S. Badaire *et al.*, "Liquid crystals of DNA-stabilized carbon nanotubes," *Advanced Materials*. 2005.

[24] E. Penzo *et al.*, "Directed Assembly of Single Wall Carbon Nanotube Field Effect Transistors," *ACS Nano*, 2016.

[25] M. L. Cohen and A. Zettl, "The physics of boron nitride nanotubes," *Phys. Today*, vol. 63, no. 11, pp. 34–38, 2010.

[26] M. W. Smith *et al.*, "Very long single- and few-walled boron nitride nanotubes via the pressurized vapor/condenser method," *Nanotechnology*, vol. 20, no. 50, p. 505604, 2009.

[27] R. Saito, G. Dresselhaus, M. Dresselahus, S. R, D. G, and D. M. S, *Physical Properties of Carbon Nanotubes*. 1998.

[28] and C. Z. Dmitri Golberg,* Yoshio Bando, Yang Huang, Takeshi Terao, Masanori Mitome, Chengchun Tang, "Boron nitride nanotubes and Nanosheets," *ACS Nano*, vol. 4, no. 6, pp. 2979–2993, 2010.

[29] X. Blase, A. Rubio, S. G. Louie, and M. L. Cohen, "Stability and band gap constancy of boron nitride nanotubes," *EPL*, vol. 28, no. 5, pp. 335–340, 1994.

[30] C. W. Chen, M. H. Lee, and S. J. Clark, "Band gap modification of single-walled

carbon nanotube and boron nitride nanotube under a transverse electric field," *Nanotechnology*, 2004.

[31] J. Zhang, K. P. Loh, S. W. Yang, and P. Wu, "Exohedral doping of single-walled boron nitride nanotube by atomic chemisorption," *Appl. Phys. Lett.*, 2005.

[32] W. An, X. Wu, J. L. Yang, and X. C. Zeng, "Adsorption and surface reactivity on single-walled boron nitride nanotubes containing stone-wales defects," *J. Phys. Chem. C*, 2007.

[33] X. Wu, J. L. Yang, and X. C. Zeng, "Adsorption of hydrogen molecules on the platinum-doped boron nitride nanotubes," *J. Chem. Phys.*, 2006.

[34] Y. Chen, J. Zou, S. J. Campbell, and G. Le Caer, "Boron nitride nanotubes: Pronounced resistance to oxidation," *Appl. Phys. Lett.*, vol. 84, no. 13, pp. 2430–2432, 2004.

[35] C. Zhi, Y. Bando, W. Wang, C. Tang, H. Kuwahara, and D. Golberg, "DNA-mediated assembly of boron nitride nanotubes," *Chem. - An Asian J.*, vol. 2, no. 12, pp. 1581–1585, 2007.

[36] C. H. Lee, J. Drelich, and Y. K. Yap, "Superhydrophobicity of boron nitride nanotubes grown on silicon substrates," *Langmuir*, 2009.

[37] A. Rubio, J. L. Corkill, and M. L. Cohen, "Theory of graphitic boron nitride nanotubes," *Phys. Rev. B*, vol. 49, no. 7, pp. 5081–5084, 1994.

[38] Y. Chen, L. T. Chadderton, J. F. Gerald, and J. S. Williams, "A solid-state process for formation of boron nitride nanotubes," *Appl. Phys. Lett.*, 1999.

[39] W. Han, Y. Bando, K. Kurashima, and T. Sato, "Synthesis of boron nitride nanotubes from carbon nanotubes by a substitution reaction," *Appl. Phys. Lett.*,

1998.

[40] A. Pakdel, C. Zhi, Y. Bando, T. Nakayama, and D. Golberg, "A comprehensive analysis of the CVD growth of boron nitride nanotubes," *Nanotechnology*, vol. 23, no. 21, 2012.

[41] A. Loiseau, F. Willaime, N. Demoncy, G. Hug, and H. Pascard, "Boron nitride nanotubes with reduced numbers of layers synthesized by arc discharge," *Phys. Rev. Lett.*, vol. 76, no. 25, pp. 4737–4740, 1996.

[42] S. M. C. Vieira and D. L. Carroll, "Purification of Boron Nitride Multiwalled Nanotubes," *J. Nanosci. Nanotechnol.*, vol. 7, p. 331803322, 2007.

[43] D. M. Marincel *et al.*, "Scalable Purification of Boron Nitride Nanotubes via Wet Thermal Etching," *Chem. Mater.*, 2019.

[44] M. Adnan *et al.*, "Extraction of Boron Nitride Nanotubes and Fabrication of Macroscopic Articles Using Chlorosulfonic Acid," *Nano Lett.*, 2018.

[45] K. S. Kim *et al.*, "Hydrogen-catalyzed, pilot-scale production of small-diameter boron nitride nanotubes and their macroscopic assemblies," *ACS Nano*, vol. 8, no. 6, pp. 6211–6220, 2014.

[46] H. Chen, Y. Chen, J. Yu, and J. S. Williams, "Purification of boron nitride nanotubes," *Chem. Phys. Lett.*, vol. 425, no. 4–6, pp. 315–319, 2006.

[47] O. Kleinerman *et al.*, "Dissolution and Characterization of Boron Nitride Nanotubes in Superacid," *Langmuir*, p. acs.langmuir.7b03461, 2017.

[48] W. Lei, V. N. Mochalin, D. Liu, S. Qin, Y. Gogotsi, and Y. Chen, "Boron nitride colloidal solutions, ultralight aerogels and freestanding membranes through one-step exfoliation and functionalization," *Nat. Commun.*, 2015.

[49] N. Alem, R. Erni, C. Kisielowski, M. D. Rossell, W. Gannett, and A. Zettl, "Atomically thin hexagonal boron nitride probed by ultrahigh-resolution transmission electron microscopy," *Phys. Rev. B - Condens. Matter Mater. Phys.*, 2009.

[50] C. Li, Y. Bando, C. Zhi, Y. Huang, and D. Golberg, "Thickness-dependent bending modulus of hexagonal boron nitride nanosheets," *Nanotechnology*, 2009.

[51] A. Nag, K. Raidongia, K. P. S. S. Hembram, R. Datta, U. V. Waghmare, and C. N. R. Rao, "Graphene analogues of BN: Novel synthesis and properties," *ACS Nano*, 2010.

[52] C. A. De Los Reyes *et al.*, "Tunable Alkylation of White Graphene (Hexagonal Boron Nitride) Using Reductive Conditions," *J. Phys. Chem. C*, 2019.

[53] A. Falin *et al.*, "Mechanical properties of atomically thin boron nitride and the role of interlayer interactions," *Nat. Commun.*, 2017.

[54] I. Jo *et al.*, "Thermal conductivity and phonon transport in suspended few-layer hexagonal boron nitride," *Nano Lett.*, 2013.

[55] K. Watanabe, T. Taniguchi, and H. Kanda, "Direct-bandgap properties and evidence for ultraviolet lasing of hexagonal boron nitride single crystal," *Nat. Mater.*, 2004.

[56] L. H. Li, J. Cervenka, K. Watanabe, T. Taniguchi, and Y. Chen, "Strong oxidation resistance of atomically thin boron nitride nanosheets," *ACS Nano*, 2014.

[57] X. Wang, C. Zhi, Q. Weng, Y. Bando, and D. Golberg, "Boron nitride nanosheets: Novel syntheses and applications in polymeric composites," in *Journal of Physics: Conference Series*, 2013.

[58] W. Lei *et al.*, "Oxygen-doped boron nitride nanosheets with excellent performance in hydrogen storage," *Nano Energy*, 2014.

[59] Z. G. Chen and J. Zou, "Field emitters: Ultrathin BN nanosheets protruded from BN fibers," *J. Mater. Chem.*, 2011.

[60] T. C. Doan, J. Li, J. Y. Lin, and H. X. Jiang, "Growth and device processing of hexagonal boron nitride epilayers for thermal neutron and deep ultraviolet detectors," *AIP Adv.*, 2016.

[61] K. Uosaki *et al.*, "Boron nitride nanosheet on gold as an electrocatalyst for oxygen reduction reaction: Theoretical suggestion and experimental proof," *J. Am. Chem. Soc.*, 2014.

[62] W. Lei, D. Portehault, D. Liu, S. Qin, and Y. Chen, "Porous boron nitride nanosheets for effective water cleaning," *Nat. Commun.*, 2013.

[63] C.-Y. Su, H.-Z. Tang, K. Chu, and C.-K. Lin, "Cosmetic properties of TiO2/mica-BN composite powder prepared by spray drying," *Ceram. Int.*, vol. 40, no. 5, pp. 6903–6911, 2014.

[64] T. Masui, M. Yamamoto, T. Sakata, H. Mori, and G. ya Adachi, "Synthesis of BN-coated CeO2 fine powder as a new UV blocking material," *J. Mater. Chem.*, 2000.

[65] O. R. Lourie, C. R. Jones, B. M. Bartlett, P. C. Gibbons, R. S. Ruoff, and W. E. Buhro, "CVD growth of boron nitride nanotubes," *Chem. Mater.*, vol. 12, no. 7, pp. 1808–1810, 2000.

[66] J. Cumings and A. Zettl, "Mass-production of boron nitride double-wall nanotubes and nanococoons," *Chem. Phys. Lett.*, 2000.

[67] R. Arenal, O. Stephan, J. Lou Cochon, and A. Loiseau, "Root-growth mechanism

for single-walled boron nitride nanotubes in laser vaporization technique," *J. Am. Chem. Soc.*, vol. 129, no. 51, pp. 16183–16189, 2007.

[68] D. Golberg, Y. Bando, M. Eremets, K. Takemura, K. Kurashima, and H. Yusa, "Nanotubes in boron nitride laser heated at high pressure," *Appl. Phys. Lett.*, 1996.

[69] C. Y. Zhang, X. L. Zhong, J. B. Wang, and G. W. Yang, "Room-temperature growth of cubic nitride boron film by RF plasma enhanced pulsed laser deposition," *Chem. Phys. Lett.*, 2003.

[70] R. Haubner, M. Wilhelm, R. Weissenbacher, and B. Lux, "Boron Nitrides — Properties, Synthesis and Applications," 2002.

[71] C. Zhi, Y. Bando, C. Tang, H. Kuwahara, and D. Golberg, "Large-scale fabrication of boron nitride nanosheets and their utilization in polymeric composites with improved thermal and mechanical properties," *Adv. Mater.*, 2009.

[72] T. Guo, P. Nikolaev, A. G. Rinzler, D. Tomanek, D. T. Colbert, and R. E. Smalley, "Self-assembly of tubular fullerenes," *J. Phys. Chem.*, 1995.

[73] Z. Zheng, M. C. Cox, and B. Li, "Surface modification of hexagonal boron nitride nanomaterials: a review," *Journal of Materials Science*. 2018.

[74] Z. Cui, A. J. Oyer, A. J. Glover, H. C. Schniepp, and D. H. Adamson, "Large scale thermal exfoliation and functionalization of boron nitride," *Small*, 2014.

[75] C. Zhi, N. Hanagata, Y. Bando, and D. Golberg, "Dispersible shortened boron nitride nanotubes with improved molecule-loading capacity," *Chem. - An Asian J.*, 2011.

[76] A. Pakdel, Y. Bando, and D. Golberg, "Plasma-assisted interface engineering of boron nitride nanostructure films," *ACS Nano*, 2014.

[77] X. J. Dai *et al.*, "Controlled surface modification of boron nitride nanotubes," *Nanotechnology*, 2011.

[78] L. Li, X. W. Liu, X. J. J. Dai, L. H. Li, and Y. Chen, "Surface wetting processing on BNNT films by selective plasma modes," *Chinese Sci. Bull.*, 2013.

[79] Y. Lin, T. V. Williams, W. Cao, H. E. Elsayed-Ali, and J. W. Connell, "Defect functionalization of hexagonal boron nitride nanosheets," *J. Phys. Chem. C*, 2010.

[80] X. Lu and Z. Chen, "Curved Pi-conjugation, aromaticity, and the related chemistry of small fullerenes (<C60) and single-walled carbon nanotubes," *Chemical Reviews*. 2005.

[81] Y. Z. Tan, S. Y. Xie, R. Bin Huang, and L. S. Zheng, "The stabilization of fused-pentagon fullerene molecules," *Nature Chemistry*. 2009.

[82] C. Y. Zhi, Y. Bando, T. Terao, C. C. Tang, H. Kuwahara, and D. Golberg, "Chemically activated boron nitride nanotubes," *Chem. - An Asian J.*, 2009.

[83] Y. Lin, T. V. Williams, T. B. Xu, W. Cao, H. E. Elsayed-Ali, and J. W. Connell, "Aqueous dispersions of few-layered and monolayered hexagonal boron nitride nanosheets from sonication-assisted hydrolysis: Critical role of water," *J. Phys. Chem. C*, vol. 115, no. 6, pp. 2679–2685, 2011.

[84] T. Sainsbury *et al.*, "Oxygen radical functionalization of boron nitride nanosheets," *J. Am. Chem. Soc.*, 2012.

[85] T. Ikuno, T. Sainsbury, D. Okawa, J. M. J. Fréchet, and A. Zettl, "Amine-functionalized boron nitride nanotubes," *Solid State Commun.*, 2007.

[86] Y. Liao *et al.*, "Chemical sharpening, shortening, and unzipping of boron nitride nanotubes," *Adv. Funct. Mater.*, 2014.

[87] S. Y. Xie, W. Wang, K. A. S. Fernando, X. Wang, Y. Lin, and Y. P. Sun, "Solubilization of boron nitride nanotubes," *Chem. Commun.*, 2005.

[88] Y. Lin, T. V. Williams, and J. W. Connell, "Soluble, exfoliated hexagonal boron nitride nanosheets," *J. Phys. Chem. Lett.*, 2010.

[89] T. Sainsbury *et al.*, "Dibromocarbene functionalization of boron nitride nanosheets: Toward band gap manipulation and nanocomposite applications," *Chem. Mater.*, 2014.

[90] H. Shin, J. Guan, M. Z. Zgierski, K. S. Kim, C. T. Kingston, and B. Simard, "Covalent Functionalization of Boron Nitride Nanotubes via Reduction Chemistry," *ACS Nano*, 2015.

[91] C. Zhi *et al.*, "Covalent functionalization: Towards soluble multiwalled boron nitride nanotubes," *Angew. Chemie - Int. Ed.*, vol. 44, no. 48, pp. 7932–7935, 2005.

[92] C. Tang *et al.*, "Fluorination and electrical conductivity of BN nanotubes," *J. Am. Chem. Soc.*, 2005.

[93] X. Huang, C. Zhi, P. Jiang, D. Golberg, Y. Bando, and T. Tanaka, "Polyhedral oligosilsesquioxane-modified boron nitride nanotube based epoxy nanocomposites: An ideal dielectric material with high thermal conductivity," *Adv. Funct. Mater.*, 2013.

[94] C. A. De Los Reyes *et al.*, "Chemical Decoration of Boron Nitride Nanotubes Using the Billups-Birch Reaction: Toward Enhanced Thermostable Reinforced Polymer and Ceramic Nanocomposites," *ACS Appl. Nano Mater.*, 2018.

[95] S. Velayudham *et al.*, "Noncovalent functionalization of boron nitride nanotubes

with poly(p-phenylene-ethynylene)s and polythiophene," *ACS Appl. Mater. Interfaces*, 2010.

[96] A. Star *et al.*, "Noncovalent side-wall functionalization of single-walled carbon nanotubes," *Macromolecules*, 2003.

[97] R. J. Chen, Y. Zhang, D. Wang, and H. Dai, "Noncovalent sidewall functionalization of single-walled carbon nanotubes for protein immobilization [11]," *Journal of the American Chemical Society*. 2001.

[98] C. Xing, L. Zhao, J. You, W. Dong, X. Cao, and Y. Li, "Impact of ionic liquid-modified multiwalled carbon nanotubes on the crystallization behavior of poly(vinylidene fluoride)," *J. Phys. Chem. B*, 2012.

[99] A. Llanes-Pallas *et al.*, "Modular engineering of H-bonded supramolecular polymers for reversible functionalization of carbon nanotubes," *J. Am. Chem. Soc.*, 2011.

[100] J. Yu, Y. Chen, and B. M. Cheng, "Dispersion of boron nitride nanotubes in aqueous solution with the help of ionic surfactants," *Solid State Commun.*, 2009.

[101] H. B. Kulkarni, P. B. Tambe, and G. M. Joshi, "Influence of surfactant assisted exfoliation of hexagonal boron nitride nanosheets on mechanical, thermal and dielectric properties of epoxy Nanocomposites," *Compos. Interfaces*, 2020.

[102] A. Chae, S. J. Park, B. Min, and I. In, "Enhanced dispersion of boron nitride nanosheets in aqueous media by using bile acid-based surfactants," *Mater. Res. Express*, 2018.

[103] D. Kim, T. Sawada, C. Zhi, Y. Bando, D. Golberg, and T. Serizawa, "Dispersion of Boron Nitride Nanotubes in Aqueous Solution by Simple Aromatic Molecules,"

J. Nanosci. Nanotechnol., vol. 14, no. 4, pp. 3028–3033, 2014.

[104] J. S. Maria Nithya and A. Pandurangan, "Aqueous dispersion of polymer coated boron nitride nanotubes and their antibacterial and cytotoxicity studies," *RSC Adv.*, vol. 4, no. 60, pp. 32031–32046, 2014.

[105] P. Ma and J. T. Spencer, "Non-covalent stabilization and functionalization of boron nitride nanosheets (BNNSs) by organic polymers: formation of complex BNNSs-containing structures," *J. Mater. Sci.*, 2015.

[106] N. A. Rice *et al.*, "Noncovalent functionalization of boron nitride nanotubes using poly(2,7-carbazole)s," *J. Polym. Sci.*, 2020.

[107] E. C. Anota, Y. Tlapale, M. S. Villanueva, and J. A. R. Márquez, "Non-covalent functionalization of hexagonal boron nitride nanosheets with guanine," *J. Mol. Model.*, 2015.

[108] Z. Gao, C. Zhi, Y. Bando, D. Golberg, and T. Serizawa, "Isolation of individual boron nitride nanotubes via peptide wrapping," *J. Am. Chem. Soc.*, vol. 132, no. 14, pp. 4976–4977, 2010.

[109] Z. Gao, T. Sawada, C. Zhi, Y. Bando, D. Golberg, and T. Serizawa, "Nucleotide-assisted decoration of boron nitride nanotubes with semiconductor quantum dots endows valuable visible-light emission in aqueous solution," *Soft Matter*, 2011.

[110] S. Pal, S. R. C. Vivekchand, A. Govindaraj, and C. N. R. Rao, "Functionalization and solubilization of BN nanotubes by interaction with Lewis bases," *J. Mater. Chem.*, 2007.

[111] Z. Gao *et al.*, "Noncovalent functionalization of boron nitride nanotubes using water-soluble synthetic polymers and the subsequent preparation of

superhydrophobic surfaces," *Polym. J.*, 2013.

[112] A. D. Smith McWilliams *et al.*, "Surfactant-assisted individualization and dispersion of boron nitride nanotubes," *Nanoscale Adv.*, 2019.

[113] A. D. Smith McWilliams *et al.*, "Understanding the Exfoliation and Dispersion of Hexagonal Boron Nitride Nanosheets by Surfactants: Implications for Antibacterial and Thermally Resistant Coatings," *ACS Appl. Nano Mater.*, 2021.

[114] T. Morishita and H. Okamoto, "Facile Exfoliation and Noncovalent Superacid Functionalization of Boron Nitride Nanosheets and Their Use for Highly Thermally Conductive and Electrically Insulating Polymer Nanocomposites," *ACS Appl. Mater. Interfaces*, 2016.

[115] L. Zhao *et al.*, "Aqueous-Phase Exfoliation and Functionalization of Boron Nitride Nanosheets Using Tannic Acid for Thermal Management Applications," *Ind. Eng. Chem. Res.*, 2020.

[116] M. Adnan *et al.*, "Extraction of Boron Nitride Nanotubes and Fabrication of Macroscopic Articles Using Chlorosulfonic Acid," *Nano Lett.*, vol. 18, no. 3, pp. 1615–1619, 2018.

[117] O. Kleinerman *et al.*, "Dissolution and Characterization of Boron Nitride Nanotubes in Superacid," *Langmuir*, 2017.

[118] Z. Gao, C. Zhi, Y. Bando, D. Golberg, and T. Serizawa, "Noncovalent functionalization of disentangled boron nitride nanotubes with flavin mononucleotides for strong and stable visible-light emission in aqueous solution," *ACS Appl. Mater. Interfaces*, 2011.

[119] C. H. Lee, D. Zhang, and Y. K. Yap, "Functionalization, dispersion, and cutting of

boron nitride nanotubes in water," *J. Phys. Chem. C*, 2012.

[120] L. Liang, W. Hu, Z. Zhang, and J. W. Shen, "Theoretic Study on Dispersion Mechanism of Boron Nitride Nanotubes by Polynucleotides," *Sci. Rep.*, vol. 6, pp. 1–9, 2016.

[121] P. V. Jena, M. M. Safaee, D. A. Heller, and D. Roxbury, "DNA-Carbon Nanotube Complexation Affinity and Photoluminescence Modulation Are Independent," *ACS Appl. Mater. Interfaces*, 2017.

[122] X. Tu, S. Manohar, A. Jagota, and M. Zheng, "DNA sequence motifs for structure-specific recognition and separation of carbon nanotubes," *Nature*, 2009.

[123] A. N. G. Parra-Vasquez *et al.*, "Simple length determination of single-walled carbon nanotubes by viscosity measurements in dilute suspensions," *Macromolecules*, 2007.

[124] Q. Wu, X. Li, S. Fu, Q. Li, and S. Wang, "Estimation of aspect ratio of cellulose nanocrystals by viscosity measurement: influence of surface charge density and NaCl concentration," *Cellulose*, 2017.

[125] A. D. Smith McWilliams, Z. Tang, S. Ergülen, C. A. de Los Reyes, A. A. Martí, and M. Pasquali, "Real-Time Visualization and Dynamics of Boron Nitride Nanotubes Undergoing Brownian Motion," *J. Phys. Chem. B*, 2020.

[126] V. A. Davis *et al.*, "Phase Behavior and Rheology of SWNT in Superacids," *Macromolecules*, vol. 37, pp. 154–160, 2004.

[127] G. Ao, D. Nepal, and V. A. Davis, "Rheology of lyotropic cholesteric liquid crystal forming single-wall carbon nanotube dispersions stabilized by double-stranded DNA," *Rheol. Acta*, vol. 55, no. 9, pp. 717–725, 2016.

[128] A. M. Wierenga and A. P. Philipse, "Low-shear viscosities of dilute dispersions of colloidal rodlike silica particles in cyclohexane," *J. Colloid Interface Sci.*, 1996.

[129] Y. Boluk, R. Lahiji, L. Zhao, and M. T. McDermott, "Suspension viscosities and shape parameter of cellulose nanocrystals (CNC)," *Colloids Surfaces A Physicochem. Eng. Asp.*, 2011.

[130] P. Axelrad and K. M. Larson, "The structure and rheology of complex fluids," *Eos, Transactions American Geophysical Union*. 2006.

[131] Q. Wu *et al.*, "Rheological behavior of cellulose nanocrystal suspension: Influence of concentration and aspect ratio," *J. Appl. Polym. Sci.*, 2014.

[132] L. C. F. Andrade, J. A. Petronílio, C. E. D. A. Maneschy, and D. O. D. A. Cruz, "The carreau-yasuda fluids: A skin friction equation for turbulent flow in pipes and kolmogorov dissipative scales," *J. Brazilian Soc. Mech. Sci. Eng.*, 2007.

[133] J. G. Kirkwood and P. L. Auer, "The visco-elastic properties of solutions of rod-like macromolecules," *J. Chem. Phys.*, 1951.

[134] M. Pasquali, V. A. Davis, I. Stepanek-Basset, A. N. G. Parra-Vasquez, and R. H. Hauge, "Method and apparatus for determining the length of single-walled carbon nanotubes." Google Patents, 08-Nov-2005.

[135] A. Schindler, J. Brill, N. Fruehauf, J. P. Novak, and Z. Yaniv, "Solution-deposited carbon nanotube layers for flexible display applications," *Phys. E Low-Dimensional Syst. Nanostructures*, 2007.

[136] M. Jeong, K. Lee, E. Choi, A. Kim, and S. B. Lee, "Spray-coated carbon nanotube thin-film transistors with striped transport channels," *Nanotechnology*, 2012.

[137] Y. Li, T. Yu, T. Pui, P. Chen, L. Zheng, and K. Liao, "Fabrication of transparent

and conductive carbon nanotube/polyvinyl butyral films by a facile solution surface dip coating method," *Nanoscale*, vol. 3, no. 6, pp. 2469–2471, 2011.

[138] J. W. Jo, J. W. Jung, J. U. Lee, and W. H. Jo, "Fabrication of highly conductive and transparent thin films from single-walled carbon nanotubes using a new non-ionic surfactant via spin coating," *ACS Nano*, 2010.

[139] C. Luo *et al.*, "Flexible carbon nanotube-polymer composite films with high conductivity and superhydrophobicity made by solution process," *Nano Lett.*, 2008.

[140] L. Fu and A. M. Yu, "Carbon nanotubes based thin films: Fabrication, characterization and applications," *Rev. Adv. Mater. Sci.*, 2014.

[141] K. S. Kim *et al.*, "Polymer nanocomposites from free-standing, macroscopic boron nitride nanotube assemblies," *RSC Adv.*, 2015.

[142] N. Behabtu *et al.*, "Strong, light, multifunctional fibers of carbon nanotubes with ultrahigh conductivity," *Science (80-.).*, 2013.

[143] B. Vigolo *et al.*, "Macroscopic fibers and ribbons of oriented carbon nanotubes," *Science (80-.).*, 2000.

[144] G. Ao, D. Nepal, M. Aono, and V. A. Davis, "Cholesteric and nematic liquid crystalline phase behavior of double-stranded DNA stabilized single-walled carbon nanotube dispersions," *ACS Nano*, vol. 5, no. 2, pp. 1450–1458, 2011.

[145] L. S. Li, M. Marjanska, G. H. J. Park, A. Pines, and A. P. Alivisatos, "Isotropic-liquid crystalline phase diagram of a CdSe nanorod solution," *J. Chem. Phys.*, 2004.

[146] T. Xu and V. A. Davis, "Liquid crystalline phase behavior of silica nanorods in

dimethyl sulfoxide and water," *Langmuir*, 2014.

[147] P. Jaffrennou *et al.*, "Optical properties of multiwall boron nitride nanotubes," *Phys. status solidi*, vol. 244, no. 11, pp. 4147–4151, 2007.

[148] L. Vaccarini, C. Goze, L. Henrard, E. Hernández, P. Bernier, and A. Rubio, "Mechanical and electronic properties of carbon and boron-nitride nanotubes," *Carbon N. Y.*, vol. 38, no. 11, pp. 1681–1690, 2000.

[149] T. Terao *et al.*, "Alignment of Boron Nitride Nanotubes in Polymeric Composite Films for Thermal Conductivity Improvement," *J. Phys. Chem. C*, vol. 114, pp. 4340–4344, 2010.

[150] X. Zeng, J. Sun, Y. Yao, R. Sun, J. Bin Xu, and C. P. Wong, "A Combination of Boron Nitride Nanotubes and Cellulose Nanofibers for the Preparation of a Nanocomposite with High Thermal Conductivity," *ACS Nano*, vol. 11, no. 5, pp. 5167–5178, 2017.

[151] K. S. Kim *et al.*, "Scalable manufacturing of boron nitride nanotubes and their assemblies: A review," *Semiconductor Science and Technology*. 2017.

[152] A. Fathalizadeh, T. Pham, W. Mickelson, and A. Zettl, "Scaled synthesis of boron nitride nanotubes, nanoribbons, and nanococoons using direct feedstock injection into an extended-pressure, inductively-coupled thermal plasma," *Nano Lett.*, 2014.

[153] A. L. Tiano *et al.*, "Boron nitride nanotube: synthesis and applications," no. Cvd, p. 906006, 2014.

[154] Z. Gao, C. Zhi, Y. Bando, D. Golberg, and T. Serizawa, "Functionalization of boron nitride nanotubes for applications in nanobiomedicine," in *Boron Nitride Nanotubes in Nanomedicine*, 2016.

[155] C. Y. Khripin, N. Arnold-Medabalimi, and M. Zheng, "Molecular-crowding-induced clustering of DNA-wrapped carbon nanotubes for facile length fractionation," *ACS Nano*, vol. 5, no. 10, pp. 8258–8266, 2011.

[156] J. K. Streit, J. A. Fagan, and M. Zheng, "A Low Energy Route to DNA-Wrapped Carbon Nanotubes via Replacement of Bile Salt Surfactants," *Anal. Chem.*, 2017.

[157] S. Badaire *et al.*, "Liquid crystals of DNA-stabilized carbon nanotubes," *Advanced Materials*. 2005.

[158] S. Burge, G. N. Parkinson, P. Hazel, A. K. Todd, and S. Neidle, "Quadruplex DNA: Sequence, topology and structure," *Nucleic Acids Res.*, 2006.

[159] S. Iliafar, J. Mittal, D. Vezenov, and A. Jagota, "Interaction of single-stranded DNA with curved carbon nanotube is much stronger than with flat graphite," *J. Am. Chem. Soc.*, 2014.

[160] M. M. Safaee, M. Gravely, C. Rocchio, M. Simmeth, and D. Roxbury, "DNA Sequence Mediates Apparent Length Distribution in Single-Walled Carbon Nanotubes," *ACS Appl. Mater. Interfaces*, 2019.

[161] Y. Kato, A. Inoue, Y. Niidome, and N. Nakashima, "Thermodynamics on soluble carbon nanotubes: How do DNA molecules replace surfactants on carbon nanotubes?," *Sci. Rep.*, 2012.

[162] S. Kruss *et al.*, "Neurotransmitter detection using corona phase molecular recognition on fluorescent single-walled carbon nanotube sensors," *J. Am. Chem. Soc.*, 2014.

[163] L. Wirtz, A. Rubio, R. De La Concha, and A. Loiseau, "Ab initio calculations of the lattice dynamics of boron nitride nanotubes," *Phys. Rev. B - Condens. Matter*

Mater. Phys., 2003.

[164] S. C. Glotzer and M. J. Solomon, "Anisotropy of building blocks and their assembly into complex structures," *Nat. Mater.*, 2007.

[165] V. N. Manoharan, "Colloidal matter: Packing, geometry, and entropy," *Science*. 2015.

[166] V. Davis, "Liquid crystalline assembly of nanocylinders," *J. Mater. Res.*, vol. 26, no. June 2010, pp. 140–153, 2011.

[167] L. M. Ericson *et al.*, "Macroscopic, neat, single-walled carbon nanotube fibers," *Science (80-.).*, 2004.

[168] C. Zhang *et al.*, "Self-Assembled Boron Nitride Nanotube Reinforced Graphene Oxide Aerogels for Dielectric Nanocomposites with High Thermal Management Capability," *ACS Appl. Mater. Interfaces*, 2020.

[169] P. Wang *et al.*, "Enhanced In-Plane Thermal Conductance of Thin Films Composed of Coaxially Combined Single-Walled Carbon Nanotubes and Boron Nitride Nanotubes," *ACS Nano*, 2020.

[170] L. Liang *et al.*, "Computer simulation of water desalination through boron nitride nanotubes," *Phys. Chem. Chem. Phys.*, 2017.

[171] L. Zhang *et al.*, "Understanding the effect of chemical modification on water desalination in boron nitride nanotubes via molecular dynamics simulation," *Desalination*. 2019.

[172] H. Cho *et al.*, "Single- and double-walled boron nitride nanotubes: Controlled synthesis and application for water purification," *Sci. Rep.*, 2020.

[173] M. M. Rahman *et al.*, "High temperature and high rate lithium-ion batteries with

boron nitride nanotubes coated polypropylene separators," *Energy Storage Mater.*, 2019.

[174] M. Kıvanç, B. Barutca, A. T. Koparal, Y. Göncü, S. H. Bostancı, and N. Ay, "Effects of hexagonal boron nitride nanoparticles on antimicrobial and antibiofilm activities, cell viability," *Mater. Sci. Eng. C*, 2018.

[175] W. M. da Silva *et al.*, "Boron nitride nanotubes radiolabeled with 153Sm and 159Gd: Potential application in nanomedicine," *Appl. Radiat. Isot.*, 2020.

[176] G. Ciofani, S. Danti, G. G. Genchi, B. Mazzolai, and V. Mattoli, "Boron nitride nanotubes: Biocompatibility and potential spill-over in nanomedicine," *Small*. 2013.

[177] Y. Martinez Rubi, Z. J. Jakubek, M. Chen, S. Zou, and B. Simard, "Quality assessment of bulk boron nitride nanotubes for advancing research, commercial, and industrial applications," *ACS Appl. Nano Mater.*, 2019.

[178] V. R. Kode *et al.*, "Purification and Assembly of DNA-Stabilized Boron Nitride Nanotubes into Aligned Films," *ACS Appl. Nano Mater.*, 2019.

[179] J. Augustine *et al.*, "Assessing size-dependent cytotoxicity of boron nitride nanotubes using a novel cardiomyocyte AFM assay," *Nanoscale Adv.*, 2019.

[180] C. S. Torres Castillo, C. Bruel, and J. R. Tavares, "Chemical affinity and dispersibility of boron nitride nanotubes," *Nanoscale Adv.*, 2020.

[181] A. L. Tiano *et al.*, "Thermodynamic approach to boron nitride nanotube solubility and dispersion," *Nanoscale*, vol. 8, no. 7, pp. 4348–4359, 2016.

[182] K. R. Hinkle and F. R. Phelan, "Solvation of Carbon Nanoparticles in Water/Alcohol Mixtures: Using Molecular Simulation to Probe Energetics,

Structure, and Dynamics," *J. Phys. Chem. C*, 2017.

[183] T. Habib *et al.*, "Cosolvents as Liquid Surfactants for Boron Nitride Nanosheet (BNNS) Dispersions," *Langmuir*, 2016.

[184] X. Nie, G. Li, Z. Jiang, W. Li, T. Ouyang, and J. Wang, "Co-solvent exfoliation of hexagonal boron nitride: Effect of raw bulk boron nitride size and co-solvent composition," *Nanomaterials*, 2020.

[185] K. G. Zhou, N. N. Mao, H. X. Wang, Y. Peng, and H. L. Zhang, "A mixed-solvent strategy for efficient exfoliation of inorganic graphene analogues," *Angew. Chemie - Int. Ed.*, 2011.

[186] E. J. Petersen, X. Tu, M. Dizdaroglu, M. Zheng, and B. C. Nelson, "Protective roles of single-wall carbon nanotubes in ultrasonication-induced DNA base damage," *Small*, 2013.

[187] A. N. G. Parra-Vasquez, J. G. Duque, M. J. Green, and M. Pasquali, "Assessment of length and bundle distribution of dilute single-walled carbon nanotubes by viscosity measurements," *AIChE J.*, 2014.

[188] R. R Development Core Team, *R: A Language and Environment for Statistical Computing*. 2011.

[189] C. Zhi, Y. Bando, C. Tang, and D. Golberg, "Specific heat capacity and density of multi-walled boron nitride nanotubes by chemical vapor deposition," *Solid State Commun.*, 2011.

[190] M. Mutz, E. Eastwood, and M. D. Dadmun, "Quantifying the solubility of boron nitride nanotubes and sheets with static light scattering and refractometry," *J. Phys. Chem. C*, 2013.

[191] M. Doi and S. F. Edwards, "The theory of polymer dynamics," *Claredon Press. Oxford*, 1986.

[192] M. J. Abraham *et al.*, "Gromacs: High performance molecular simulations through multi-level parallelism from laptops to supercomputers," *SoftwareX*, 2015.

[193] W. L. Jorgensen, J. Chandrasekhar, J. D. Madura, R. W. Impey, and M. L. Klein, "Comparison of simple potential functions for simulating liquid water," *J. Chem. Phys.*, 1983.

[194] J. Huang and A. D. Mackerell, "CHARMM36 all-atom additive protein force field: Validation based on comparison to NMR data," *J. Comput. Chem.*, 2013.

[195] Y. Wu, L. K. Wagner, and N. R. Aluru, "Hexagonal boron nitride and water interaction parameters," *J. Chem. Phys.*, 2016.

[196] B. Hess, "P-LINCS: A parallel linear constraint solver for molecular simulation," *J. Chem. Theory Comput.*, 2008.

[197] G. Bussi, D. Donadio, and M. Parrinello, "Canonical sampling through velocity rescaling," *J. Chem. Phys.*, 2007.

[198] M. Parrinello and A. Rahman, "Polymorphic transitions in single crystals: A new molecular dynamics method," *J. Appl. Phys.*, 1981.

[199] M. R. Shirts, J. W. Pitera, W. C. Swope, and V. S. Pande, "Extremely precise free energy calculations of amino acid side chain analogs: Comparison of common molecular mechanics force fields for proteins," *J. Chem. Phys.*, 2003.

[200] C. H. Bennett, "Efficient estimation of free energy differences from Monte Carlo data," *J. Comput. Phys.*, 1976.

[201] A. Pohorille, C. Jarzynski, and C. Chipot, "Good practices in free-energy

calculations," *J. Phys. Chem. B*, 2010.

[202] K. R. Hinkle and F. R. Phelan, "Solvation Free Energy of Self-Assembled Complexes: Using Molecular Dynamics to Understand the Separation of ssDNA-Wrapped Single-Walled Carbon Nanotubes," *J. Phys. Chem. C*, 2020.

[203] D. Roxbury, J. Mittal, and A. Jagota, "Molecular-basis of single-walled carbon nanotube recognition by single-stranded DNA," *Nano Lett.*, 2012.

[204] T. V. Galassi *et al.*, "An optical nanoreporter of endolysosomal lipid accumulation reveals enduring effects of diet on hepatic macrophages in vivo," *Sci. Transl. Med.*, 2018.

[205] Y. Hu *et al.*, "Targeting of CD38 by the tumor suppressor miR-26a serves as a novel potential therapeutic agent in multiple myeloma," *Cancer Res.*, 2020.

[206] W. Wenseleers, I. L. Vlasov, E. Goovaerts, E. D. Obraztsova, A. S. Lobach, and A. Bouwen, "Efficient isolation and solubilization of pristine single-walled nanotubes in bile salt micelles," *Adv. Funct. Mater.*, 2004.

[207] M. J. O'Connell *et al.*, "Band gap fluorescence from individual single-walled carbon nanotubes," *Science (80-.).*, 2002.

[208] J. A. Fagan *et al.*, "Analyzing surfactant structures on length and chirality resolved (6,5) single-wall carbon nanotubes by analytical ultracentrifugation," *ACS Nano*, 2013.

[209] G. Akerlof, "Dielectric constants of some organic solvent-water mixtures at various temperatures," *J. Am. Chem. Soc.*, 1932.

[210] M. R. Green and J. Sambrook, "Precipitation of DNA with isopropanol," *Cold Spring Harb. Protoc.*, 2017.

[211] F. Xhyliu and G. Ao, "Chirality-pure carbon nanotubes show distinct complexation with recognition DNA sequences," *Carbon N. Y.*, 2020.

[212] R. J. Hijmans, "Package 'raster' - Geographic Data Analysis and Modeling," *CRAN Repository*. 2019.

[213] J. K. Streit, S. M. Bachilo, A. V. Naumov, C. Khripin, M. Zheng, and R. B. Weisman, "Measuring single-walled carbon nanotube length distributions from diffusional trajectories," *ACS Nano*, 2012.

[214] R. G. Larson, *The structure and rheology of complex fluids*, vol. 150. Oxford university press New York, 1999.

[215] P. Cassagnau, W. Zhang, and B. Charleux, "Viscosity and dynamics of nanorod (carbon nanotubes, cellulose whiskers, stiff polymers and polymer fibers) suspensions," *Rheologica Acta*. 2013.

[216] T. A. Hilder *et al.*, "Validity of current force fields for simulations on boron nitride nanotubes," *Micro Nano Lett.*, 2010.

[217] J. F. Campbell, I. Tessmer, H. H. Thorp, and D. A. Erie, "Atomic force microscopy studies of DNA-wrapped carbon nanotube structure and binding to quantum dots," *J. Am. Chem. Soc.*, 2008.

[218] X. Chen, C. M. Dmuchowski, C. Park, C. C. Fay, and C. Ke, "Quantitative Characterization of Structural and Mechanical Properties of Boron Nitride Nanotubes in High Temperature Environments," *Sci. Rep.*, 2017.

[219] X. Chen, L. Zhang, C. Park, C. C. Fay, X. Wang, and C. Ke, "Mechanical strength of boron nitride nanotube-polymer interfaces," *Appl. Phys. Lett.*, 2015.

[220] P. Schroeder, C. Calles, T. Benesova, F. MacAluso, and J. Krutmann,

"Photoprotection beyond ultraviolet radiation - Effective sun protection has to include protection against infrared a radiation-induced skin damage," *Skin Pharmacology and Physiology*. 2010.

[221] B. L. Diffey, "Human exposure to solar ultraviolet radiation.," *Journal of cosmetic dermatology*. 2002.

[222] C.-Y. Su, H.-Z. Tang, G.-D. Zhu, C.-C. Li, and C.-K. Lin, "The optical properties and sunscreen application of spherical h-BN–TiO2/mica composite powder," *Ceram. Int.*, vol. 40, no. 3, pp. 4691–4696, 2014.

[223] C. C. Lin and W. J. Lin, "Sun protection factor analysis of sunscreens containing titanium dioxide nanoparticles," *J. Food Drug Anal.*, 2011.

[224] R. Arenal, M. S. Wang, Z. Xu, A. Loiseau, and D. Golberg, "Young modulus, mechanical and electrical properties of isolated individual and bundled single-walled boron nitride nanotubes," *Nanotechnology*, 2011.

[225] A. E. Tanur, J. Wang, A. L. M. Reddy, D. N. Lamont, Y. K. Yap, and G. C. Walker, "Diameter-dependent bending modulus of individual multiwall boron nitride nanotubes," *J. Phys. Chem. B*, 2013.

[226] J. Garel *et al.*, "Ultrahigh torsional stiffness and strength of boron nitride nanotubes," *Nano Lett.*, 2012.

[227] Q. Luo, C. Wirth, and E. Pentzer, "Efficient sizing of single layer graphene oxide with optical microscopy under ambient conditions," *Carbon N. Y.*, 2020.

APPENDIX A

PURIFICATION AND ASSEMBLY OF DNA-STABILIZED BORON NITRIDE NANOTUBES INTO ALIGNED FILMS

1. SEM of As-Synthesized BNNT Material

SEM images of as-synthesized BNNT material are shown in Figure A1. Both nanotube structures (arrows), and the presence of impurities (arrowheads) which stick to nanotubes in the form of star-shaped structures,[116] are observed.

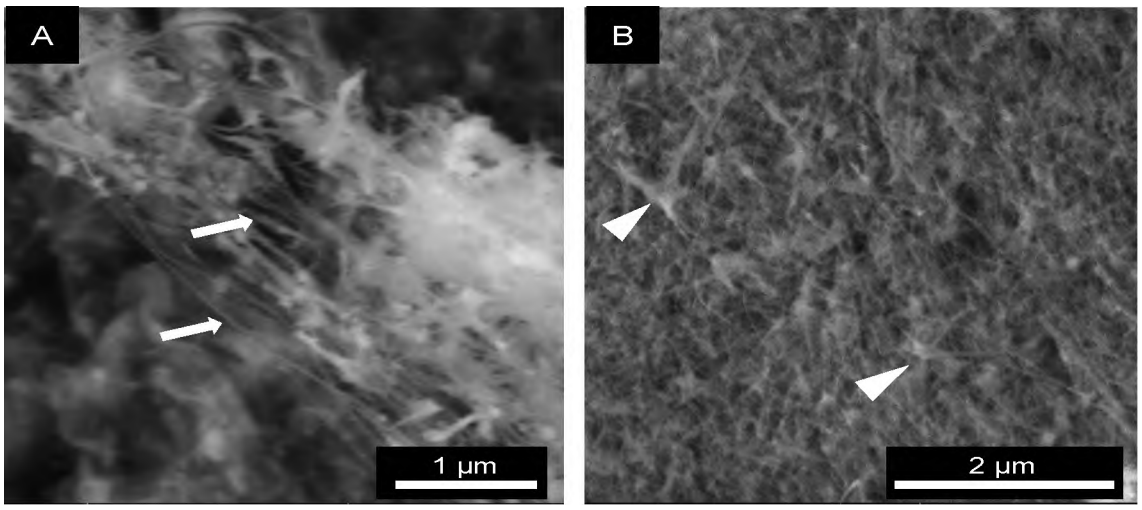

Figure A.1. SEM images of a synthetic BNNT material, where (A) arrows indicate nanotubes and (B) arrowheads represent impurities in the form of star-shaped structures.

2. UV-vis Absorption of DNA-BNNT Dispersions

Figure A2 shows the UV-vis absorbance spectra of aqueous dispersions of DNA-BNNTs with different preparation methods. Here, absorbance spectra for bulk and supernatant dispersions with BNNTs:DNA = 1:1 were measured after removing excess DNA using a precipitation method. However, BNNT:DNA = 1:0 sample was measured without precipitation. We observed that with precipitation and re-dispersion in water, the peak at 190 nm in BNNT:DNA = 1:0 sample disappeared indicating that DNA may also assist the stabilization of impurities in water to a certain extent.

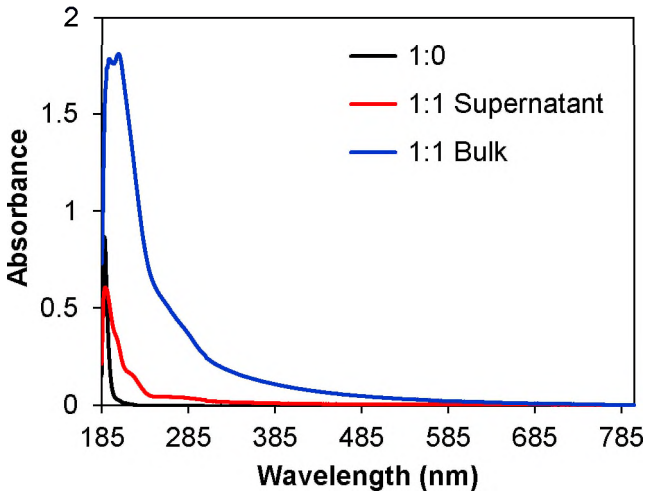

Figure A.2. Absorbance spectra of aqueous dispersions of $(GT)_{20}$-BNNTs with BNNTs/DNA mass ratios of 1:0 and 1:1 before (*i.e.*, bulk) and after (*i.e.*, supernatant) centrifugation. All samples were diluted by a factor of 100× in DI water for UV-vis absorbance measurements.

3. Extinction Coefficient of DNA-BNNTs

The extinction coefficient of DNA-BNNT hybrids was measured using non-centrifuged dispersions of DNA-BNNT at a ratio BNNTs:DNA = 1:1 on a mass basis after purification by membrane filtration. After membrane-filtration, the dispersion is highly enriched in DNA-BNNT hybrids. In Figure A3, the extinction coefficient of DNA-BNNT hybrids was calculated to be 0.0926 $L \cdot mg^{-1} \cdot cm^{-1}$ at 205 nm using Beer-Lambert's law. Specifically, six replicates of a concentrated DNA-BNNT dispersion were dried in an oven up to 350 °C for three days to obtain the average mass of dried DNA-BNNT hybrids using a Cahn Instruments C31 Microbalance with a readability of 0.1 μg. The same DNA-BNNT dispersion was serially diluted to obtain absorbance values of DNA-BNNT hybrids at 205 nm at different concentrations. In addition, the overall percentage of non-nanotube impurities in an as-synthesized BNNT material was estimated as ≈ 45.17 mass % by measuring the average mass of dried DNA-BNNT samples before and after purification

with membrane filtration, assuming that only DNA-BNNT hybrids remained in the dispersion, and that all nanotubes were recovered after membrane filtration. Our estimation is close to that of ≈ 50 mass % impurities provided for the specification of a synthetic BNNT material by the supplier.

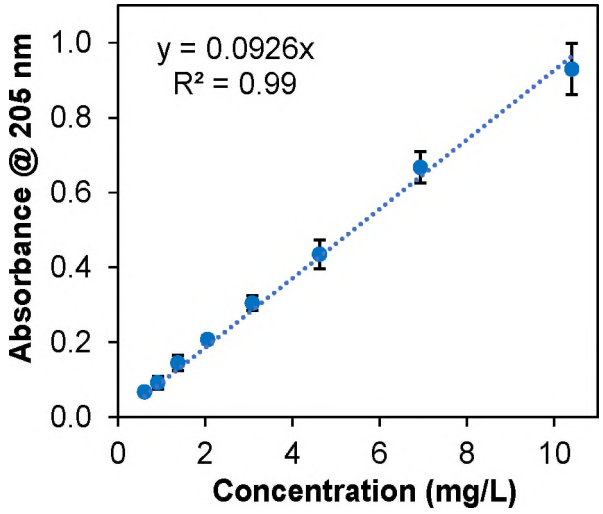

Figure A.3. The calibration curve of DNA-BNNT hybrids obtained at 205 nm. Error bars were generated from the standard deviation of three repeats. All samples were serially diluted by a factor of two-thirds in DI water for measurements.

4. SEM of DNA-BNNT films

The purified, concentrated DNA-BNNT dispersion used for producing dried films contains excess $(GT)_{20}$ ssDNA not bound to nanotubes with free DNA:DNA-BNNT hybrids ≈ 1.1:1 mass ratio. SEM images of dried films obtained from purified dispersions containing ≈ 11.5 mass% DNA-BNNT hybrids and ≈ 12.6 mass% excess $(GT)_{20}$ (Figure A4.A,B) and from 12.6 mass % of $(GT)_{20}$ only (Figure A4.C,D) are shown below. Relative to the DNA-stabilized BNNT films, the films without nanotubes exhibit high brittleness and break in glassy pieces when scribing to reveal the smooth underside of the films.

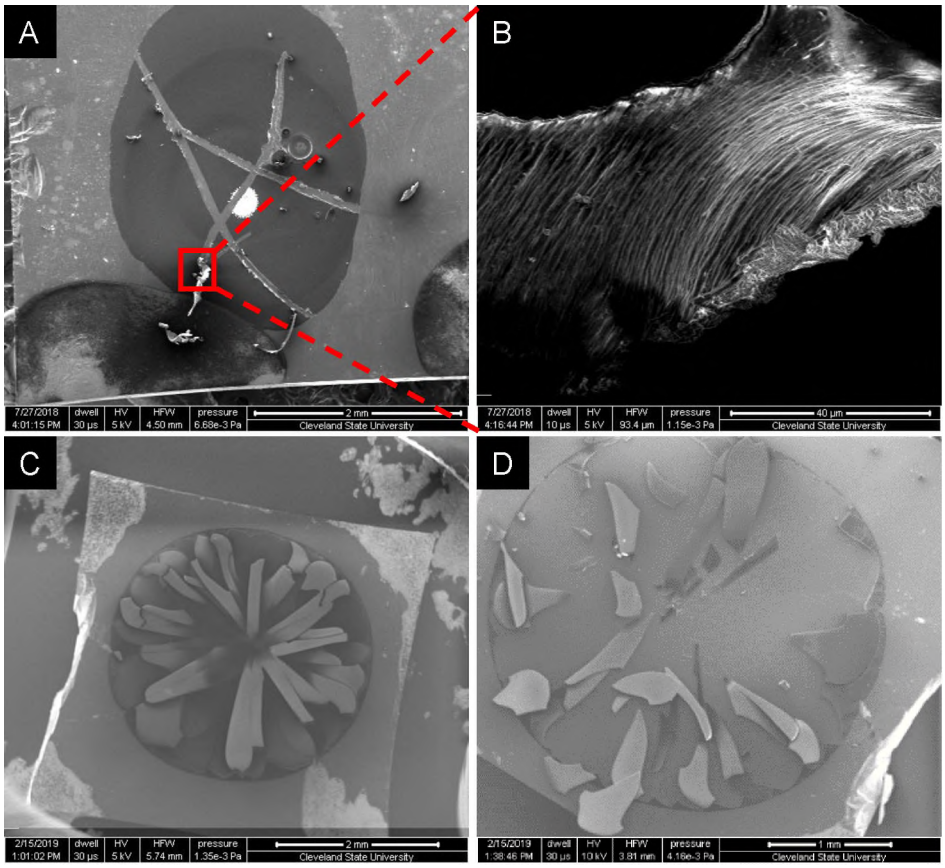

Figure A.4. SEM images of dried films. (A,B) Films obtained from purified, concentrated dispersions containing ≈ 11.5 mass % DNA-BNNT hybrids and ≈ 12.6 mass % excess $(GT)_{20}$ ssDNA. Films obtained from drying 12.6 mass % $(GT)_{20}$ only without nanotubes before (C) and after (D) scribing.

APPENDIX B

COSOLVENT-ASSISTED COMPLEXATION OF BORON NITRIDE NANOTUBES WITH DNA

Table S1. Detail of BNNT-Water-IPA Simulated Systems

Alcohol vol%	Alcohol mol%	# Water Molecules	# Alcohol Molecules
0	0	3339	0
20	5.6	2671	158
40	13.6	2003	316
60	26.2	1336	474
80	48.6	668	631
100	100	0	789

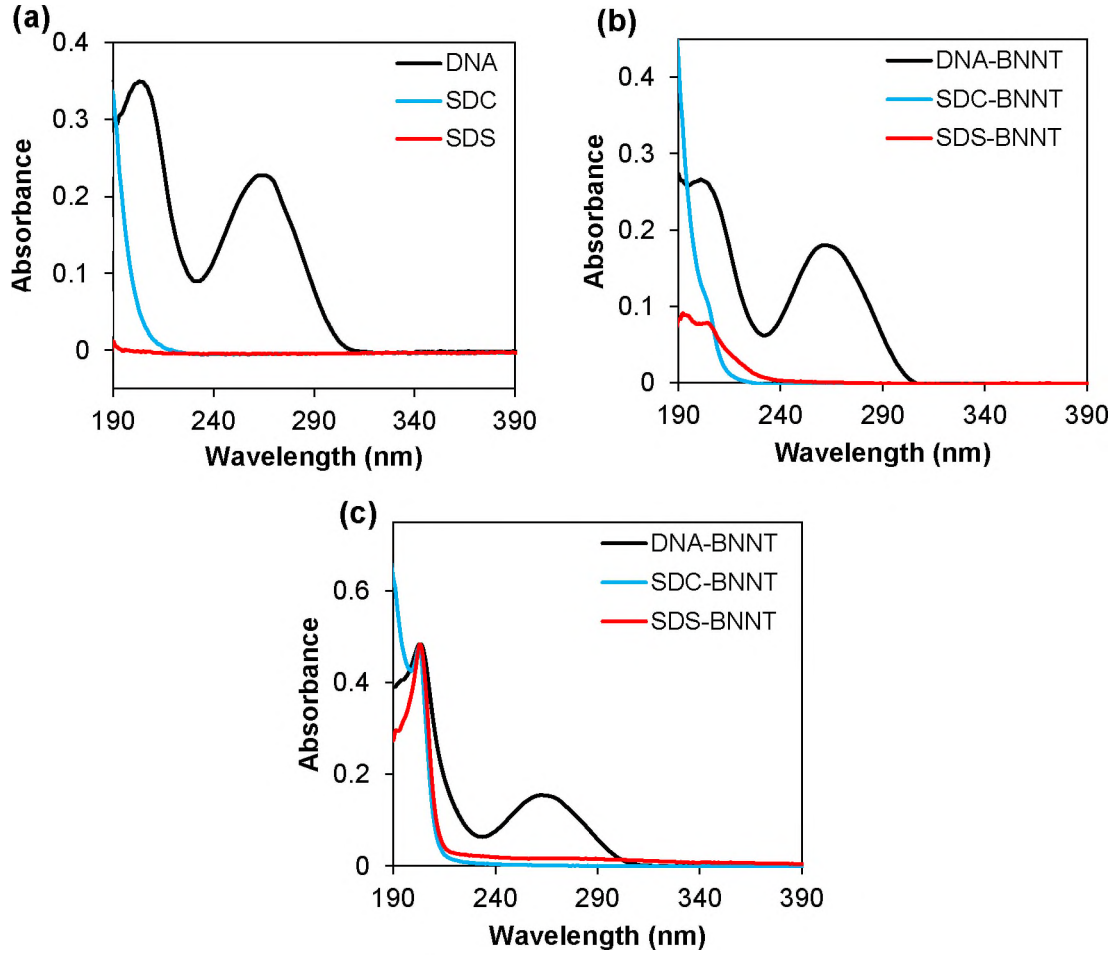

Figure B.1. Absorbance spectra of (a) aqueous solutions of 1 mg/mL DNA, 1 mass% SDC and 1 mass% SDS, respectively, and dispersions of BNNTs coated by DNA, SDC, SDS in water prepared by (b) 24 hr bath sonication and (c) 1 hr probe tip sonication based on our previous work.[178]

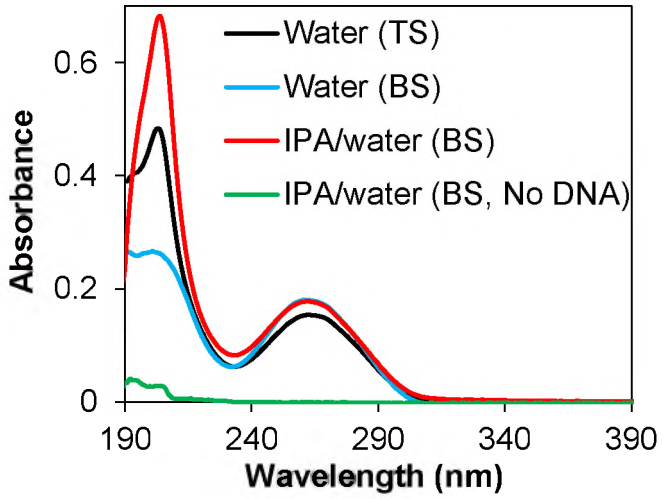

Figure B.2. Absorbance spectra of supernatant dispersions of DNA-BNNT complexes prepared using three different methods: 1 hr probe tip sonication (TS) in water based on our previous work,[178] 24 hr bath sonication (BS) in water, and 24 hr bath sonication in an IPA/water mixture containing 50 % (v/v) IPA, respectively. Absorbance spectra of BNNTs only (without adding DNA) in IPA/water mixture containing 50 % (v/v) IPA with 24 hr bath sonication was included for comparison.

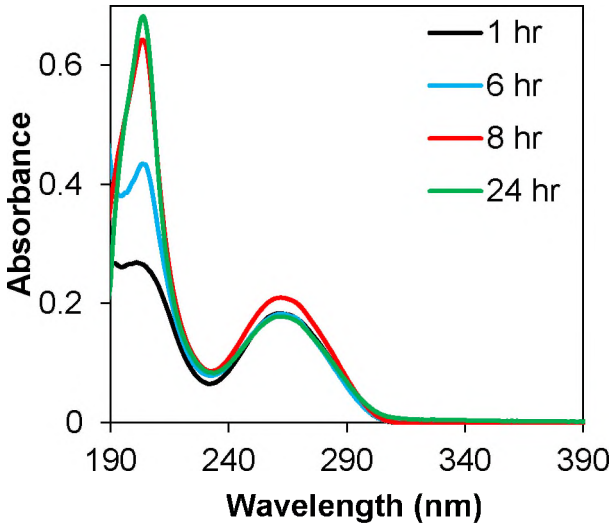

Figure B.3. Absorbance spectra of supernatant dispersions of DNA-BNNT complexes prepared in an IPA/water mixture containing 50 % (v/v) IPA by bath sonication for different time periods including 1, 6, 8, and 24 hours.

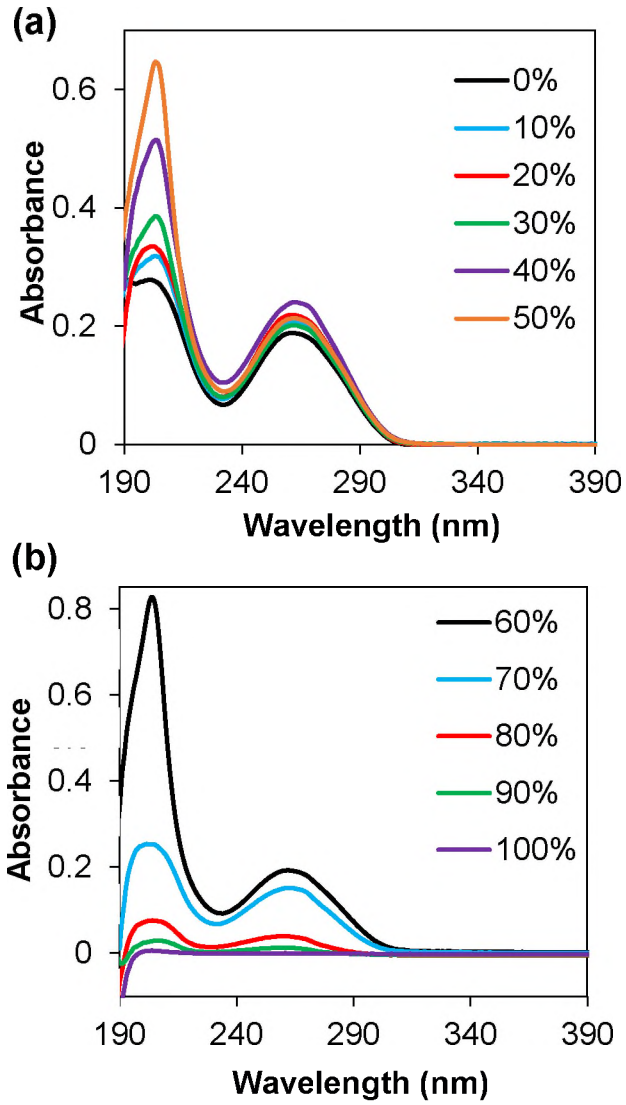

Figure B.4. Absorbance spectra of supernatant dispersions of DNA-BNNT complexes prepared in IPA/water mixtures with increasing amount of IPA including (a) 0 - 50 % (v/v) IPA and (b) 60 - 100 % (v/v) IPA.

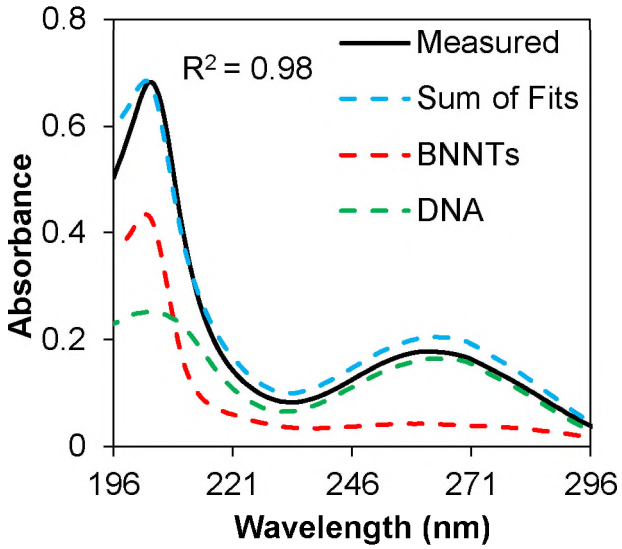

Figure B.5. Absorbance spectra of supernatant dispersions of DNA-BNNTs prepared in an IPA/water mixture containing 60 % (v/v) IPA and the corresponding peak fitting through linear regression of absorption peaks of each component (i.e., free DNA and BNNTs, respectively) to obtain a global fitting of the measured absorbance spectra.

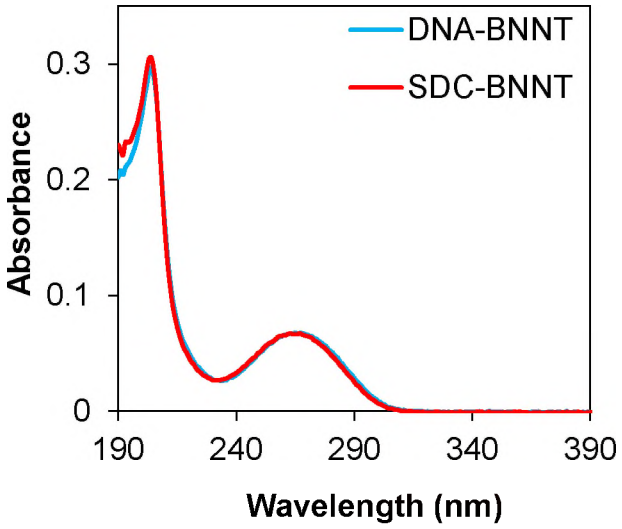

Figure B.6. Absorbance spectra of aqueous dispersions of purified DNA-BNNTs by membrane filtration and SDC-BNNT complexes after DNA/surfactant exchange.

A. Python code for global fitting of absorbance spectra of DNA-BNNTs in IPA/water mixtures

```
Created on Mon Dec 14 16:26:57 2020

@author: VENKATESWARA RAO KODE

Spyder Editor

import numpy as np

import pandas as pd

from sklearn import linear_model

from sklearn.metrics import r2_score


data=pd.read_csv('test.csv')

X=data[['nanotubes','dna']]

y=data['cummulative']

X=np.array(X)

y=np.array(y)


clf_linear = linear_model.LinearRegression()

clf_linear.fit(X,y)

clf_linear.coef_

r2_score(y,clf_linear.predict(X))
```

B. R code for statistical analysis on length distributions of DNA-BNNTs before and after surfactant exchange

```
# Created by VENKATESWARA RAO KODE On April 27th, 2020

# Developed for Statistical Analysis on Length Distributions of DNA-BNNTs Before and After Surfactant Exchange

rm(list=ls(all=TRUE)) #clearing all history

library(readxl)

#importing datafile

VRK_Final_Project_Data <- read_excel("E:/RESEARCH/project/VRK_Final Project Data.xlsx")

View(VRK_Final_Project_Data)

#viewing each column in the data set

attach(VRK_Final_Project_Data)

View(`DNA-BNNTs`)

View(`SDC-BNNTs`)

#plotting histogram of DNA-BNNTs

hist(`DNA-BNNTs`, prob=T, breaks = 50, col = "4", main = " ", xlab = "Length of BNNTs (nm)", ylab = "Frequency")

#plottig histogram of SDC-BNNTs

hist(`SDC-BNNTs`, breaks = 50, add = TRUE, prob=T, col = "5", main = " ")

legend("topright", legend=c("DNA-BNNTs", "SDC-BNNTs"), col=c("orange", "blue"), fill=topo.colors(2), cex=0.5)

#boxplot

boxplot(`DNA-BNNTs`,`SDC-BNNTs`, col = "orange", ylab = "Lengths of BNNTs (nm)", names = c("DNA-BNNTs", "SDC-BNNTs"))

text(x=1.5, y=800, "P< 0.001") #inserting the p-value in the box plot

#summary of each case

summary(`DNA-BNNTs`,na.rm=T)

summary(`SDC-BNNTs`,na.rm=T)

#testing the normality of each case

#Q-Q plot

qqnorm(`DNA-BNNTs`, col="orange", pch=19, font=1.5,font.lab=2, main = "DNA-BNNTs")

qqline(`DNA-BNNTs`)
```

```
qqnorm(`SDC-BNNTs`, pch=19,col="orange",font=1.5,font.lab=2, main = "SDC-BNNTs")
qqline(`SDC-BNNTs`)
#testing the normality
#Shapiro-Wilk test
shapiro.test(`DNA-BNNTs`)
shapiro.test(`SDC-BNNTs`)
#standard deviation of each case
sd(`DNA-BNNTs`)
sd(`SDC-BNNTs`)
#nonparametric method
#The Mann-Whitney U-test
wilcox.test(`DNA-BNNTs`,`SDC-BNNTs`)
```

APPENDIX C

LIQUID DISPERSIONS OF HEXAGONAL BORON NITRIDE NANOSHEETS STABILIZED BY DNA

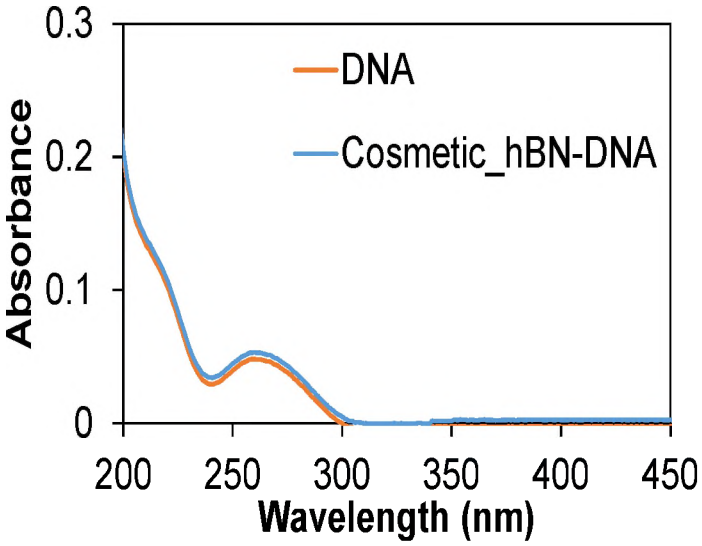

Figure C.1. Absorbance spectra of precipitated samples of both DNA-hBN prepared at a mass ratio of hBN:DNA = 1:2 and DNA only samples. Samples were diluted 12,800x for absorbance measurements.

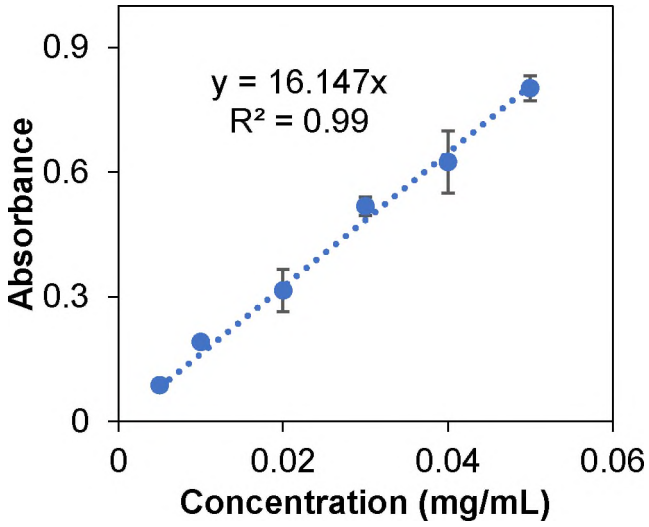

Figure C.2. The calibration curve of DNA obtained at 260 nm. All samples are diluted 100x. The error bars were obtained from the standard deviation of minimum three replicates.

Table C.1. The quantitative data for dispersion yield calculation of DNA-hBN sheets in PBS.

S. No	Mass of empty pan (mg)	Total mass of empty pan + dried sample (mg)	Mass of dried sample (mg)	Measured volume in each pan (μL)	Measured mass of excess DNA (mg)	Measured mass of hBN (mg)	Maximum mass of hBN (mg)	Dispersion yield (%)
Pan1	13.33	16.28	2.95	45	1.891	1.058	4.43	23.89
Pan2	13.61	16.09	2.48	45	1.891	0.588	4.43	13.28
Pan3	13.06	16.03	2.97	45	1.891	1.078	4.43	24.34
Pan4	13.27	15.81	2.54	45	1.891	0.648	4.43	14.64

Sample calculation for pan 1:

Excess DNA concentration in hBN-DNA precipitated sample:

C= (0.053/0.01614) mg/L= 0.00328 mg/mL × 12,800x (dilution factor) = 42.032 mg/mL

The measured mass of excess DNA = 42.032 mg/mL × 45.0 μL= 1.8914 mg

The measured mass of hBN (mg):

Mass of dried sample – measured mass of excess DNA

= 2.950 mg – 1.891 mg = 1.058 mg

Dispersion yield of hBN:

Measured mass of hBN (mg) / Maximum mass of hBN in each pan (mg)

= **(**1.058/4.430) × 100 % = 23.89 % (assuming mass of PEG and NaSCN is negligible)

The average dispersion yield of hBN = 19.04 ± 5.10 %